Phenomenological Yield and Failure Criteria

Holm Altenbach, Alexandre Bolchoun and Vladimir A. Kolupaev

Abstract Models for isotropic materials based on the equivalent stress concept are discussed. At first, so-called classical models which are useful in the case of absolutely brittle or ideal ductile materials are presented. Tests for basic stress states are suggested. At second, standard models describing the intermediate range between the absolutely brittle and ideal-ductile behavior are introduced. Any criterion is expressed by various mathematical equations formulated, for example, in terms of invariants. At the same time the criteria can be visualized which simplifies the application. At third, in the main part pressure-insensitive, pressure-sensitive and combined models are separated. Fitting methods based on mathematical, physical and geometrical criteria are necessary. Finally, three examples (gray cast iron, poly(oxymethylene) (POM) and poly(vinyl chloride) (PVC) hard foam) demonstrates the application of different approaches in modeling certain limit behavior. Two appendices are necessary for a better understanding of this chapter: in Chap. 2 applied invariants are briefly introduced and a table of discussed in this chapter criteria with references is given.

Keywords Strength criteria · Yield criteria · Equivalent stress · Pressure-insensitive criteria · Pressure-sensitive criteria · Limit surfaces

H. Altenbach (✉)
Lehrstuhl für Technische Mechanik, Institut für Mechanik, Fakultät für Maschinenbau, Otto-von-Guericke-Universtät Magdeburg, Universitätsplatz 2, 39106 Magdeburg, Germany
e-mail: holm.altenbach@ovgu.de

A. Bolchoun
Abteilung Werkstoffe und Bauteile, Fraunhofer-Institut für Betriebsfestigkeit und Systemzuverlässigkeit LBF, Bartningstr. 47, 64289 Darmstadt, Germany
e-mail: alexandre.bolchoun@lbf.fraunhofer.de

V. A. Kolupaev
Deutsches Kunststoff-Institut (DKI), Schloßgartenstr. 6, 64289 Darmstadt, Germany
e-mail: VKolupaev@dki.tu-darmstadt.de

H. Altenbach and A. Öchsner (eds.), *Plasticity of Pressure-Sensitive Materials*, Engineering Materials, DOI: 10.1007/978-3-642-40945-5_2,

1 Need of Criteria

The strength theory assumes that the mechanical loading states can be characterized, for example, by stresses [62]. It is known that the stresses in each point of the material or structure are presented by the stress tensor $\boldsymbol{\sigma}$ [5]. For comparison purposes of various stress states the stress tensor cannot be applied that means a scalar quantity should be used. Let us introduce the following expression for such quantity

$$\sigma_{\mathrm{EQ}} = \sigma_{\mathrm{eq}}(\boldsymbol{\sigma}) + f(\nabla\boldsymbol{\sigma})\, R, \qquad R \geq 0. \tag{1}$$

∇ is the nabla operator, f denotes an arbitrary scalar-valued function and R is a structural parameter, which can be associated with the grain size in gray iron, with the cell size of a hard foam, with the particle size in nanomaterials, etc. This parameter represents the influence of the stress distribution expressed by the stress gradient $\nabla\boldsymbol{\sigma}$. The parameter R is positive-definit and bounded by the minimal dimension of the structural component, e. g. the plate or sheet thickness, cf. [214]. Equation (1) can be extended by introducing higher order stress gradients, however the application is limited. The additional material parameters should be estimated experimentally, but tests for their estimation are unknown.

Ignoring the microstructure influence Eq. (1) can be simplified

$$\sigma_{\mathrm{EQ}} = \sigma_{\mathrm{eq}}(\boldsymbol{\sigma}). \tag{2}$$

This implies that the stress state in each point can be described through the stresses at this point only [71]. This formulation has multiple limitations and must be applied with care if the calculation of stresses is performed for parts with significant stress gradients:

- stress concentration areas,
- load application areas,
- sharp corners, etc.

Nevertheless, the concept of the equivalent stress (2) is widely applicable. This concept allows to compare multi-axial stress states with material parameters, e. g. the tensile yield or failure stress σ_+

$$\sigma_{\mathrm{eq}} = \sigma_+. \tag{3}$$

Strength hypotheses and yield criteria for isotropic materials can be formulated using principal stresses

$$\Phi(\sigma_{\mathrm{I}},\ \sigma_{\mathrm{II}},\ \sigma_{\mathrm{III}},\ \sigma_{\mathrm{eq}}) = 0, \tag{4}$$

or other invariants, e. g. axiatoric-deviatoric invariants

$$\Phi(I_1,\ I_2',\ I_3',\ \sigma_{\mathrm{eq}}) = 0, \tag{5}$$

or cylindrical invariants (Novozhilov's invariants)

$$\Phi(I_1,\ I_2',\ \theta,\ \sigma_{\mathrm{eq}}) = 0. \tag{6}$$

The invariants are named in accordance to [234] and detailed presented in Appendix 15. The three formulations (4), (5) and (6) are equivalent. Note that in the case of incompressible material behavior it can be shown that the first invariant I_1 has no influence on Φ

$$\Phi(I_2',\ I_3',\ \sigma_{\mathrm{eq}}) = 0, \qquad \Phi(I_2',\ \theta,\ \sigma_{\mathrm{eq}}) = 0. \tag{7}$$

The remaining invariants are named deviatoric invariants.

The equivalent stress concept (2) allows to formulate the material response under multi-axial loading in a compact form using only few parameters. Such formulations are used in

- elasticity theory (elastic potential) [8, 9, 130, 212],
- plasticity theory (plastic potential, yield criterion) [8, 139, 163, 234],
- creep theory (creep potential) [8, 125],
- strength of materials (strength hypothesis or criterion) [8, 35, 91, 157, 220, 229],
- low cyclic fatigue [8, 126] and
- phase transformation conditions [158, 165].

Phenomenological yield and failure criteria are widely discussed in the literature. Some reviews are given in [8, 16, 45, 71, 74, 157, 174, 204, 221, 228, 229, 234] among others.

2 Classical Strength Theories

The dimensioning of structural members is usually carried out under the assumption, that materials behave either brittle or ductile. The following hypotheses (sometimes named theories), which correspond to one of the two assumptions, are often used for strength or yield evaluation [65, 74, 132, 174].

The three classical models (normal stress hypothesis, Tresca, von Mises), which are presented as usual in textbooks on strength of materials and implemented in commercial finite element codes as a standard tool, and the model of Schmidt-Ishlinsky represent particular cases of material behavior and are sometimes unable to describe the behavior of materials properly. Because of their simplicity they are used in the engineering practice. For applied problems the computations can be performed using these models, if no information on the particular material properties is available. The normal stress hypothesis (Fig. 1) describes the "absolutely brittle" material behavior, the models of Tresca, von Mises and Schmidt-Ishlinsky—the "ideal ductile" behavior.

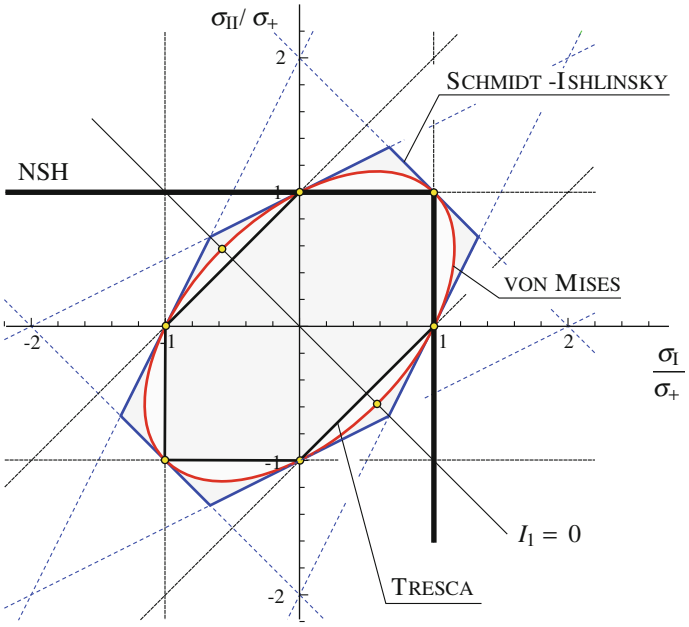

Fig. 1 Models for incompressible "ideal ductile" material behavior (von Mises, Tresca and Schmidt-Ishlinsky) and the normal stress hypothesis (NSH) for "absolutely brittle" material behavior in the plane $\sigma_{\mathrm{I}}-\sigma_{\mathrm{II}}$, $\sigma_{\mathrm{III}} = 0$ (after [93])

2.1 Normal Stress Hypothesis

The normal stress hypothesis (Clapeyron, Galilei, Leibniz, Lamé, Maxwell, Navier, Rankine), Fig. 2, i.e. the maximum tensile stress is responsible for the failure [75, 94, 166, 175], can be expressed as it as follows

$$\sigma_{\mathrm{eq}} = \max(\sigma_{\mathrm{I}},\ \sigma_{\mathrm{II}},\ \sigma_{\mathrm{III}}). \tag{8}$$

Another formulation is

$$(\sigma_{\mathrm{I}} - \sigma_{\mathrm{eq}})\,(\sigma_{\mathrm{II}} - \sigma_{\mathrm{eq}})\,(\sigma_{\mathrm{III}} - \sigma_{\mathrm{eq}}) = 0. \tag{9}$$

Equation (9) is a cubic equation with respect to σ_{eq}. With the help of a parameter identification this equation can be transformed into a third order polynomial of I_1^3, $I_1^2\,\sigma_{\mathrm{eq}}$, $I_1\,\sigma_{\mathrm{eq}}^2$, σ_{eq}^3, $I_2'\,\sigma_{\mathrm{eq}}$ and I_3'. It can be obtained using the model [178]

$$\frac{3\,I_2'\,\sigma_{\mathrm{eq}} + c_3\,I_3'}{1 + 2\,c_3/3^3} = \sigma_{\mathrm{eq}}^3, \tag{10}$$

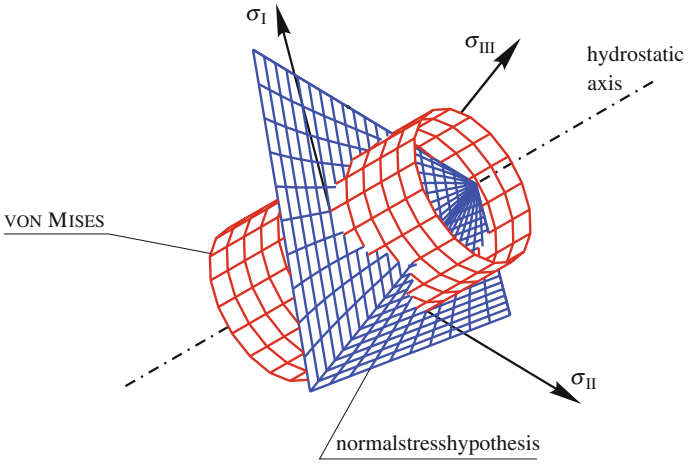

Fig. 2 Normal stress hypothesis (8) and cylinder of von Mises (16) in the principal stress space $(\sigma_I, \sigma_{II}, \sigma_{III})$

and the substitution [103, 178]

$$\sigma_{eq} \rightarrow \frac{\sigma_{eq} - \gamma_1 I_1}{1 - \gamma_1} \tag{11}$$

with the parameter values

$$c_3 = \frac{3^2}{2}, \qquad \gamma_1 = \frac{1}{3} \tag{12}$$

for the better analysis, unified visualization techniques and systematization.

2.2 Tresca Hypothesis

The shear stress hypothesis (Coulomb, Guest, Mohr, Saint Venant, Tresca), i. e. the maximum difference of the principal stresses is relevant for the failure [48, 163, 209], can be written as follows (Fig. 1)

$$\tau_{max} = \frac{1}{2} \max(|\sigma_I - \sigma_{II}|,\ |\sigma_{II} - \sigma_{III}|,\ |\sigma_{III} - \sigma_I|). \tag{13}$$

The equivalent stress can be expressed in this case as

$$\sigma_{eq} = 2\,\tau_{max}. \tag{14}$$

In analogy to Eq. (9) one can write

$$(\sigma_{\mathrm{eq}} - |\sigma_{\mathrm{I}} - \sigma_{\mathrm{II}}|)\,(\sigma_{\mathrm{eq}} - |\sigma_{\mathrm{II}} - \sigma_{\mathrm{III}}|)\,(\sigma_{\mathrm{eq}} - |\sigma_{\mathrm{III}} - \sigma_{\mathrm{I}}|) = 0.$$

This hypothesis (often called Tresca hypothesis) can be also expressed by the deviatoric invariants [163, 171]

$$\left(I_2' - \sigma_{\mathrm{eq}}^2\right)^2 \left(2^2\, I_2' - \sigma_{\mathrm{eq}}^2\right) - 3^3\, I_3'^{\,2} = 0. \tag{15}$$

2.3 Huber-von Mises-Hencky Hypothesis

The distortion energy hypothesis (Huber, von Mises, Hencky),[1] Fig. 2, has different interpretations among them that the failure occurs if a critical amount of accumulated distortion energy is achieved [85, 91, 139, 194, 234]

$$\sigma_{\mathrm{eq}}^2 = \frac{1}{2}\left[(\sigma_{\mathrm{I}} - \sigma_{\mathrm{II}})^2 + (\sigma_{\mathrm{II}} - \sigma_{\mathrm{III}})^2 + (\sigma_{\mathrm{III}} - \sigma_{\mathrm{I}})^2\right] = 3\, I_2'. \tag{16}$$

This hypothesis is often called von Mises hypothesis.

2.4 Schmidt-Ishlinsky Hypothesis

The criterion of the maximum deviatoric stress (Burzyński, Schmidt, Ishlinsky, Hill, Haythornthwaite), i. e. the failure occurs if a critical value of deviatoric components of the stress tensor is achieved [35, 84, 87, 92, 182] (Fig. 1)

$$\max\left[\left|\sigma_{\mathrm{I}} - \frac{1}{3}\, I_1\right|,\ \left|\sigma_{\mathrm{II}} - \frac{1}{3}\, I_1\right|,\ \left|\sigma_{\mathrm{III}} - \frac{1}{3}\, I_1\right|\right] = \frac{2}{3}\,\sigma_{\mathrm{eq}} \tag{17}$$

or in analogy to Eq. (9)

$$\left[\sigma_{\mathrm{eq}} - \left|\sigma_{\mathrm{I}} - \frac{1}{2}(\sigma_{\mathrm{II}} + \sigma_{\mathrm{III}})\right|\right]\left[\sigma_{\mathrm{eq}} - \left|\sigma_{\mathrm{II}} - \frac{1}{2}(\sigma_{\mathrm{III}} + \sigma_{\mathrm{I}})\right|\right]\left[\sigma_{\mathrm{eq}} - \left|\sigma_{\mathrm{III}} - \frac{1}{2}(\sigma_{\mathrm{I}} + \sigma_{\mathrm{II}})\right|\right] = 0. \tag{18}$$

This model can be expressed with the deviatoric invariants [11, 222, 224, 225]

$$\left[\frac{3^3}{2^3}\, I_3' + \frac{3^2}{2^2}\, I_2'\,\sigma_{\mathrm{eq}} - \sigma_{\mathrm{eq}}^3\right]\left[\frac{3^3}{2^3}\, I_3' - \frac{3^2}{2^2}\, I_2'\,\sigma_{\mathrm{eq}} + \sigma_{\mathrm{eq}}^3\right] = 0. \tag{19}$$

The naming Schmidt-Ishlinsky hypothesis has become established.

[1] This criterion was also formulated 1865 in a letter of Maxwell to Lord Kelvin [204].

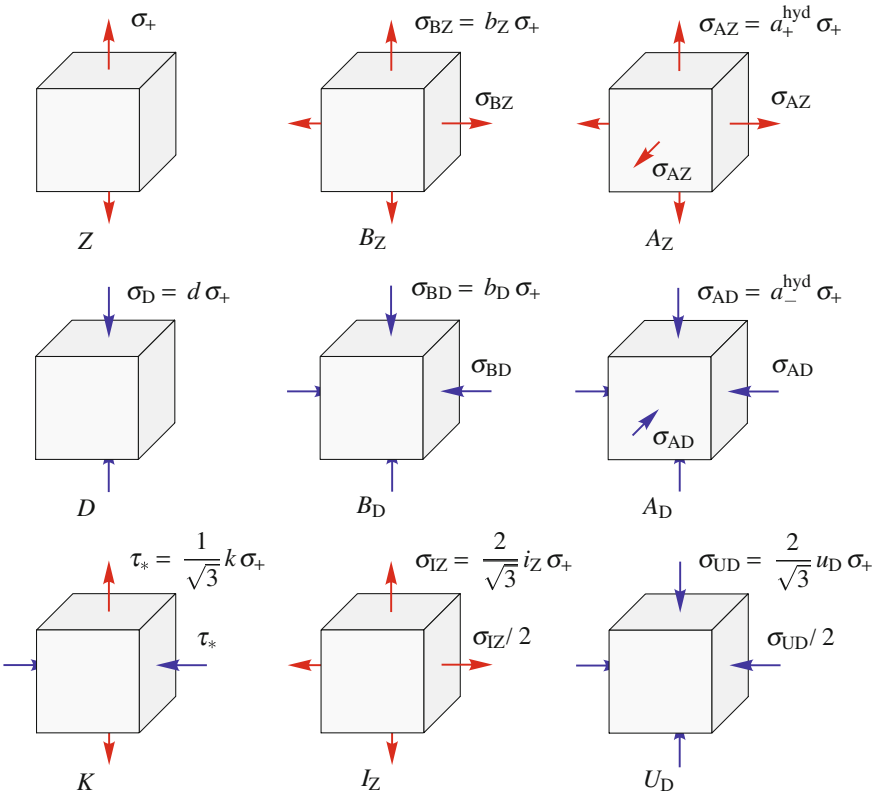

Fig. 3 *Nine* basic tests. The stresses, values and labels of loading are given in Table 1

3 Basic Stress States

All criteria can be visualized as a limit surface Φ. Nine tests (Fig. 3) are chosen for the analysis and comparison of the surfaces Φ:

- two loadings corresponding to one-dimensional stress states (tension, compression),
- five loadings corresponding to plane stress states (torsion, two balanced plane states, two thin-walled tube specimens with closed ends under inner and outer pressure) and
- two loadings corresponding to hydrostatic (3D balanced) tension and compression.

The relevant stresses are listed in Table 1. All these loading cases have approved verbal formulations and can be considered as basic tests.[2]

[2] Note that in material testing another definition of basic tests is given [32].

Table 1 Basic stress states, relations, normalized coordinates in the principal stress space, normalized axiatoric-deviatoric invariants (Appendix A.3), and the stress angle θ (224) [107]

Loading	Stress	Label	Relation	$\left(\frac{\sigma_{\mathrm{I}}}{\sigma_+}, \frac{\sigma_{\mathrm{II}}}{\sigma_+}, \frac{\sigma_{\mathrm{III}}}{\sigma_+}\right)$	$\frac{I_1}{\sigma_+}$	$\frac{\sqrt{3I_2'}}{\sigma_+}$	$\frac{3\sqrt[3]{I_3'/2}}{\sigma_+}$	θ
Basic stress states								
Tension	σ_+	Z	1	$(1,\ 0,\ 0)$	1	1	1	0
Compression	σ_-	D	d	$(-d,\ 0,\ 0)$	$-d$	d	d	$\frac{\pi}{3}$
Torsion	τ_*	K	k	$\left(\frac{k}{\sqrt{3}}, -\frac{k}{\sqrt{3}}, 0\right)$	0	k	0	$\frac{\pi}{6}$
Biaxial tension	σ_{BZ}	B_{Z}	b_{Z}	$(b_{\mathrm{Z}},\ b_{\mathrm{Z}},\ 0)$	$2\,b_{\mathrm{Z}}$	b_{Z}	$-b_{\mathrm{Z}}$	$\frac{\pi}{3}$
Biaxial compression	σ_{BD}	B_{D}	b_{D}	$(-b_{\mathrm{D}},\ -b_{\mathrm{D}},\ 0)$	$-2\,b_{\mathrm{D}}$	b_{D}	b_{D}	0
Inner pressure	σ_{IZ}	I_{Z}	i_{Z}	$\left(\frac{2}{\sqrt{3}}\,i_{\mathrm{Z}},\ \frac{1}{\sqrt{3}}\,i_{\mathrm{Z}},\ 0\right)$	$\sqrt{3}\,i_{\mathrm{Z}}$	i_{Z}	0	$\frac{\pi}{6}$
Outer pressure	σ_{UD}	U_{D}	u_{D}	$\left(-\frac{2}{\sqrt{3}}\,u_{\mathrm{D}}, -\frac{1}{\sqrt{3}}\,u_{\mathrm{D}},\ 0\right)$	$-\sqrt{3}\,u_{\mathrm{D}}$	u_{D}	0	$\frac{\pi}{6}$
Hydrostatic tension	σ_{AZ}	A_{Z}	a_+^{hyd}	$\left(a_+^{\mathrm{hyd}},\ a_+^{\mathrm{hyd}},\ a_+^{\mathrm{hyd}}\right)$	$3\,a_+^{\mathrm{hyd}}$	0	0	–
Hydrostatic compression	σ_{AD}	A_{D}	a_-^{hyd}	$\left(-a_-^{\mathrm{hyd}}, -a_-^{\mathrm{hyd}}, -a_-^{\mathrm{hyd}}\right)$	$-3\,a_-^{\mathrm{hyd}}$	0	0	–
Additional tests								
Tension-torsion	σ_{H}	H	h	$\left(\sqrt{\frac{2}{3}}\,h,\ \sqrt{\frac{2}{3}}\,\frac{1-\sqrt{3}}{2}\,h,\ 0\right)$	$\sqrt{2-\sqrt{3}}\,h$	h	$\frac{h}{2^{1/6}}$	$\frac{\pi}{12}$
Compression-torsion	σ_{Q}	Q	q	$\left(-\sqrt{\frac{2}{3}}\,q,\ \sqrt{\frac{2}{3}}\,\frac{\sqrt{3}-1}{2}\,q,\ 0\right)$	$-\sqrt{2-\sqrt{3}}\,q$	q	$-\frac{q}{2^{1/6}}$	$\frac{\pi}{4}$

These nine tests are sufficient for the comparison of the most important features of surfaces. Their selection is however not unambiguous and can be expanded according to the available equipment, expected phenomena and requested precision, see e. g. loading cases labeled by Q and H (Table 1 and Sect. 9.2). Further considerations for the choice of loadings are discussed in [8, 36, 37].

The values (Table 1) relating the respective stresses to σ_+ are introduced in order to obtain

$$k = d = i_Z = u_D = b_Z = b_D = 1 \qquad \text{and} \qquad a_-^{hyd},\ a_+^{hyd} \to \infty \tag{20}$$

for the von Mises hypotheses (16).

For the models of incompressible material behavior the values on the angle $\theta = 0$, $\frac{\pi}{6}$ and $\frac{\pi}{3}$ are computed to [16, 103, 234]

$$b_D = 1, \qquad k = i_Z = u_D \qquad \text{and} \qquad d = b_Z. \tag{21}$$

For the classical models (Sect. 2) it follows [113]

$$b_Z = 1, \qquad b_D = d. \tag{22}$$

The models for incompressible behavior can be compared in the $d-k$-diagram (Fig. 4) [104, 105, 110]. In this diagram the models of Haythornthwaite and Sayir II (Sect. 9.1) limit the convex shapes of the surface Φ in the π-plane [33]. For the models of compressible material behavior (Sect. 10) the $\frac{1}{d}-k$-diagram, which allows to represent the properties $d \to \infty$, $k = \sqrt{3}$ of the normal stress hypothesis among others, is recommended (Fig. 5) [122, 156, 157]. In this diagram the areas of validity of all criterions and various ideas of generalization can be visualized.

The measurements σ_+, σ_- and τ_* for some materials are presented in [18, 41, 124, 157, 229]. Examples of experimental data for some polymers are given in Table 2.

The data are taken from various sources and they are related to different manufacturers. They can be used as first estimates only. Note that the experiments were performed for specimens with different geometries and using different techniques. The relations d and k of the materials can be represented in Figs. 4 and 5 together with the models in order to simplify the choice of the suitable model [104].

4 Inelastic Poisson's Ratio

In the linear theory of elasticity the Poisson's ratio is defined as the negative ratio of the strain $\varepsilon_{II} = \varepsilon_{III}$ in the direction orthogonal to the applied load and the strain ε_I in the tension direction [20, 89]:

$$\nu^{el} = -\frac{\varepsilon_{II}}{\varepsilon_I} = -\frac{\varepsilon_{III}}{\varepsilon_I}, \qquad \nu^{el} \in \left]-1,\ \frac{1}{2}\right[. \tag{23}$$

Table 2 Parameters for brittle and ductile failure at room temperature collected in [18, 184, 185] on the base of [13, 19, 60, 137, 164, 183, 184, 189, 190, 198, 203] and elastic Poisson's ratios

Polymer	σ_+ [MPa]	d [−]	k [−]	ν_+^{el}, [10] [−]	ν_+^{el}, [119] [−]	ν_+^{el}, [59] [−]	ν_+^{el}, [58] [−]	Remarks
Failure as the result of yielding								
PS	72.67	1.33	1.18	0.33…0.35	0.32…0.34	0.38	0.33	
PVC	57.08	1.17	1.25	–	0.32…0.35[1]	–	–	[1]PVC unplasticized
PVC	53.94	1.30	1.18	–	0.32…0.35[1]	–	–	[1]PVC unplasticized
PVC	32.36	1.33	1.11	–	0.32…0.35[1]	–	–	[1]PVC unplasticized
PMMA	–	1.00	–	–	0.30…0.35	–	0.33	
PMMA	37.27	1.30	–	–	–	–	–	at 80°C
PC	45.11	1.20	1.06	0.37…0.38	0.30…0.35	–	0.42	
PC	58.84	1.22	1.13	0.37…0.38	0.32…0.35	–	0.42	
CAB	33.15	1.00	1.00	–	–	–	–	
PE	10.69	1.34	1.49*	0.40…0.44[2]	0.35…0.40[2]	–	0.38[2]	[2]high density
					0.40…0.45[3]	0.49[3]	0.45[3]	[3]low density
PP	32.26	1.32	1.44*	0.37…0.38	0.35…0.40	–	0.4	
PA	66.29	0.92	1.04	–	0.32…0.40	0.44[4]	–	[4]PA6.6
							0.33[5]	[5]PA6, PA6.6 (dried)
							0.45[6]	[6]PA6, PA6.6 (dried) at 100°C

(continued)

Table 2 (continued)

Polymer	σ_+ [MPa]	d [−]	k [−]	ν_+^{el}, [10] [−]	ν_+^{el}, [119] [−]	ν_+^{el}, [59] [−]	ν_+^{el}, [58] [−]	Remarks
ABS	44.62	0.95	0.94	0.35…0.36	0.32…0.35	–	–	
Brittle fracture								
PMMA	62.08	1.50	1.20	–	0.30…0.35	–	0.33	
PMMA	59.04	1.40	1.16	–	0.30…0.35	–	0.33	
PMMA	–	1.00	–	–	0.30…0.35	–	0.33	
CAB	33.64	0.91	1.30	–	–	–	–	
CA	40.50	1.23	1.70*	–	–	–	–	
PVCA	65.90	1.29	1.80*	–	–	–	–	
EP resin	81.40	1.45	1.20	–	–	–	0.4	Araldit CY232
EP resin	78.45	1.33	1.13	–	–	–	0.4	Legutherm K57

* These values contradict our own experiences [104]

⁻ Molar mass of the thermoplastic polymers was not specified

⁻ Crystallinity of PE, PP and PA is unknown

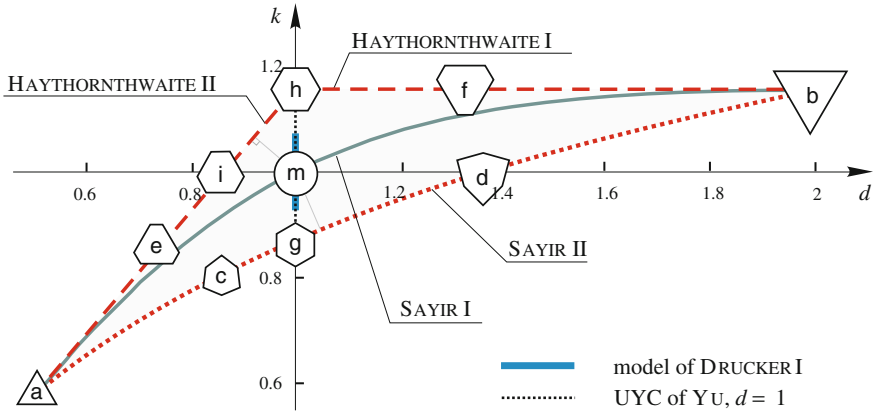

Fig. 4 Diagram $d-k$ for convex models of incompressible material behavior compared with the hypothesis of von Mises [110]. Certain cross sections in the π-plane are visualized in order to achieve a better understanding:
a. $k = 1/\sqrt{3}, d = 1/2$ *b*. $k = 2/\sqrt{3}, d = 2$
c. $k = 3\,(2-\sqrt{3}), d = \sqrt{3}/2$ *d*. $k = 1, d = (1+\sqrt{3})/2$
e. $k = \sqrt{3}/2, d = 3/4$ *f*. $k = 2/\sqrt{3}, d = 4/3$
g. $k = \sqrt{3}/2, d = 1$(Tresca) *h*. $k = 2/\sqrt{3}, d = 1$(Schmidt − Ishlinsky)
i. $k = 1, d = \sqrt{3}/2$ *m*. $k = 1, d = 1$(von Mises)

If the elastic law is formulated on the base of the potential Φ, one can write

$$\nu^{\mathrm{el}} = -\left(\frac{\partial\,\Phi}{\partial\,\sigma_{\mathrm{II}}}\Big/\frac{\partial\,\Phi}{\partial\,\sigma_{\mathrm{I}}}\right)\Big|_{\sigma_{\mathrm{II}}=\sigma_{\mathrm{III}}=0} = -\left(\frac{\partial\,\Phi}{\partial\,\sigma_{\mathrm{III}}}\Big/\frac{\partial\,\Phi}{\partial\,\sigma_{\mathrm{I}}}\right)\Big|_{\sigma_{\mathrm{II}}=\sigma_{\mathrm{III}}=0}. \tag{24}$$

The classical theory of elasticity [20, 64, 205] makes no difference between Poisson's ratio at tension and compression

$$\nu^{\mathrm{el}}_{+} = \nu^{\mathrm{el}}_{-}. \tag{25}$$

The Poisson's ratio for yield criteria in the isotropic case can be computed in a similar way as relations of the strain or strain rates

$$\nu^{\mathrm{in}} = -\left(\frac{\partial\,\Phi}{\partial\,\sigma_{\mathrm{II}}}\Big/\frac{\partial\,\Phi}{\partial\,\sigma_{\mathrm{I}}}\right)\Big|_{\sigma_{\mathrm{II}}=\sigma_{\mathrm{III}}=0} = -\left(\frac{\partial\,\Phi}{\partial\,\sigma_{\mathrm{III}}}\Big/\frac{\partial\,\Phi}{\partial\,\sigma_{\mathrm{I}}}\right)\Big|_{\sigma_{\mathrm{II}}=\sigma_{\mathrm{III}}=0} \tag{26}$$

using the flow rule [126, 167, 234]

$$\dot{\varepsilon}_{ij} = \dot{\lambda}\,\frac{\partial\,\Phi}{\partial\,\sigma_{ij}}, \qquad \dot{\lambda} > 0 \tag{27}$$

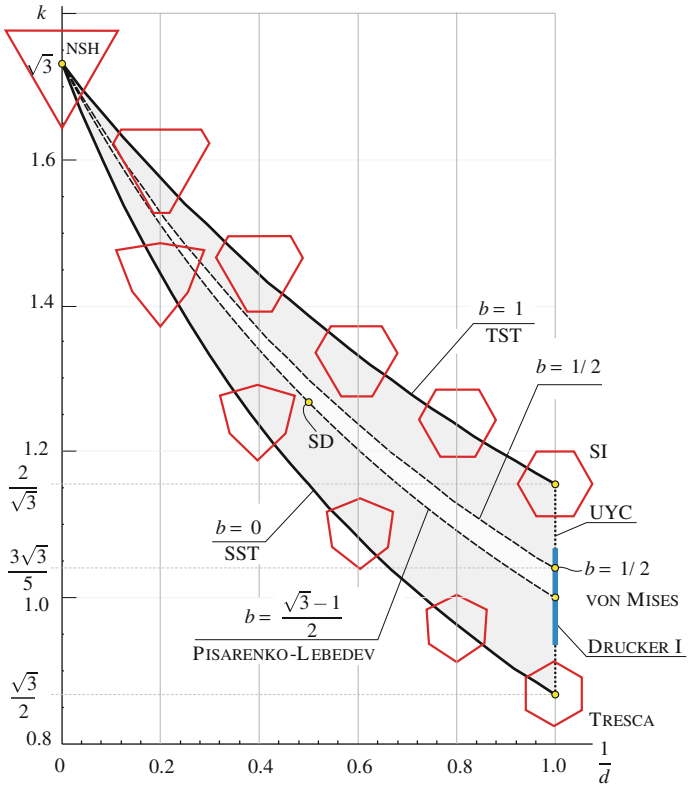

Fig. 5 $1/d$ versus k for the classical models (Sect. 2) and for the Unified Strength Theory of Yu (Sect. 10.2) as a function of $d \geq 1$ and $b \in [0,\ 1]$:
$d \geq 1, k \in \left[1,\ \sqrt{3}\right]$—Pisarenko-Lebedev model (48),
$d = 1, k \in \left[(2/3)^{1/6},\ (3/2)^{1/6}\right]$—model of Drucker I (Sect. 9.2),
$d = 1, k \in \left[\sqrt{3}/2,\ 2/\sqrt{3}\right]$—Unified Yield Criterion of Yu with $b \in [0,\ 1]$ (Sect. 9.2),
$d \to \infty, k = \sqrt{3}$—normal stress hypothesis (Sect. 2.1).
SI—model of Schmidt-Ishlinsky (Sect. 2.4), SD—model of Sdobirev with $d = 2, k = 3 - \sqrt{3} \approx 1.27$ (Sect. 6.3), UYC—Unified Yield Criterion (Sect. 9.2), SST—Single-Shear-Theory of Yu (model of Mohr-Coulomb), Sect. 10.2, TST—Twin-Shear-Theory of Yu. The cross-sections in the π-plane on $I_1 = \sigma_{eq}$ are provided for better understanding [104, 105, 115]

for $\dot{\varepsilon}_{II}$ and $\dot{\varepsilon}_{I}$. Further definitions of ν^{in} are given in [109]. There is a difference between the inelastic Poisson's ratios at tension ν_{+}^{in} with $\sigma_I = \sigma_+$ and compression ν_{-}^{in} with $\sigma_I = -d\,\sigma_+$, $d \geq 0$.

The convexity condition (necessary condition) for the meridian with the angle $\theta = 0$ and the associated point Z (tension) yields [105]

$$\nu_{+}^{in} \in \left]-1,\ \frac{1}{2}\right]. \tag{28}$$

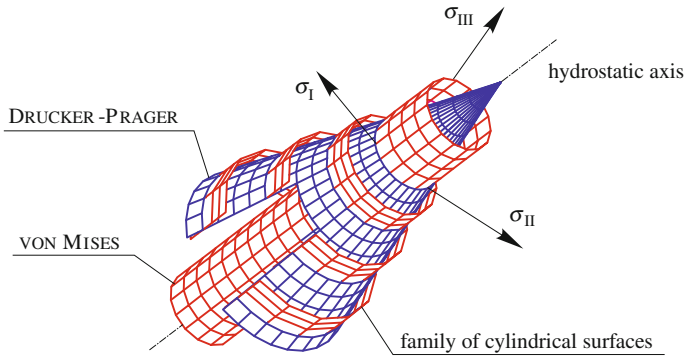

Fig. 6 *Cone* of Drucker-Prager with the family of cylindric surfaces and cylinder of von Mises in the principal stress space (the *cone* is cut in order to achieve better visualization)

For the surfaces that do not cross the hydrostatic axis in the compression region ($a_-^{\text{hyd}} \to \infty$), it follows [103, 181]

$$\nu_-^{\text{in}} \geq \frac{1}{2}. \tag{29}$$

For those surfaces (e. g. Drucker-Prager, Mohr-Coulomb, Pisarenko-Lebedev) a non-associated flow rule with

$$\nu_-^{\text{in}} = \frac{1}{2} \tag{30}$$

is often used [103]. The model of Drucker-Prager can be used as an example (Fig. 6). In this figure for each stress state in the region $I_1 \leq 0$ a cylindrical surface is defined. This results in a "family" of rings, which define the incompressible behavior for each stress state in the compression region.

For closed surfaces in the principal stress space will be assumed [105, 216]

$$\nu_-^{\text{in}} \in \left]-1,\ \frac{1}{2}\right]. \tag{31}$$

The restriction can be clarified in the $\left(\sqrt{3\,I_2'},\ I_1\right)$-plane (Sect. 8.2): the maximum of a meridian lies in the region

$$\frac{I_1}{\sigma_+} \in [-d,\ 1].$$

Using (26) the inclination of the tangent line at the points Z (tension) and D (compression) of the surface Φ in the principal stress space with respect to the hydrostatic axis can be characterized:

- from the inclination $\psi = 0$ (tangent line parallel to the hydrostatic axis) follows $\nu^{\text{in}} = 1/2$ (Fig. 2, model of von Mises) and
- the inclination $\psi = \pi/2$ (tangent line is orthogonal to the hydrostatic axis) yields $\nu^{\text{in}} = -1$.

The Poisson's ratio $\nu_+^{\text{in}} = 0$ (Fig. 2, normal stress hypothesis (8)) yields[3] the inclination angle with

$$\tan\psi = \sqrt{2}\left[\frac{3}{2\,(1+\nu_+^{\text{in}})} - 1\right] \tag{32}$$

to $\psi = \arctan\left(\sqrt{2}/2\right) \approx 35.26°$ in the principal stress space (Fig. 7).

This geometrical interpretation of (26) can be used for description of the limit surface Φ. It completes the relations (Table 1) for the analytical comparison of different surfaces by fitting of measurements.

The following estimates are available for evaluation of the quality of the model:

- For ductile materials the experience-based inequality

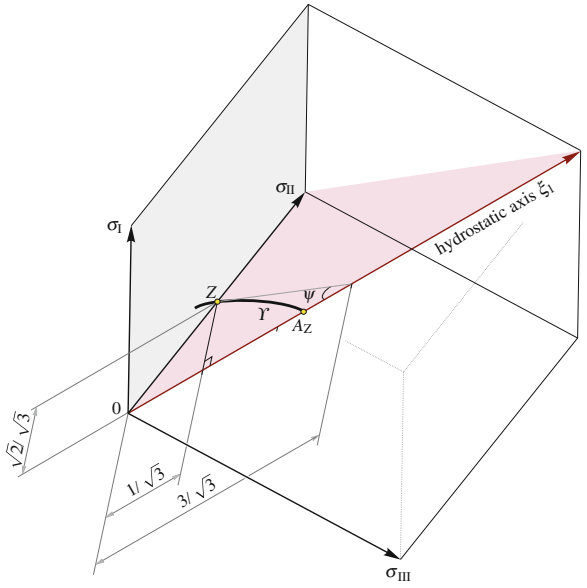

Fig. 7 Principal stress space (σ_{I}, σ_{II}, σ_{III}): inclination of the tangent line $\psi \approx 35.26°$ at the point Z (tension) of the surface Φ correlates with the Poisson's ratio at tension $\nu_+^{\text{in}} = 0$, Υ—intersection of the surface Φ with the surface (ξ_1, 0, σ_{II}) or meridian with $\theta = 0$ of the surface Φ

[3] Here the substitution $I_3' = \frac{2\sqrt{3}}{3^2}\,(I_2')^{3/2}$ is used, which corresponds to the meridian with the angle $\theta = 0$ (Sect. 8.2). The point Z (tension) belongs to this meridian (Table 1).

$$\nu_+^{\text{in}} \in \left[\nu_+^{\text{el}},\ \frac{1}{2}\right] \tag{33}$$

can be used in order to check the quality of fitting to the measured data.

- The term "slight compressibility", see [140], can estimated by [110]

$$\nu_+^{\text{in}} \in \left[0.48,\ \frac{1}{2}\right]. \tag{34}$$

This range is recommended for yield criteria.

- For "very ductile" behavior [126] it can be required additionally

$$\nu_+^{\text{in}} \to \frac{1}{2}, \tag{35}$$

and one gets the desired parameters of the yield criterion in the fitting (Sect. 12).

- For brittle material behavior the following constraints can be formally written down

$$\nu_+^{\text{in}} \in]-1,\ \nu_+^{\text{el}}], \tag{36}$$

cf. the maximum strain hypothesis (Sect. 6.1) for the upper bound and the strain hypotheses with $\sigma_{\text{eq}} = I_1$ for the lower bound.

- For "absolutely" brittle material behavior failure occurs without plastic deformations in the cross sectional area of the tensile bar [206, 208]. In this case it can be assumed from the normal stress hypothesis (Sect. 2)

$$\nu_+^{\text{in}} \approx 0. \tag{37}$$

5 Ratios for a Torsion Bar

In addition to value k, one can define other values relating to torsion using the yield condition (27). By analogy to the Poisson's ratio the elongation/contraction ratio for a torsion bar or tubes can be established, cf. [8]:

$$\chi = \frac{\partial \Phi}{\partial \sigma_{11}} \Big/ \frac{\partial \Phi}{\partial \sigma_{12}} \tag{38}$$

with $\sigma_{12} = k\,\sigma_{\text{eq}}/\sqrt{3}$ and $\sigma_{11} = \sigma_{22} = \sigma_{33} = \sigma_{13} = \sigma_{23} = 0$. With the help of this ratio the Poynting-effect and the Poynting-Swift-effect [160–162, 200] can be described (Figs. 8 and 9). These effects are discussed in the literature, see [3, 8, 16, 27, 29, 69, 81, 168, 206, 215] among others. The material behavior of the von Mises-type results in $\chi = 0$. In the case of the application of the normal stress hypothesis (Sect. 2) one gets $\chi = 1/2$ [6, 110].

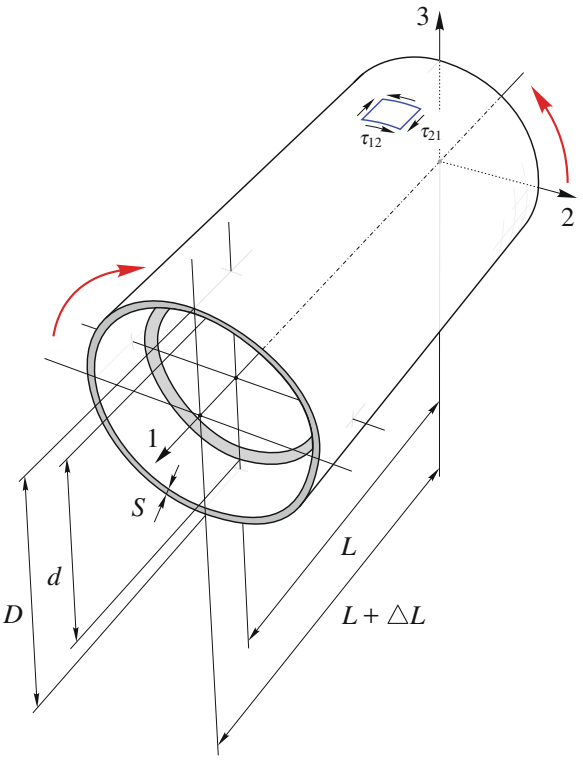

Fig. 8 Change of the geometry of a tube clamped on the right side at torsion

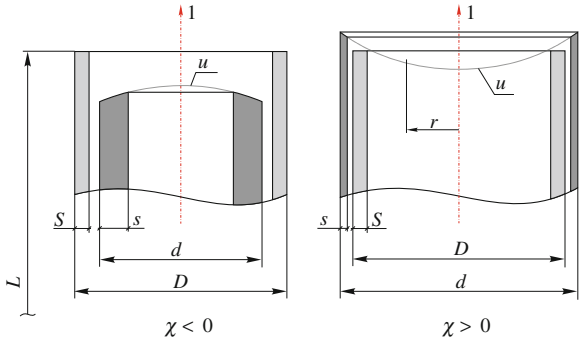

Fig. 9 Change of the geometry of a tube at torsion. D and d—outer diameter of the tube before and after loading, S and s—wall thickness before and after loading, $u(r)$—distribution law for the displacements in the direction 1

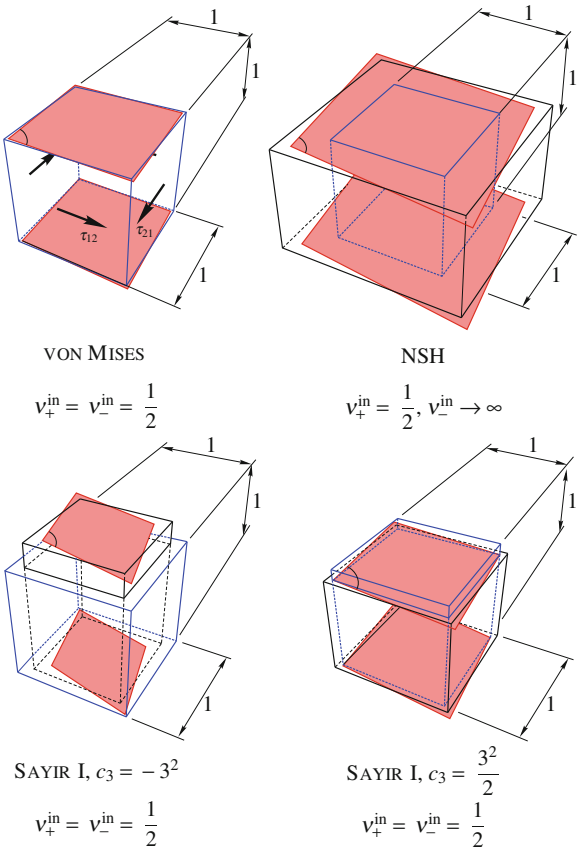

Fig. 10 Change of the geometry and the shape of a cube with the size $1 \times 1 \times 1$ under stress action τ_{12} for four settings of the Sayir I model (Table 3)

Furthermore, the volume strain caused by torsion (volume dilatation, see Kelvin-effect [8, 16]) can be computed as follows:

$$\varepsilon_{V\tau} = \left(\frac{\partial \Phi}{\partial \sigma_{11}} + \frac{\partial \Phi}{\partial \sigma_{22}} + \frac{\partial \Phi}{\partial \sigma_{33}} \right) \Big/ \frac{\partial \Phi}{\partial \sigma_{12}}. \tag{39}$$

In addition, a transverse contraction ratio can be obtained [110]:

$$\nu_\tau^{in} = -\frac{\partial \Phi}{\partial \sigma_{33}} \Big/ \frac{\partial \Phi}{\partial \sigma_{11}}. \tag{40}$$

By this way one gets more information about the material behavior from the torsion test. Some special cases are analyzed in Fig. 10 and Table 3 on the base of model of

Table 3 Effects computed at torsion considering the model of Sayir I (10) with the linear substitution (11)

Cross section in the π-plane (Fig. 4)	a	m		b	
$c_3 \in \left[-3^2,\ \frac{3^2}{2}\right]$	-3^2	0		$\frac{3^2}{2}$	
$\gamma_1 \in [0,\ 1[$		0			$\frac{1}{3}$
$\nu_+^{\text{in}} = \frac{1}{2}\ (1 - 3\,\gamma_1)$		$\frac{1}{2}$			0
Classical model	–	von Mises		–	NSH
$k = \frac{1}{1-\gamma_1}\sqrt{1 + \frac{2}{3^3}\,c_3}$	$\frac{1}{\sqrt{3}}$	1		$\frac{2}{\sqrt{3}}$	$\sqrt{3}$
d	$\frac{1}{2}$	1		2	∞
$\chi = \sqrt{3}\sqrt{1 + \frac{2}{3^3}\,c_3}\,\frac{c_3\,(1-\gamma_1) + 2\cdot 3^2\,\gamma_1}{2\cdot 3^3\,(1-\gamma_1)}$	$-\frac{1}{6}$	0		$\frac{1}{6}$	$\frac{1}{2}$
$\nu_\tau^{\text{in}} = 2\,\frac{c_3\,(1-\gamma_1) - 3^2\,\gamma_1}{c_3\,(1-\gamma_1) + 2\cdot 3^2\,\gamma_1}$	2	$\frac{0}{0}$		2	0
$\varepsilon_{V\tau} = \sqrt{3}\,\frac{\gamma_1}{1-\gamma_1}\sqrt{1 + \frac{2}{3^3}\,c_3}$		0			1

The von Mises hypothesis describes the torsion of the tubular specimen without elongation $\chi = 0$. The hypotheses for incompressible material behavior (von Mises and Sayir I with $c_3 = -3^2$ und $c_3 = 3^2/2$) reflect no volume change. The hypotheses of von Mises and of normal stress do not result in changes of the wall thickness $\partial\,\Phi/\partial\,\sigma_{33} = 0$, cf. the Mohr-Coulomb hypothesis [73, 79] and Pisarenko-Lebedev hypothesis [157].

Sayir I (10). It is obvious that the influence of I_1 and I_3' cannot be separated by these measurements.

For rotational-symmetric models with $a_-^{\text{hyd}} \to \infty$ one obtains $\chi \geq 0$. For various materials the cross-sections of the surface Φ in the π-plane result in the part g – b – h of the $d-k$-diagram (Fig. 4, $d \geq 1$) yielding $\chi > 0$. From this it follows that the length and the diameter increase at torsion is more realistic, cf. [25, 168, 206]. This effect is significantly influenced by:

- defects in the material,
- material anisotropy,
- loading-induced anisotropy,
- technological characteristics,
- deviation of the specimen shape from the ideal geometry,
- non-coaxial fixation of the specimen in the testing machine,
- temperature changing during the test, etc.

This is the reason for different suggestions to describe such behavior in the literature. The ratios χ, $\varepsilon_{V\tau}$ and ν_τ^{in} are properties of the model.

If the torsion test is carried out with $\varepsilon_{11} = 0$ (strain is constrained), the axial force can be computed using the flow rule [172]. The sign of this force gives clues about the shape of the surface Φ.

6 Standard Criteria

The standard models (strain hypothesis, model of Mohr-Coulomb, model of Pisarenko-Lebedev and model of Burzyński-Yagn [157, 194, 234]) are frequently used models for first approximations of measurements: they are easy to handle, can be used to describe different material types (brittle-ductile range) and their parameters can be obtained using simple tests.

6.1 Strain Criterion

Strain model (strain hypothesis) is obtained assuming Hooke's law [20, 64, 205]

$$\sigma_{\mathrm{I}} - \nu_{+}^{\mathrm{in}} \left(\sigma_{\mathrm{II}} + \sigma_{\mathrm{III}}\right) - \sigma_{\mathrm{eq}} = 0. \tag{41}$$

The other two equations are obtained by cyclic permutation of indices. The model (10) together with the substitution (11) and the parameter values

$$c_3 = \frac{3^2}{2}, \qquad \gamma_1 = \frac{1}{3}\left(1 - 2\,\nu_{+}^{\mathrm{in}}\right). \tag{42}$$

gives rise to the representation in invariants.

The Poisson's ratio for the strain hypothesis follows, cf. [88, 201]

$$\nu_{-}^{\mathrm{in}} = \frac{1}{2}\,(d-1)\,, \qquad \nu_{+}^{\mathrm{in}} = \frac{1}{d}. \tag{43}$$

Further values are

$$d \geq 2, \qquad k = \frac{\sqrt{3}}{1+\nu_{+}^{\mathrm{in}}}, \qquad a_{+}^{\mathrm{hyd}} = \frac{1}{1-2\,\nu_{+}^{\mathrm{in}}}. \tag{44}$$

This model contains

- the normal stress hypothesis with $\nu_{+}^{\mathrm{in}} = 0$ (Sect. 2),
- the maximum strain hypothesis[4] (Mariotte [134], Navier [146], St. Venant [175], Poncelet [159], Grashof [77], Resal [170] or Bach [15]) with $\nu_{+}^{\mathrm{el}} = \nu_{+}^{\mathrm{in}}$.

The limit cases are the following surfaces Φ

- triangular prism in the principal stress space with $\nu_{-}^{\mathrm{in}} = \nu_{+}^{\mathrm{in}} = 1/2$, [8, 31, 66, 97, 174, 177, 192] and
- plane through point Z orthogonal to hydrostatic axis with $\nu_{+}^{\mathrm{in}} = -1$ [97, 102].

[4] This hypothesis is analyzed in [38, 65, 94, 220, 221]. It does not reflect the experimental results [22, 50, 78, 157, 213] and is used in combinations of various hypotheses (Sect. 11).

6.2 Mohr-Coulomb Criterion

The model is introduced on the basis of geometrical considerations [76, 127, 141–143]. It arises as equations, which are obtained by permutation of indices in

$$\left[\sigma_{\mathrm{I}} - \frac{1}{d}\,\sigma_{\mathrm{II}} - \sigma_{\mathrm{eq}}\right]\left[\sigma_{\mathrm{I}} - \frac{1}{d}\,\sigma_{\mathrm{III}} - \sigma_{\mathrm{eq}}\right]\left[\sigma_{\mathrm{II}} - \frac{1}{d}\,\sigma_{\mathrm{III}} - \sigma_{\mathrm{eq}}\right] = 0. \tag{45}$$

The formulation in invariants is given in Sect. 10.2. The model leads to values

$$\nu_{-}^{\mathrm{in}} = \frac{d}{2}, \qquad \nu_{+}^{\mathrm{in}} = \frac{1}{2\,d}, \qquad d \geq 1, \tag{46}$$

and [129]

$$k = \sqrt{3}\,\frac{d}{d+1}, \qquad a_{+}^{\mathrm{hyd}} = \frac{d}{d-1}. \tag{47}$$

This model yields (Fig. 5, SST)

- with $d \to \infty$ to the normal stress hypothesis and
- with $d = 1$ to the model of Tresca.

The relation $d \geq 2$ is recommended if computations involving so called fatigue limits should be performed [30].

6.3 Pisarenko-Lebedev Criterion

The model is presented by

$$(1-\xi)\sqrt{\frac{1}{2}\left[(\sigma_{\mathrm{I}} - \sigma_{\mathrm{II}})^2 + (\sigma_{\mathrm{II}} - \sigma_{\mathrm{III}})^2 + (\sigma_{\mathrm{III}} - \sigma_{\mathrm{I}})^2\right]} + \xi\, max[\sigma_{\mathrm{I}},\, \sigma_{\mathrm{II}},\, \sigma_{\mathrm{III}}] = \sigma_{\mathrm{eq}} \tag{48}$$

with $\xi \in [0,\ 1]$ [82, 120, 121, 156, 157]. This is a linear combination of the equivalent stresses after the normal stress hypothesis ($\xi = 1$) and the von Mises hypothesis ($\xi = 0$). The relations compute to [123]

$$d = \frac{1}{1-\xi}, \qquad k = \frac{3}{3 + \left(-3 + \sqrt{3}\right)\,\xi}, \qquad a_{+}^{\mathrm{hyd}} = \frac{1}{\xi}, \tag{49}$$

and the Poisson's ratio

$$\nu_{+}^{\mathrm{in}} = \frac{1-\xi}{2}, \qquad \nu_{-}^{\mathrm{in}} = \frac{1}{2} + \frac{\xi}{1-\xi}. \tag{50}$$

The model of Sdobirev [191] follows with $\xi = 1/2$. The relations are $d = 2$, $k = 3 - \sqrt{3} \approx 1.27$, $a_+^{\text{hyd}} = 2$, $\nu_+^{\text{in}} = 1/4$ and $\nu_-^{\text{in}} = 3/2$ (Fig. 5). The average values of the parameter ξ for some materials are given in [124].

6.4 Burzyński-Yagn Criterion

The rotationally symmetric model evolves the energy consideration and is a function of two parameters [16, 36, 37, 220]

$$3\, I_2' = \frac{\sigma_{\text{eq}} - \gamma_1\, I_1}{1 - \gamma_1} \frac{\sigma_{\text{eq}} - \gamma_2\, I_1}{1 - \gamma_2}. \tag{51}$$

The values k and d compute to

$$d = \frac{1}{1 - \gamma_1 - \gamma_2}, \qquad k^2 = \frac{1}{(1 - \gamma_1)(1 - \gamma_2)}. \tag{52}$$

The position of the hydrostatic nodes one gets from

$$\left(1 - 3\,\gamma_1\, a_+^{\text{hyd}}\right) \left(1 - 3\,\gamma_2\, a^{\text{hyd}}\right) = 0. \tag{53}$$

The Poisson's ratios at tension and compression are obtained using

$$\nu_+^{\text{in}} = \frac{-1 + 2\,(\gamma_1 + \gamma_2) - 3\,\gamma_1\,\gamma_2}{-2 + \gamma_1 + \gamma_2}, \tag{54}$$

and

$$\nu_-^{\text{in}} = -\frac{-1 + \gamma_1^2 + \gamma_2^2 - \gamma_1\,\gamma_2}{(-2 + \gamma_1 + \gamma_2)\,(-1 + \gamma_1 + \gamma_2)}. \tag{55}$$

The model (51) represents the general equation of a second order surface of revolution about the hydrostatic axis in the principal stress space. In dependence of the parameter values γ_1 and γ_2 one gets:

- cone of Drucker-Prager [56], Mirolyubov [138] (Fig. 6) with equal parameters $\gamma_1 = \gamma_2 \in [0,\ 1]$;
- paraboloid of Balandin [17], Burzyński-Torre [35–37, 207, 235] (Fig. 11) with $\gamma_1 \in [0,\ 1]$, $\gamma_2 = 0$;
- ellipsoid of Beltrami (strain energy hypothesis) [21], see Fig. 12, assuming $\gamma_1 = -\gamma_2 \in [0,\ 1]$ or with equal Poisson's ratios $\nu_-^{\text{in}} = \nu_+^{\text{in}} \in]-1,\ 1/2]$;
- ellipsoid of Schleicher [179, 180] with $\gamma_1 \in [0,\ 1]$, $\gamma_2 \in [-\infty,\ 0]$. The restriction (31) yields $\nu_-^{\text{in}} \in]-1,\ 1/2]$, $\nu_+^{\text{in}} \in [-1,\ 1/2]$;
- hyperboloid of Burzyński-Yagn [39, 221] with $\gamma_1 \in [0,\ 1]$ and $\gamma_2 \in [0,\ \gamma_1]$;

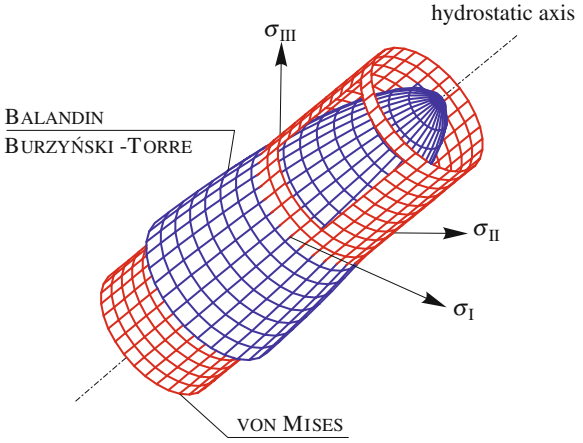

Fig. 11 Paraboloid of Balandin, Burzyński-Torre and the cylinder of von Mises in the principal stress space (the cylinder is cut for better understanding) [103]

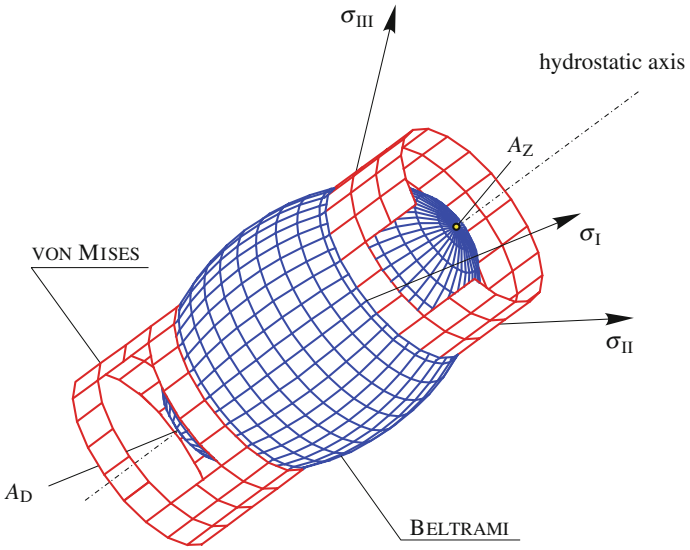

Fig. 12 Ellipsoid of Beltrami and cylinder of von Mises in the principal stress space (the cylinder is cut for better understanding) [103]

- hyperboloid of one sheet with complex conjugate γ_1 and γ_2 which is not convex (see Sect. 10.1); this model is used as partial surface in combined models (Sect. 11.2.1).

The models differ by the symmetry type in the π-plane (Fig. 4) and by the power of stresses n. The rotationally symmetric model (51) has the stress power $n = 2$. The strain hypothesis and the model of Pisarenko-Lebedev has the stress power $n = 3$

and the model of Mohr-Coulomb—$n = 6$. The last three models have a trigonal symmetry in the in the π-plane.

The models can be characterized by the shape of the meridian line. The strain hypothesis, the hypothesis of Mohr-Coulomb, the model of Pisarenko-Lebedev, the models of von Mises and of Drucker-Prager have a straight line as the meridian. The model (51) has additional to the straight line curvilinear meridians: parabola, hyperbola and ellipse.

The cross-sections of models (41) and (51) in the π-plane are unchangable. The form in the π-plane and the inclination of the meridian line of the models of Mohr-Coulomb and Pisarenko-Lebedev are controlled by a single parameter. This limits the capabilities of the models to be fitted to measured data.

There are no theoretical or experimental evidence known to support the application of models with a straight line as the meridian line. Models with further shapes of the meridian lines and independent from the shapes in the π-plane (Fig. 4) are required.

7 Mathematical Formulations

In the case of phenomenological models some mathematical framework is often applied for the formulation. The aim is to establish some general equation which includes classical models as special cases. The following three formulation ideas are known:

7.1 Criterion of Altenbach-Zolochevsky I

The criterion [7, 8]

$$\sigma_{\text{eq}} = \sqrt{3\,I_2'}\,(\lambda_1\,\sin\varphi + \lambda_2\,\cos\varphi + \lambda_3) + I_1\,(\lambda_4 + \lambda_5\,\sin\varphi + \lambda_6\,\cos\varphi) \tag{56}$$

is a combination of the first invariant of the stress tensor, the second invariant of the stress deviator and the stress angle.[5] Various special cases can be deduced by different settings of λ_i (Table 4). It should be mentioned that the systematization of models can be based on the number of these parameters.

In the formulation of this model the following relations between the principal stresses σ_{I}, σ_{II}, σ_{III} and the invariants (Appendix 15) [42, 43, 147, 149, 211, 233] are used:

[5] In the original papers the following definition of the stress angle is used

$$\sin 3\varphi = -\frac{3\sqrt{3}}{2}\frac{I_3'(\boldsymbol{s})}{I_2'(\boldsymbol{s})^{3/2}}, \qquad |\varphi| \le \frac{\pi}{6}.$$

Table 4 Settings of the criterion of Altenbach-Zolochevsky I (56)

Model	λ_1	λ_2	λ_3	λ_4	λ_5	λ_6	Reference /Equation
von Mises	0	1	0				(16)
Tresca	0	$\frac{2\sqrt{3}}{3}$		0			(13)
SH, $\nu_+^{\text{in}} = \frac{1}{2}$	$-\frac{1}{2}$	$\frac{\sqrt{3}}{2}$		0			(41)
SH, $\nu_+^{\text{in}} = \nu_+^{\text{el}}$	$-\frac{1+\nu_+^{\text{el}}}{3}$	$\left(1+\nu_+^{\text{el}}\right)\ \frac{\sqrt{3}}{3}$	0	$\frac{1-2\,\nu_+^{\text{el}}}{3}$	0		(41)
NSH	$-\frac{1}{3}$	$\frac{\sqrt{3}}{3}$	0	$\frac{1}{3}$	0		(8)
Sdobirev	$-\frac{1}{6}$	$\frac{\sqrt{3}}{6}$	$\frac{1}{2}$	$\frac{1}{6}$	0		(48)
Mohr-Coulomb	$\frac{1}{3}\left(\frac{1}{d}-1\right)$	$\frac{\sqrt{3}}{3}\left(\frac{1}{d}+1\right)$	0	$\frac{1}{3}\left(1-\frac{1}{d}\right)$	0		(45)
Drucker-Prager	0	$\frac{1}{2}\left(1+\frac{1}{d}\right)$		$\frac{1}{2}\left(1-\frac{1}{d}\right)$	0		(51)
Pisarenko-Lebedev	$\frac{1}{3}\left(\frac{1}{d}-1\right)$	$\frac{\sqrt{3}}{3}\left(1-\frac{1}{d}\right)$	$\frac{1}{d}$	$\frac{1}{3}\left(1-\frac{1}{d}\right)$	0		(48)
Sandel	0	$\frac{\sqrt{3}}{3}\left(1+\frac{1}{d}\right)$	0	$\frac{1}{2}\left(1-\frac{1}{d}\right)$	0		(58)
Edelman-Drucker	0	$\frac{2\sqrt{3}}{3}\ (1-\chi)$	χ		0		(59)
Tsvelodub	λ_1	λ_2	λ_3		0		[211]
Paul	$\frac{1}{3}\ (2\,a_2 - a_1 - a_3)$	$\frac{\sqrt{3}}{3}\ (a_1 - a_3)$	0	$\frac{1}{3}\ (a_1 + a_2 + a_3)$	0		(60)
Birger	$\frac{1}{3}\ (2\,a_2 - a_1 - a_3)$	$\frac{\sqrt{3}}{3}\ (a_1 - a_3)$	a_4	$\frac{1}{3}\ (a_1 + a_2 + a_3)$	0		(61)
Tarasenko	0	λ_2	0	λ_4	λ_5	λ_6	[201]

$$\begin{aligned}
\sigma_{\mathrm{I}} &= \frac{1}{3}\left[2\sqrt{3\,I_2'}\,\sin\left(\varphi+\frac{2\,\pi}{3}\right)+I_1\right],\\
\sigma_{\mathrm{II}} &= \frac{1}{3}\left[2\sqrt{3\,I_2'}\,\sin(\varphi)+I_1\right],\\
\sigma_{\mathrm{III}} &= \frac{1}{3}\left[2\sqrt{3\,I_2'}\,\sin\left(\varphi+\frac{4\,\pi}{3}\right)+I_1\right],
\end{aligned} \tag{57}$$

and $\sigma_{\mathrm{I}} \geq \sigma_{\mathrm{II}} \geq \sigma_{\mathrm{III}}$ is assumed.

This model includes not only the standard models (Sect. 6). The following models can be obtained:

- criterion of Sandel [176]

$$\sigma_{\mathrm{eq}} = \sigma_{\mathrm{I}} + \frac{1}{2}\left(1-\frac{1}{d}\right)\sigma_{\mathrm{II}} - \frac{1}{d}\,\sigma_{\mathrm{III}}, \tag{58}$$

- convex combination of von Mises and Tresca models after Edelman-Drucker, Koval'chuk [57, 117]

$$\chi\,\sqrt{3\,I_2'} + (1-\chi)\,(\sigma_{\mathrm{I}} - \sigma_{\mathrm{III}}) = \sigma_{\mathrm{eq}}, \qquad \chi \in [0,\,1], \tag{59}$$

- criterion of Paul [154]

$$a_1\,\sigma_{\mathrm{I}} + a_2\,\sigma_{\mathrm{II}} + a_3\,\sigma_{\mathrm{III}} = \sigma_{\mathrm{eq}}, \tag{60}$$

- criterion of Birger [30]

$$a_1\,\sigma_{\mathrm{I}} + a_2\,\sigma_{\mathrm{II}} + a_3\,\sigma_{\mathrm{III}} + a_4\,\sqrt{3\,I_2'} = \sigma_{\mathrm{eq}}. \tag{61}$$

A disadvantage of this model is the number of parameters, which should be identified by six independent tests.

7.2 Model in Terms of the Integrity Basis

This model results from the invariants I_1, $\left(I_2'\right)^{1/2}$ and I_3', cf. [23, 24, 51, 188]. The basic idea is the formulation of scalar valued functions of a given order:

$$\begin{aligned}
S_1 &= a_1\,I_1 + b_1\,\left(I_2'\right)^{1/2},\\
S_2 &= a_2\,I_1^2 + b_2\,I_2',\\
S_3 &= a_3\,I_1^3 + b_3\,\left(I_2'\right)^{3/2} + c_3\,I_3 + d_3\,I_1\,I_2 + e_3\,I_1^2\,\left(I_2'\right)^{1/2},\\
&\ldots
\end{aligned} \tag{62}$$

The sum of the S_i with the same power n yields

$$(S_1)^n + (S_2)^{n/2} + (S_3)^{n/3} + \ldots = \sigma_{\text{eq}}^n. \tag{63}$$

The choice of integer exponents n/i is recommended for the terms S_i. In [103] the following exponents are suggested

$$n = 1,\ 2,\ 3,\ 6,\ 9 \text{ and } 12. \tag{64}$$

The model of Altenbach-Zolochevsky II follows with $n = 1$ for S_1, S_2 and S_3 [2, 8, 103]. The parameters of the model are related to the scaling (3). The advantage of this model is that the equivalent stress σ_{eq} can be expressed explicitly.

Another modification one gets if the weight σ_{eq}^{n-i} for S_i is introduced

$$\sigma_{\text{eq}}^{n-1}\, S_1 + \sigma_{\text{eq}}^{n-2}\, S_2 + \sigma_{\text{eq}}^{n-3}\, S_3 + \ldots + \sigma_{\text{eq}}\, S_{n-1} + S_n = \sigma_{\text{eq}}^n. \tag{65}$$

By this way we get the same power of the stresses in each term [103]. The exponent $n > 1$ and the terms in (65) can be selected in such a manner that an analytical solution is possible with respect to σ_{eq}. Equation (51) is an example of a quadratic equation, models which are given cubic, bi-cubic and tri-quadratic equations are

$$S_1\, \sigma_{\text{eq}}^2 + S_2\, \sigma_{\text{eq}} + S_3 = \sigma_{\text{eq}}^3, \tag{66}$$

$$S_2\, \sigma_{\text{eq}}^4 + S_4\, \sigma_{\text{eq}}^2 + S_6 = \sigma_{\text{eq}}^6, \tag{67}$$

$$S_3\, \sigma_{\text{eq}}^3 + S_6 = \sigma_{\text{eq}}^6. \tag{68}$$

More examples are presented in [103]. Disadvantages of this approach can be summarized as follows:

- increasing number of parameters,
- difficult convexity limits for the parameters and
- missing geometrical interpretation of the parameters.

7.3 Models Based on the Stress Deviator

The functions of the invariants of the stress deviator can be defined as follows

$$\begin{aligned} S_2' &= b_2\, I_2', \\ S_3' &= b_3\, \left(I_2'\right)^{3/2} + c_3\, I_3, \\ S_4' &= b_4\, \left(I_2'\right)^2 + f_4\, \left(I_2'\right)^{1/2}\, I_3, \\ &\ldots \end{aligned} \tag{69}$$

The sum of S_i' with the same power results in

$$\left(S_2'\right)^{n/2} + \left(S_3'\right)^{n/3} + \left(S_4'\right)^{n/4} + \ldots = \sigma_{\mathrm{eq}}^n \tag{70}$$

and

$$\sigma_{\mathrm{eq}}^{n-2}\, S_2' + \sigma_{\mathrm{eq}}^{n-3}\, S_3' + \ldots + \sigma_{\mathrm{eq}}\, S_{n-1}' + S_n' = \sigma_{\mathrm{eq}}^n, \tag{71}$$

cf. Eqs. (63) and (65). Another possibility is [106]

$$\sigma_{\mathrm{eq}}^{n-2\,m_2}\, \left(S_2'\right)^{m_2} + \sigma_{\mathrm{eq}}^{n-3\,m_3}\, \left(S_3'\right)^{m_3} + \ldots + \sigma_{\mathrm{eq}}\, \left(S_{n-1}'\right) + \left(S_n'\right) = \sigma_{\mathrm{eq}}^n. \tag{72}$$

The formulations (70), (71) and (72) yield in the models of incompressible material behavior (Sect. 9): Sayir I, Drucker I, Dodd-Naruse, TQM, BCM, Spitzig, Iyer, Freudenthal [16, 68, 90] and Maitra [131, 226].

Multiplicative combinations of various S_i' are possible, for example,

$$\left(S_2'\right)^{(n-j)/2}\, S_j' = \sigma_{\mathrm{eq}}^n. \tag{73}$$

This equation results in the geometrical-mechanical model (Sect. 9.1.6).

The formulation of the models with the deviatoric basis (69) should be preferred since they are simpler in comparison with models on the basis of Eq. (62). The compressible generalization can be performed using the substitution presented in Sect. 10.1. In the case of rational functions of I_3' (functions of I_3' with integer power) one gets convex shapes in the π-plane.

8 Visualization Methods

Several possibilities of the visualization of the limit surface Φ are presented in the literature. In this section main approaches are briefly discussed and examples are given.

8.1 Spatial Representation of the Limit Surface

Strength hypotheses and flow criteria can be represented in the principal stress space (σ_{I}, σ_{II}, σ_{III}) [43, 219, 234], which is also known as the Haigh-Westergaard space [80, 218]. By means of an orthogonal transform the decomposition of the stress tensor in the hydrostatic and deviatoric components can be carried out. For this purpose the coordinates (ξ_1, ξ_2, ξ_3) are introduced (Fig. 13), which are related to the coordinates (σ_{I}, σ_{II}, σ_{III}) as follows [23, 123, 186, 187, 210]:

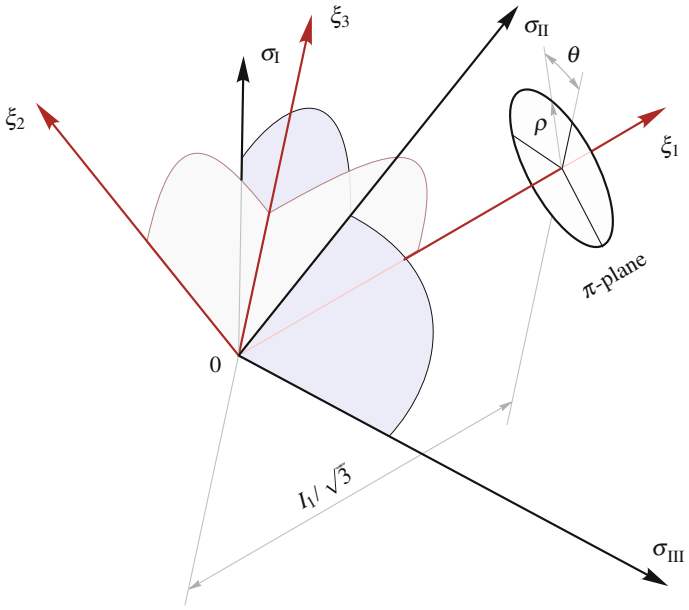

Fig. 13 Principal stress space (σ_{I}, σ_{II}, σ_{III}), coordinates (ξ_1, ξ_2, ξ_3) and (ξ_1, ρ, θ)

$$\begin{pmatrix} \sigma_{\mathrm{I}} \\ \sigma_{\mathrm{II}} \\ \sigma_{\mathrm{III}} \end{pmatrix} = \begin{pmatrix} \frac{1}{\sqrt{3}} & \frac{1}{\sqrt{2}} & -\frac{1}{\sqrt{6}} \\ \frac{1}{\sqrt{3}} & 0 & \frac{2}{\sqrt{6}} \\ \frac{1}{\sqrt{3}} & -\frac{1}{\sqrt{2}} & -\frac{1}{\sqrt{6}} \end{pmatrix} \begin{pmatrix} \xi_1 \\ \xi_2 \\ \xi_3 \end{pmatrix}. \tag{74}$$

In these coordinates

$$\xi_1 = \frac{1}{\sqrt{3}} (\sigma_{\mathrm{I}} + \sigma_{\mathrm{II}} + \sigma_{\mathrm{III}}) = \frac{1}{\sqrt{3}} I_1 \tag{75}$$

is the hydrostatic axis ($\sigma_{\mathrm{I}} = \sigma_{\mathrm{II}} = \sigma_{\mathrm{III}}$). The axis

$$\xi_3 = \frac{1}{\sqrt{6}} (-\sigma_{\mathrm{I}} + 2\,\sigma_{\mathrm{II}} - \sigma_{\mathrm{III}}) \tag{76}$$

lies in the plane $\xi_1 - \sigma_{\mathrm{II}}$. The axis

$$\xi_2 = \frac{1}{\sqrt{2}} (\sigma_{\mathrm{I}} - \sigma_{\mathrm{III}}) \tag{77}$$

constitutes together with the axes ξ_1 and ξ_3 an orthogonal coordinate system (Fig. 13).

The surface Φ can be formulated in cylindrical coordinates or the Haigh-Westergaard coordinates $(\xi_1,\ \rho,\ \theta)$ [234]. The value of the radius ρ is computed to [23, 43]

$$\rho = \sqrt{2\, I_2'} = \sqrt{\xi_2^2 + \xi_3^2} \tag{78}$$

and represents a function of the second invariant of the stress deviator. The angle θ is given by Eq. (224).

The representation of the surface Φ in the principal stress space $(\sigma_{\mathrm{I}},\ \sigma_{\mathrm{II}},\ \sigma_{\mathrm{III}})$ is widely used because of its simplicity and clearness. For the analysis of the surface properties the Haigh-Westergaard space with the coordinates $(\xi_1,\ \xi_2,\ \xi_3)$ is better. Such a surface can be characterized by two projections:

- the meridian cross section $(\xi_1,\ \xi_3)$ and
- the planes with the cuts $\xi_1 = \text{const.}$ (π-plane with the coordinates $(\xi_2,\ \xi_3)$).

8.2 Burzyński-Plane

Instead of the meridian cross section $(\xi_1,\ \xi_3)$ the Burzyński-plane is often used. The Burzyński-plane is introduced for the rotationally symmetric models [35, 39]

$$\Phi\left(I_1,\ I_2',\ \sigma_{\mathrm{eq}}\right) = 0. \tag{79}$$

For these models the surface is represented by a line in the upper half-plane in the diagram $(\xi_1,\ \rho)$ (Fig. 14, model of von Mises).

The whole surface Φ is obtained by the rotation of this line about the axis ξ_1 [234]. For a better clearness the coordinates $\left(I_1,\ \sqrt{3\, I_2'}\right)$ are used [103]. This scaling is due to the relation

$$I_1^2 = 3\, I_2' \tag{80}$$

at tension and compression. It simplifies the comparison of the presented models with the model of von Mises (16) and leads to a geometrical interpretation of the relations (Table 1). Other scalings are used in [86, 95, 101, 133, 155, 174, 181, 194, 231, 234]. A normalization of axes with respect to the tensile stress

$$\left(\frac{I_1}{\sigma_+},\ \frac{\sqrt{3\, I_2'}}{\sigma_+}\right)$$

can be applied in order to compare the shape of the surfaces for different materials [105, 113].

The surface Φ (5) or (6) can be presented in the Burzyński-plane by the meridians defined using the stress angle [136, 145, 155]

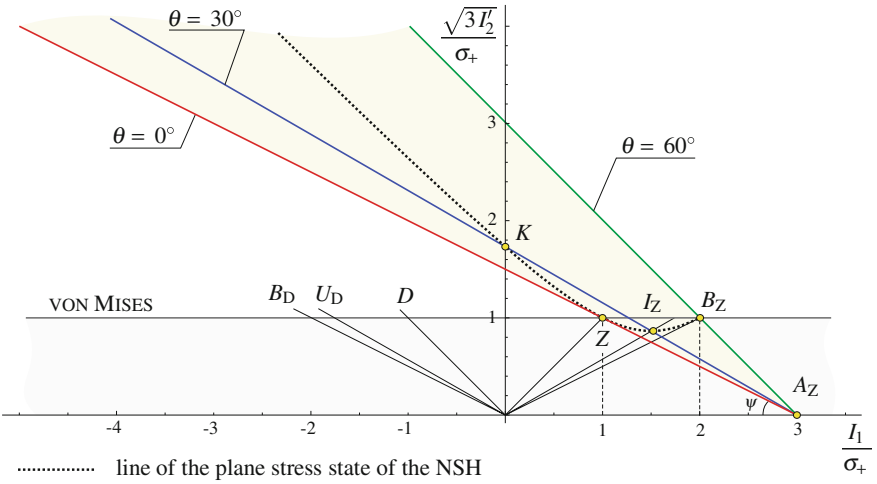

Fig. 14 Normal stress hypothesis (NSH) and the model of von Mises in the Burzyński-plane [105]. The inclination of the tangent line at the point Z (tension) of the surface Φ is $\psi = \arctan 1/2 \approx 27.56°$, cf. (Fig. 7)

- $\theta = 0 \Rightarrow I_3' = \dfrac{2\sqrt{3}}{3^2}\,(I_2')^{3/2}$,
- $\theta = \dfrac{\pi}{6} \Rightarrow I_3' = 0$,
- $\theta = \dfrac{\pi}{3} \Rightarrow I_3' = -\dfrac{2\sqrt{3}}{3^2}\,(I_2')^{3/2}$.

These meridians for the normal stress hypothesis (8) are shown in Fig. 14.

The three meridians are enough to display the most important properties (Table 1). The line of the plane stress state, which results from

$$\sigma_{\mathrm{I}}\,\sigma_{\mathrm{II}}\,\sigma_{\mathrm{III}} = 0, \tag{81}$$

is obtained in this diagram using the substitution [103]

$$I_3' = \frac{1}{3}\,I_1\,I_2' - \frac{1}{3^3}\,I_1^3. \tag{82}$$

This line contains the points B_{D}, U_{D}, D, K, Z, I_{Z} and B_{Z} (Figs. 15 and 16) and it is convex for axisymmetric models only, e. g. the model of Burzyński-Yagn (51), Fig. 17.

The introduced representation allows to show all the measurements on their respective meridians. Different extrapolations of the measurements to the point A_{Z} (hydrostatic tension) with the relation

$$a_+^{\text{hyd}} > \frac{1}{3} \quad \text{or} \quad \nu_+^{\text{in}} \in \left[-1, \frac{1}{2} \right]$$

can be easily evaluated.

8.3 π-Plane

The cross-section of the surface Φ with the cut $\xi_1 = \text{const.}$ (Fig. 13) is denoted as the π-plane [12, 43, 167, 234]. For incompressible material behavior these cross-sections do not depend on the coordinate ξ_1. For a compressible material it is important to consider the cross-sections, which contain certain points of the plane stress state for the most important loading cases, e. g.:

- point Z (tension): $\xi_1 = \dfrac{1}{\sqrt{3}}\,\sigma_{\text{eq}}$,
- point K (torsion): $\xi_1 = 0$ and
- point D (compression): $\xi_1 = -\dfrac{1}{\sqrt{3}}\,d\,\sigma_{\text{eq}}$.

The line of the plane stress state defined, for instance, by the condition $\sigma_{\text{III}} = 0$ can be projected onto the π-plane. The projection is given by the equality, see (74),

$$\xi_1 = \frac{1}{\sqrt{2}}\,(\sqrt{3}\,\xi_2 + \xi_3), \tag{83}$$

which must be substituted into the equation of the surface Φ.

In the most general case the surface Φ has a trigonal symmetry in the π-plane (Fig. 4). If only even powers of the third invariant of deviators are present, then the model has a hexagonal symmetry (e. g. models of Tresca and Schmidt-Ishlinsky, Fig. 4). The absence of the third invariant leads to a rotationally symmetric surface, e. g. Eq. (51) [105].

9 Pressure-Insensitive Criteria

In this section the most important models with the property

$$\nu_+^{\text{in}} = \nu_-^{\text{in}} = \frac{1}{2} \tag{84}$$

are discussed. These models are of the form

$$\Phi(I_2',\ I_3',\ \sigma_{\text{eq}}) = 0 \tag{85}$$

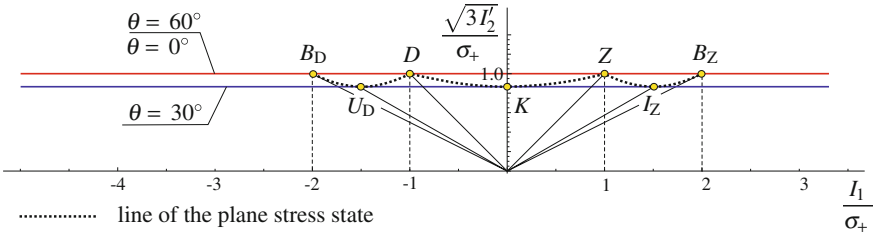

Fig. 15 Model of Tresca in the Burzyński-plane [103]

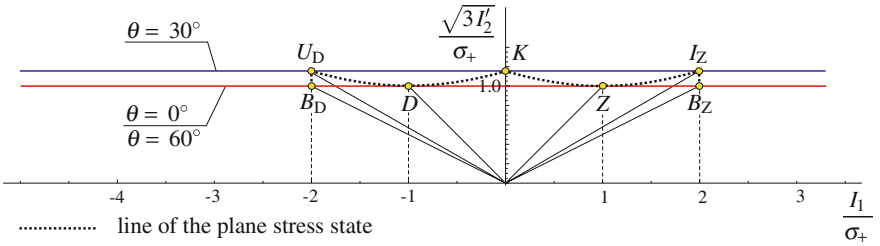

Fig. 16 Model of Schmidt-Ishlinsky in the Burzyński-plane

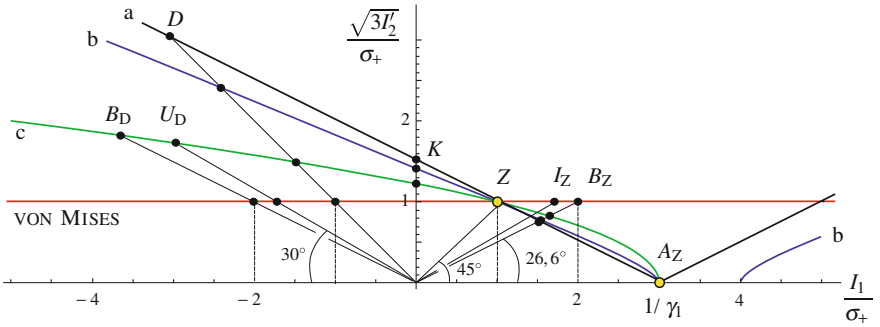

Fig. 17 Quadratic rotationally symmetric models (51) with the hydrostatic node A_Z ($\gamma_1 = 1/3$) in the Burzyński-plane [105]: *a* cone of Drucker-Prager: $\gamma_2 = 1/3$, $\nu_-^{\text{in}} = 2$, $\nu_+^{\text{in}} = 0$, $d = 3$, $k = 3/2$; *b* hyperboloid of Burzyński-Yagn: $\gamma_2 = 1/4$, $\nu_-^{\text{in}} = 1.54$, $\nu_+^{\text{in}} = 0.06$, $d = 2.4$, $k = 1.41$; *c* paraboloid of Balandin: $\gamma_2 = 0$, $\nu_-^{\text{in}} = 0.8$, $\nu_+^{\text{in}} = 0.2$, $d = 3/2$, $k = 1.22$

or

$$\Phi(I_2', \theta, \sigma_{\text{eq}}) = 0, \tag{86}$$

and hence are cylindric or prismatic surfaces aligned along the hydrostatic axis. They do not restrict the hydrostatic stresses. These models can only be used in the region $I_1 \leq 0$ in combined models (Sect. 11), cf. [139].

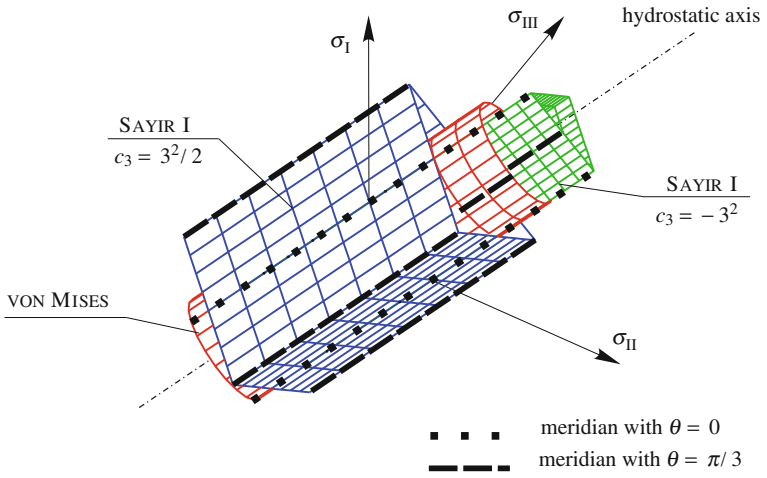

Fig. 18 *Triangular prisms* of Sayir I (87) with the limit convexity values of the parameter $c_3 \in \left[-3^2,\ 3^2/2\right]$ and the cylinder of von Mises (16) in the principal stress space [103]

9.1 Yield Surfaces with Trigonal Symmetry

Theoretical considerations allow conclusions about the symmetry of the yield surface Φ in the π-plane only. This surface shows trigonal, hexagonal or rotational symmetry. No suggestions can be made based on microstructure. The material behavior is described by neglecting the real structure with its microscopic defects and inhomogeneity. The effects of material behavior could be captured correctly only in average [8].

9.1.1 Model of Sayir I

The cylinder of Sayir I [178] is defined as follows

$$\frac{\sigma_{\mathrm{eq}}\, 3\, I_2' + c_3\, I_3'}{1 + 2\, c_3/3^3} = \sigma_{\mathrm{eq}}^3, \qquad c_3 \in \left[-3^2,\ \frac{3^2}{2}\right]. \tag{87}$$

The model has the structure of the reduced cubic equation with respect to σ_{eq}. For $c_3 = 0$ the cylinder of von Mises arises (Fig. 18). The relations k and d compute to

$$k^2 = 1 + \frac{2}{3^3}\, c_3, \qquad d = \frac{3^3 + 2\, c_3 - \sqrt{3\,(3^2 - 2\, c_3)\,(3^3 + 2\, c_3)}}{2^2\, c_3} \tag{88}$$

and shown in Fig. 4.

9.1.2 Model of Sayir II

The hexagonal prism of Sayir II [178] is defined by

$$\sigma_{\mathrm{I}} - \frac{1}{1+b_1}\,(b_1\,\sigma_{\mathrm{II}} + \sigma_{\mathrm{III}}) - \sigma_{\mathrm{eq}} = 0, \qquad b_1 \in \left[-\frac{1}{2},\ 1\right]. \tag{89}$$

Further equations result from the cyclic permutations of indices. The model is formulated in the deviatoric invariants

$$\begin{aligned}\Phi_{\mathrm{SAY}} = {} & \alpha_{41}\,\sigma_{\mathrm{eq}}^4\,I_2' + \alpha_{31}\,\sigma_{\mathrm{eq}}^3\,I_3' + \alpha_{21}\,\sigma_{\mathrm{eq}}^2\,(I_2')^2 \\ & + \alpha_{11}\,\sigma_{\mathrm{eq}}\,I_2'\,I_3' + \beta_{21}\,(I_2')^3 + \beta_{31}\,(I_3')^2 - \sigma_{\mathrm{eq}}^6\end{aligned} \tag{90}$$

with

$$\begin{aligned}\alpha_{41} &= \frac{2\cdot 3\,(1+b_1+b_1^2)}{(1+b_1)^2}, & \alpha_{31} &= \frac{3^3\,b_1}{(1+b_1)^2}, \\ \alpha_{21} &= -3^2\,\frac{(1+b_1+b_1^2)^2}{(1+b_1)^4}, & \alpha_{11} &= -3^4\,b_1\,\frac{1+b_1+b_1^2}{(1+b_1)^4}, \\ \beta_{21} &= \frac{(-1+b_1)^2\,(2+b_1)^2\,(1+2b_1)^2}{(1+b_1)^6}, & \beta_{31} &= -\frac{3^3\,(1+b_1+b_1^2)^3}{(1+b_1)^6}.\end{aligned} \tag{91}$$

For $b_1 = 0$ the model of Tresca (15) arises (Figs. 1, 15). With $b_1 = -1/2$ and $b_1 = 1$ the model corresponds to the limit convexity cases of the model of Sayir I (87).

The relations are

$$k = \sqrt{3}\,\frac{1+b_1}{2+b_1}, \qquad d = 1 + b_1. \tag{92}$$

The model is representing the lower bound of the convexity region in the $d-k$-diagram (Fig. 4). For the model of Sayir II the point, which has the shortest distance to the point $M(1,\ 1)$ can be obtained from the equation

$$(d-1)^2 + (k-1)^2 \to \min., \tag{93}$$

which results in $b_1 \approx 0.0471$, $d \approx 1.05$ and $k \approx 0.89$.

9.1.3 Model of Haythornthwaite

The model of Haythornthwaite [40, 83, 107] consists of two overlapping triangles in the π-plane described with the model (87) with $c_3 = -3^2$ and $c_3 = 3^2/2$

$$\left[\frac{(2\,d\,\sigma_{\rm eq})\,3\,I_2' + (-3^2)\,I_3'}{1+2\,(-3^2)/3^3} - (2\,d\,\sigma_{\rm eq})^3\right]\left[\frac{\sigma_{\rm eq}\,3\,I_2' + (3^2/2)\,I_3'}{1+2\,(3^2/2)/3^3} - \sigma_{\rm eq}^3\right] = 0. \tag{94}$$

It is separated in two regions in the $d-k$ diagram (Fig. 4)

$$Haythornthwaite\,I: \quad k = \frac{2}{\sqrt{3}} \qquad \text{for} \quad d \in [1,\,2], \tag{95}$$

$$Haythornthwaite\,II: \quad k = \frac{2d}{\sqrt{3}} \qquad \text{for} \quad d \in \left[\frac{1}{2},\,1\right]. \tag{96}$$

The model is representing the upper bound of the convexity region of the $d-k$-diagram. The boundaries, where $d = 1/2$ and $d = 2$, correspond to the limit convexity cases of the models of Sayir I and Sayir II. For $d = 1$ the model of Schmidt-Ishlinsky (18) arises (Figs. 1, 16). The point, which has the shortest distance to the point $M(1,\,1)$ (Fig. 4), can be obtained from Eq. (93). This results in $d = (3+2\sqrt{3})/7 \approx 0.9234$ and $k \approx 1.07$.

9.1.4 Convex π-Plane Model

The model of Haythornthwaite (94)

$$\begin{aligned}\Phi_{\rm HAY} = {} & \frac{3^6}{2^6}\frac{1}{d^3}\,(I_3')^2 - \frac{3^5}{2^5}\frac{d-1}{d^3}\,I_2'\,I_3'\,\sigma_{\rm eq} - \frac{3^4}{2^4}\frac{1}{d^2}\,(I_2')^2\,\sigma_{\rm eq}^2 \\ & - \frac{3^3}{2^3}\frac{1-d^3}{d^3}\,I_3'\,\sigma_{\rm eq}^3 + \frac{3^2}{2^2}\frac{1+d^2}{d^2}\,I_2'\,\sigma_{\rm eq}^4 - \sigma_{\rm eq}^6\end{aligned} \tag{97}$$

and the model of Sayir II (90) with the parameters

$$\begin{aligned}\alpha_{41} &= 6\,\frac{(d-1)^2+d}{d^2}, & \alpha_{31} &= 3^3\,\frac{d-1}{d^2}, \\ \alpha_{21} &= -3^2\,\frac{\left((d-1)^2+d\right)^2}{d^4}, & \alpha_{11} &= -3^4\,\frac{(d-1)\,\left((d-1)^2+d\right)}{d^4}, \\ \beta_{21} &= \frac{(1-2\,d)^2\,(d-2)^2\,(1+d)^2}{d^6}, & \beta_{31} &= -3^3\,\frac{\left((d-1)^2+d\right)^3}{d^6}\end{aligned} \tag{98}$$

are functions of $d \in [1/2,\,2]$. With the linear combination [33]

$$\Phi_6 = \xi\,\Phi_{\rm HAY} + (1-\xi)\,\Phi_{\rm SAY}, \qquad \xi \in [0,\,1] \tag{99}$$

one obtains the model with the power of stress $n = 6$ in each term. The resulting model describes with two parameters $(d,\,\xi)$ all points in the $d-k$-diagram (Fig. 4) with a convex form in the π-plane. A drawback is that an explicit solution of (99) with respect to $\sigma_{\rm eq}$ is not possible.

The model contains as special cases:

- the model of hexagonal symmetry in the π-plane with $d = 1$ (bicubic model, Sect. 9.2),
- the value $k = 1$ of the model of von Mises results with $d = 1$ in the parameter $\xi = \frac{2^6}{7 \cdot 13} \approx 0.7033$ and
- the approximation of the model of Sayir I (87) with $\xi = \frac{2^6}{7 \cdot 13}$ and $\xi \in [0,\ 1]$.

9.1.5 Radcig Model

The Radcig model[6] consists of two overlapping hexagonal prisms of Sayir II (89) [105, 115]. It is deduced from the Unified Yield Criterion of Yu (Sect. 9.2.1). The defining equations are:

$$\begin{cases} \sigma_{\mathrm{I}} - \dfrac{1}{1+b_1}(b_1\,\sigma_{\mathrm{II}} + \sigma_{\mathrm{III}}) - \sigma_{\mathrm{eq}} = 0, \\ \sigma_{\mathrm{I}} - \dfrac{1}{1+b_2}(b_2\,\sigma_{\mathrm{II}} + \sigma_{\mathrm{III}}) + \eta\,\sigma_{\mathrm{eq}} = 0. \end{cases} \tag{100}$$

Further equations are obtained by cyclic permutations of indices. The cross-section of this model in the π-plane is a dodecagon (twelve-sided figure). The parameters are bounded as follows

$$b_1 \in \left[-\frac{1}{2},\ 1\right], \qquad b_2 \in \left[-\frac{1}{2},\ 1\right], \qquad \eta \in \left[\frac{1}{1+b_2},\ 2\right]. \tag{101}$$

The model (100) can be formulated in invariants of the deviator [105]:

$$\begin{aligned} &\big(\alpha_{41}\,\sigma_{\mathrm{eq}}^4\,I_2' + \alpha_{31}\,\sigma_{\mathrm{eq}}^3\,I_3' + \alpha_{21}\sigma_{\mathrm{eq}}^2\,(I_2')^2 \\ &\qquad + \alpha_{11}\sigma_{\mathrm{eq}}\,I_2'\,I_3' + \beta_{21}\,(I_2')^3 + \beta_{31}\,(I_3')^2 - \sigma_{\mathrm{eq}}^6\big)\times \\ &\big[\alpha_{42}\,(\eta\,\sigma_{\mathrm{eq}})^4\,I_2' - \alpha_{32}\,(\eta\,\sigma_{\mathrm{eq}})^3\,I_3' + \alpha_{22}\,(\eta\,\sigma_{\mathrm{eq}})^2\,(I_2')^2 \\ &\qquad - \alpha_{12}\,(\eta\,\sigma_{\mathrm{eq}})\,I_2'\,I_3' + \beta_{22}\,(I_2')^3 + \beta_{32}\,(I_3')^2 - (\eta\,\sigma_{\mathrm{eq}})^6\big] = 0. \end{aligned} \tag{102}$$

This allows a representation of the model in the Burzyński-plane. The first part corresponds to the model of Sayir II (90) with parameters which are given by (91). The parameters of the second part are computed using the substitution b_2 by b_1. The Radcig model contains the following models:

- the model of Sayir II with $b_1 \in [-1/2,\ 1]$, $\eta = 2$ and for arbitrary $b_2 \in [-1/2,\ 1]$ or $b_1 = \eta - 1$, $b_2 = (1-\eta)/\eta$ and $\eta \in [1/2,\ 2]$ with the relations (92),
- the model of Haythornthwaite with $b_1 = 1$, $b_2 = 1$ and $\eta \in [1/2,\ 2]$ with relations (95) and (96),

[6] This model is dedicated to Jurij Antonovič Radcig (1900–1976), who was a professor at the Kazan State University of Technology (KAI), Kazan, Russia.

- the continuous approximation of the model of Sayir I with $\eta \in [1/2,\ 2]$ and

$$\begin{aligned} b_1 &= (1-\sqrt{3})\,\eta^2 + \frac{1}{2}\left(5\sqrt{3}-3\right)\eta - \sqrt{3}, \\ b_2 &= (2-\sqrt{3})\,\eta^2 + \left(\frac{5}{2}\sqrt{3}-6\right)\eta + \left(\frac{7}{2}-\sqrt{3}\right). \end{aligned} \tag{103}$$

- the UYC of Yu with $\eta = 1$ and $b = b_1 = b_2 \in [0,\ 1]$ (Sect. 9.2) with

$$k = \sqrt{3}\,\frac{1+b_1}{2+b_1}, \qquad d = 1. \tag{104}$$

Further discussion of the Radcig-model can be found in the Sect. 10.2.

9.1.6 Geometrical-Mechanical Model

This model is a function of the stress angle θ (224) [6, 33, 107]

$$(3\,I_2')^{\frac{n}{2}}\,\frac{1+c_3\cos 3\theta + c_6\cos^2 3\theta}{1+c_3+c_6} = \sigma_{\mathrm{eq}}^n. \tag{105}$$

The main idea is to include the influence of the odd and the even functions of I_3' separately and to give a geometrical meaning to the parameters with respect to the mechanical properties. Computation of the equivalent stress σ_{eq} can be performed directly.

The two parameters c_3 and c_6 determine the geometry of the model in the π-plane. With $c_3 = 0$ a model with hexagonal symmetry is obtained: there is no difference between tension and compression ($d = 1$). With $c_3 = c_6 = 0$ one gets the model of von Mises.

The values d and k compute to

$$d^n = \frac{1+c_3+c_6}{1-c_3+c_6}, \qquad k^n = 1+c_3+c_6. \tag{106}$$

This leads to the two inequalities

$$1-c_3+c_6 > 0, \qquad 1+c_3+c_6 \geq 0. \tag{107}$$

The recommended values for the exponent are $n = 2, 3$ and 6. The exponent $n = 2$ is suitable, if the modeling with rational compressible substitution (Sect. 10.1) involves energy considerations [212]. The values $n = 2$ and 3 allow to solve the equation given by (105) with respect to σ_{eq} analytically even if the rational compressible substitution (Sect. 10.1) is introduced. The convexity region of the geometrical-mechanical model (105) in the parameter space $c_3 - c_6$ is shown in Figs. 19 and 20).

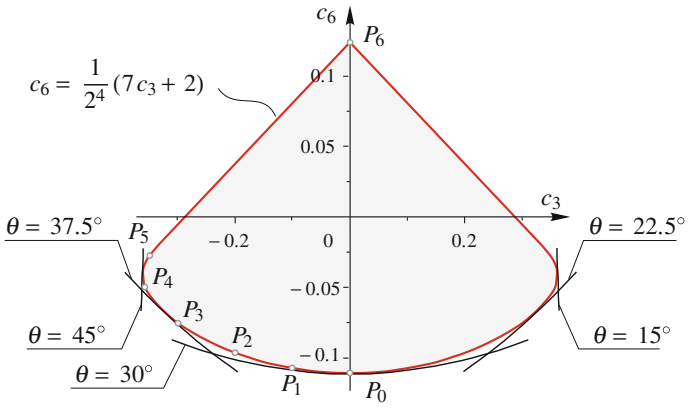

Fig. 19 Convexity region of the geometrical-mechanical model (105) with $n = 2$: with θ some curves are marked, which build the boundary of the convexity region, Coordinates at the points $P_0(0, -1/9)$, $P_1(-0.1, -0.1086)$, $P_2(-0.2, -0.1011)$, $P_3(-0.3, -0.0886)$, $P_4(-0.3560, -0.05)$, $P_5(-0.3478, -0.02717)$, $P_6(0, 1/2^3)$

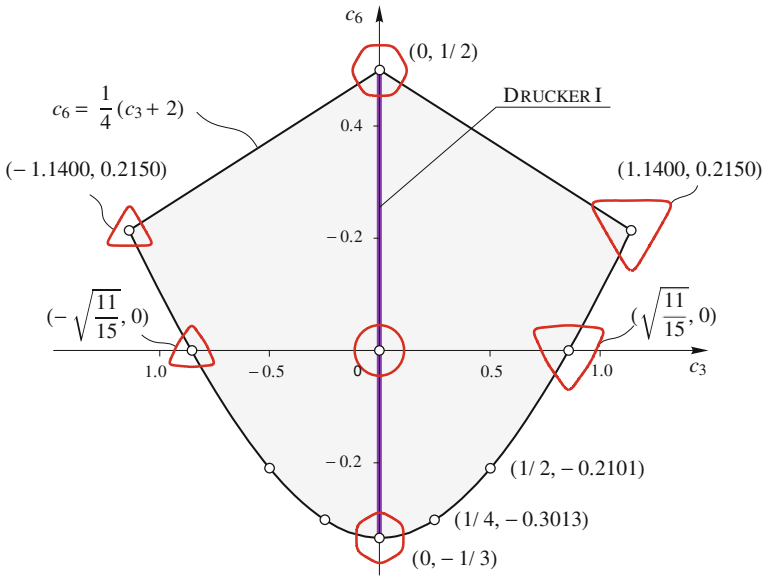

Fig. 20 Convexity region of the geometrical-mechanical model (105) with $n = 6$ (the cross-sections in the π-plane are shown for clarity)

With the exponent $n = 6$ a model is obtained, which has the largest convexity region in the $d-k$-diagram (Figs. 4 and 21).

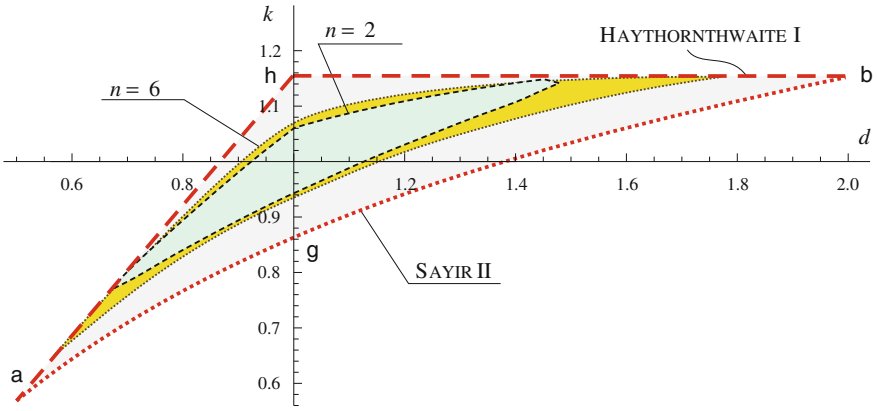

Fig. 21 Convexity condition of the geometrical-mechanical model (105) in the $d-k$-diagram together with the boundaries of the convexity region as presented in Fig. 4

9.1.7 Triquadratic Model

The triquadratic model is formulated as follows [103, 105, 107]

$$\frac{3^3\, I_2'^3 + c_3\, \sigma_{\mathrm{eq}}^3\, I_3' + c_6\, I_3'^2}{1 + \dfrac{2}{3^3}\, c_3 + \dfrac{2^2}{3^6}\, c_6} = \sigma_{\mathrm{eq}}^6. \tag{108}$$

It allows analytical estimation of the equivalent stress. This model with the power $n = 6$ contains the hexagonal symmetry model with $c_3 = 0$ (model of Drucker I, Sect. 9.2) and with $c_6 = 0$ one gets

$$c_3 \in \left[-\frac{3^3}{2^2},\ \frac{3^3}{2} \right]. \tag{109}$$

The relations are

$$k^6 = 1 + \frac{2}{3^3} c_3 + \frac{2^2}{3^6} c_6, \qquad d^3 = \frac{k^6}{1 + \dfrac{2^2}{3^6}\, c_6}. \tag{110}$$

The idea for this model is similar to the model (105). Comparing with (105) we conclude that the triquadratic model (TQM) is more difficult to use. It should be noted that the parameters c_3, c_6 have no mechanical or geometrical meaning.

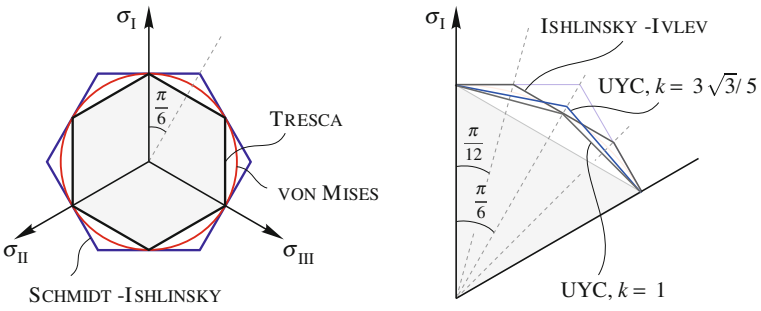

Fig. 22 Continuous surfaces with hexagonal symmetry and the model of von Mises (16) in the π-plane, incompressible material behavior, $d = 1$ [135]. On the *right hand side* an enlarged cross-section with $\theta \in [0,\ \pi/3]$ is presented [33]

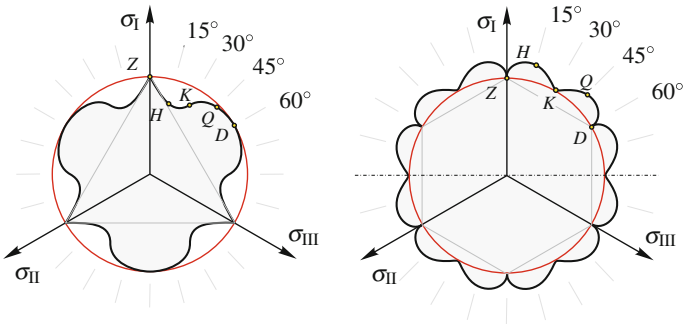

Fig. 23 Non-convex models for incompressible material behavior with $d = 1$ in the π-plane: *left hand side* model of triangular symmetry, *right hand side* model of hexagonal symmetry [96]. The rotationally symmetric model of von Mises is presented for comparison

9.2 Yield Surfaces with Hexagonal Symmetry

The models for incompressible material behavior with hexagonal symmetry have the properties $d = 1$ and $h = q$ (Table 1, Figs. 22 and 23). Such models are often used for the description of yield of ideal ductile materials in the theory of plasticity. Numerous problems are treated in the engineering practice using these criteria. These models are of the form

$$\Phi(I_2', (I_3')^2, \sigma_{eq}) = 0, \qquad \Phi(I_2', \cos^2 2\theta, \sigma_{eq}) = 0$$

The meridians with $\theta = 0$ and $\pi/3$ coincide in the Burzyński-plane (Figs. 15 and 16). Such models can be represented in the $h-k$-diagram (Fig. 24) and compared with von Mises model with $h = k = 1$.

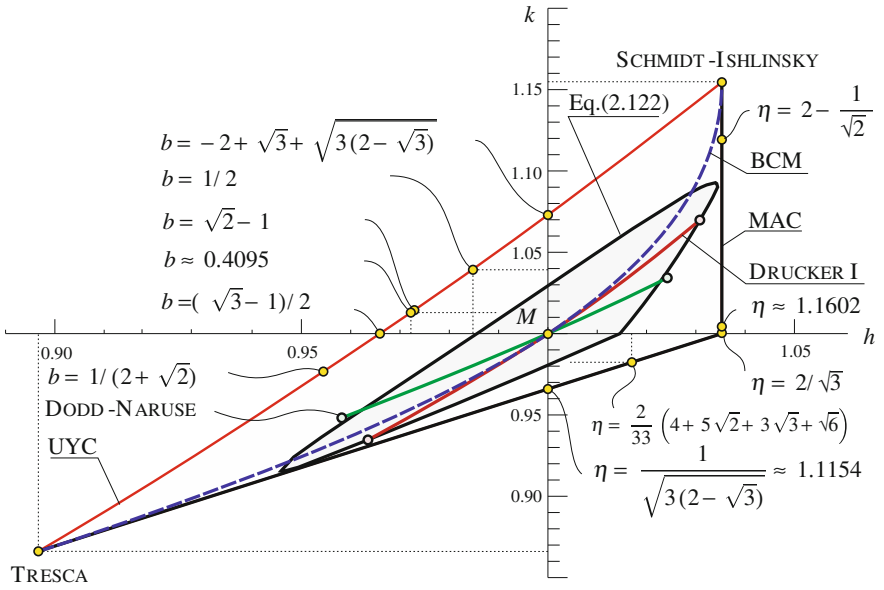

Fig. 24 $h-k$-diagram: models of hexagonal symmetry for incompressible material behavior: *M*—model of von Mises (16) with $h = k = 1$; *UYC*—yield criterion of Yu (111); *BCM*—bicubic model (113); Eq. (122)—model based on the stress angel with $n = 6$; *MAC*—multiplicative ansatz criterion, special points—s. [116]

9.2.1 Unified Yield Criterion of Yu

The criterion of Yu [222, 229] with the parameter $b \in [0,\ 1]$ can be expressed

$$\begin{cases} \sigma_{\mathrm{I}} - \dfrac{1}{1+b}(b\,\sigma_{\mathrm{II}} + \sigma_{\mathrm{III}}) - \sigma_{\mathrm{eq}} = 0, \\ \sigma_{\mathrm{I}} - \dfrac{1}{1+b}(b\,\sigma_{\mathrm{II}} + \sigma_{\mathrm{III}}) + \sigma_{\mathrm{eq}} = 0, \end{cases} \tag{111}$$

and using Eq. (102) formulated in terms of the invariants of the deviator [105]

$$\begin{aligned} \Phi_{\mathrm{UYC}} = {} & (\alpha_{41}\,\sigma_{\mathrm{eq}}^4\,I_2' + \alpha_{21}\,\sigma_{\mathrm{eq}}^2\,I_2'^2 + \beta_{21}\,I_2'^3 + \beta_{31}\,I_3'^2 - \sigma_{\mathrm{eq}}^6)^2 \\ & - (\alpha_{31}\,\sigma_{\mathrm{eq}}^3\,I_3' + \alpha_{11}\,\sigma_{\mathrm{eq}}\,I_2'\,I_3')^2 \end{aligned} \tag{112}$$

with the coefficients (91). In Table 5 some settings for special cases are presented.

The yield criterion of Yu defines the left convexity bound of the models with hexagonal symmetry in the $h-k$-diagram (Fig. 24, UYC).

Table 5 Settings of UYC (111) and the respective relations k and h (Fig. 24)

Model	b	k	h	Fig.
Tresca	0	$\frac{\sqrt{3}}{2} \approx 0.8660$	0.8966	1, 15, 22
–	$\frac{1}{2+\sqrt{2}} \approx 0.2929$	0.9767	0.9545	–
Sokolovsky[a]	$\frac{1}{2}\left(\sqrt{3}-1\right) \approx 0.3660$	1	0.9659	22
–	0.4095	1.0132	0.9723	–
–	$\sqrt{2}-1 \approx 0.4142$	$\sqrt{6}\,(\sqrt{2}-1) \approx 1.0146$	0.9729	–
–	$\frac{1}{2}$	$3\,\frac{\sqrt{3}}{5} \approx 1.0392$	0.9845	22,33
–	0.6286	1.0731	1	–
Schmidt-Ishlinsky	1	$\frac{2}{\sqrt{3}} \approx 1.1547$	1.0353	1, 16, 22

[a]The model is named after Sokolovsky following Pisarenko-Lebedev [157] "…it was attempted to introduce some intermediate criteria by replacing the hexagonal prism of Coulomb with a dodecagonal prism [195] (inscribed in the von Mises-cylinder) …". Further references to this models are [28, 222, 223, 226].

9.2.2 Bicubic Model

This model is obtained as a linear combination of the models of Tresca (15) and Schmidt-Ishlinsky (19) [33, 103]

$$\begin{aligned}&(1-\xi)\left[\left(I_2'-\sigma_{\mathrm{eq}}^2\right)^2\left(2^2\,I_2'-\sigma_{\mathrm{eq}}^2\right)-3^3\,I_3'^2\right]\\&+\xi\left[\frac{3^3}{2^3}\,I_3'+\frac{3^2}{2^2}\,I_2'\,\sigma_{\mathrm{eq}}-\sigma_{\mathrm{eq}}^3\right]\left[\frac{3^3}{2^3}\,I_3'-\frac{3^2}{2^2}\,I_2'\,\sigma_{\mathrm{eq}}+\sigma_{\mathrm{eq}}^3\right]=0.\end{aligned}\tag{113}$$

This model also results from (99) with $d = 1$.

The bicubic model divides the $h-k$-diagram into two areas. The models of Tresca and Schmidt-Ishlinsky are obtained with $\xi = 0$ and $\xi = 1$. The value $k = 1$ results in $\xi = 2^6/(7 \cdot 13) \approx 0.7033$. This model is continuously differentiable (excluding the borders of ξ) and allows an explicit solution for σ_{eq}. For this reason, the BCM is appropriate for practical use. The parameters k and h are obtained from bicubic equations

$$2^4 \cdot 3^3 + 2^3 \cdot 3^3\,k^2\,(\xi - 2^2) + 2^6\,k^6\,(\xi - 1) - 3^3\,k^4\,(7\,\xi - 2^4) = 0, \tag{114}$$

$$2^5 \cdot 3^3 + 2 \cdot 3^3\,h^4\,(2^4 - 7\,\xi) + 2^4 \cdot 3^3\,h^2\,(\xi - 2^2) + h^6\,(37\,\xi - 2^6) = 0 \tag{115}$$

as the lowest positive solutions. The analytical solution of (114) and (115) is complex and hence omitted.

Table 6 Settings of MAC (116) and the respective relations k and h (Fig. 24)

Model	η	k	h	Fig.
Tresca	1	$\frac{\sqrt{3}}{2} \approx 0.8660$	0.8966	1, 15, 22
–	$\frac{1}{\sqrt{3\,(2-\sqrt{3})}} \approx 1.1154$	$\frac{\sqrt{2+\sqrt{3}}}{2} \approx 0.9659$	1	–
–	1.1344	0.9824	1.0170	–
Ishlinsky-Ivlev[a]	$\frac{2}{\sqrt{3}} \approx 1.1547$	1	1.0353	22
–	$\frac{3}{14}\left(4+\sqrt{2}\right) \approx 1.1602$	1.0048	1.0353	–
–	$2-\frac{1}{\sqrt{2}} \approx 1.2929$	1.1197	1.0353	–
Schmidt-Ishlinsky	$\frac{4}{3}$	$\frac{2}{\sqrt{3}} \approx 1.1547$	1.0353	1, 16, 22

[a]The regular dodecagon in the π-plane is named after Ishlinsky-Ivlev [33, 105, 115], s. also [93, 98–100, 128, 193, 227].

9.2.3 Multiplicative Ansatz Criterion

Multiplicative combination of the models of Tresca (15) and Schmidt-Ishlinsky (19) [116] lies on the right boundary of the convexity region of the models of hexagonal symmetry (Fig. 24, MAC) [93, 98, 99, 193]. It is obtained as follows [105]

$$\begin{aligned}\Phi_{\mathrm{MAC}} = &\left[\left(I_2' - (\eta\,\sigma_{\mathrm{eq}})^2\right)^2 \left(2^2\,I_2' - (\eta\,\sigma_{\mathrm{eq}})^2\right) - 3^3\,I_3'^2\right] \\ &\times \left[\frac{3^3}{2^3}\,I_3' + \frac{3^2}{2^2}\,I_2'\,\sigma_{\mathrm{eq}} - \sigma_{\mathrm{eq}}^3\right]\left[\frac{3^3}{2^3}\,I_3' - \frac{3^2}{2^2}\,I_2'\,\sigma_{\mathrm{eq}} + \sigma_{\mathrm{eq}}^3\right]. \end{aligned} \tag{116}$$

The value η lies in the interval $\eta \in [1,\ 4/3]$. The parameters k and h compute to

$$k = \frac{\sqrt{3}}{2}\,\eta, \qquad h = \begin{cases} \eta\sqrt{3\,(2-\sqrt{3})}, & \eta \in \left[1,\ \dfrac{2}{\sqrt{3}}\right], \\ \sqrt{4\,(2-\sqrt{3})}, & \eta \in \left[\dfrac{2}{\sqrt{3}},\ \dfrac{4}{3}\right]. \end{cases} \tag{117}$$

The models of Tresca and Schmidt-Ishlinsky are obtained with $\eta = 1$ and $\eta = 4/3$. With $\eta = \frac{2}{\sqrt{3}}$ one gets the regular dodecagon in the π-plane (Table 6).

For UYC and MAC the points, which have the shortest distance to the point $M(1,\ 1)$ (Fig. 24, model of von Mises), can be obtained from the equation

$$(h-1)^2 + (k-1)^2 \to \min. \tag{118}$$

Using these points the model of von Mises can be approximated with the dodecagons of UYC with $b = 0.4095$ and the dodecagons of multiplicative ansatz criterion (MAC) with $\eta = 1.1344$.

9.2.4 Universal Model with Hexagonal Symmetry

The parameter $b \in [0,\ 1]$ of the UYC (111) can be replaced by the parameter $k \in \left[\sqrt{3}/2,\ 2/\sqrt{3}\right]$

$$b = \frac{\sqrt{3} - 2\,k}{k - \sqrt{3}}. \tag{119}$$

The parameter $\eta \in [1,\ 4/3]$ in MAC (116) can be replaced by $k \in \left[\sqrt{3}/2,\ 2/\sqrt{3}\right]$ with (117)

$$\eta = \frac{2}{\sqrt{3}}\,k. \tag{120}$$

With the linear (convex) combination of the two latter models [116]

$$\Phi_{12} = \xi\,\Phi_{\mathrm{MAC}} + (1 - \xi)\,\Phi_{\mathrm{UYC}}, \qquad \xi \in [0,\ 1] \tag{121}$$

the model with the power of stress $n = 12$ is obtained, cf. Eq. (99). It covers all the convex forms in the $h-k$-diagram with two parameters $(k,\ \xi)$. The values $k = 1$ and $\xi = 0.3901$ result in $h = 1$, which corresponds to the model of von Mises (Fig. 24). With $\xi = 0.3901$ and $k \in \left[\sqrt{3}/2,\ 2/\sqrt{3}\right]$ one gets the approximation of BCM (113). With $k = 1$ and $\xi \in [0,\ 1]$ one obtains a model, which links the regular dodecagon of Sokolovsky and Ishlinsky-Ivlev: $h \in [0.9659,\ 1.0353]$. The major disadvantage is, that the model (121) is not analytically solvable with respect to σ_{eq}.

9.2.5 Model Based on the Stress Angle

Cosine ansatz to the power 2 and 4 is introduced in [33]

$$(3\,I_2')^{n/2}\,\frac{1 + c_6\cos^2 3\theta + c_{12}\,\cos^4 3\theta}{1 + c_6 + c_{12}} = \sigma_{\mathrm{eq}}^n, \qquad n = 1,\ 2\ \ldots \tag{122}$$

with

$$k^n = 1 + c_6 + c_{12}, \qquad h^n = 2^2\,\frac{1 + c_6 + c_{12}}{2^2 + 2\,c_6 + c_{12}}. \tag{123}$$

This model contains the following criteria:

- Drucker I [54, 154, 199] with $n = 6$, $c_6 \in [-1/3,\ 1/2]$, $c_{12} = 0$ and

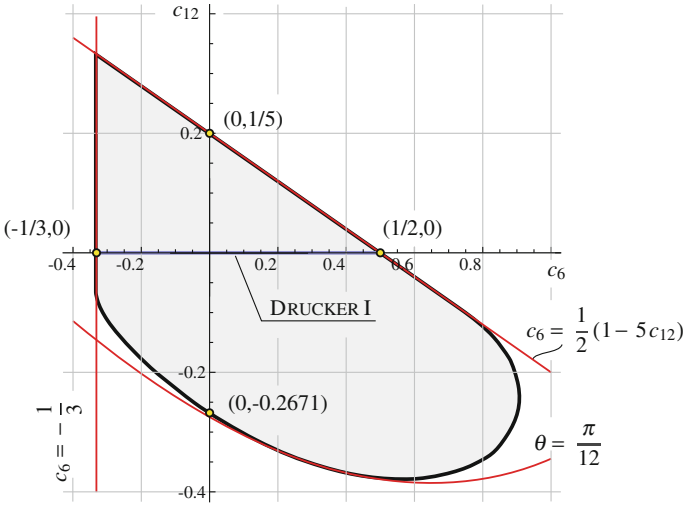

Fig. 25 Convexity region of the model (122) with $n = 6$ in the parameter space $(c_6,\ c_{12})$. The constraints at $\theta = 0$ with $c_6 = (1 - 5\,c_{12})/2$, $\theta = \pi/12$ and $\theta = \pi/6$ with $c_6 = -1/3$ are shown for clarity

- Dodd-Naruse [53, 229] with $n = 12$, $c_6 = 0$, $c_{12} \in \left[\frac{2}{3^3}\left(2\sqrt{11} - 13\right),\ \frac{1}{2}\right]$.

The boundaries of the parameters of the model (122) with $n = 6$, which result from the convexity conditions [33], are shown in Fig. 25.

10 Pressure-Sensitive Criteria

The behavior of real materials can be presented by the models (5) and (6). The first invariant of the stress tensor should be included in the pressure-insensitive criteria (Sect. 9) in such a way that the shape in the π-plane will be preserved.

10.1 Compressible Generalization

A compressible generalization of the models of incompressible material behavior (Sect. 9) is obtained by substitution [115]

$$\sigma_{\mathrm{eq}} \to \sqrt[j+l+m]{\left(\frac{\sigma_{\mathrm{eq}} - \gamma_1\, I_1}{1 - \gamma_1}\right)^{j} \left(\frac{\sigma_{\mathrm{eq}} - \gamma_2\, I_1}{1 - \gamma_2}\right)^{l} \sigma_{\mathrm{eq}}^{m}}. \tag{124}$$

The parameters γ_1 and γ_2 determine the position of the hydrostatic nodes A_Z and A_D on the hydrostatic axis (Figs. 2, 12). The powers j, l and m are chosen to be integer and positive. They are restricted by the following experience-based relation:

$$j + l + m \leq 6. \tag{125}$$

For materials, which do not fail under hydrostatic pressure (brass, plumb, steel), the surfaces Φ has a single hydrostatic node A_Z ($a_+^{\text{hyd}} > 1/3, a_-^{\text{hyd}} \to \infty$), e. g.:

- in order to obtain straight meridians the substitution with $l = m = 0$ is

$$\sigma_{\text{eq}} \to \frac{\sigma_{\text{eq}} - \gamma_1 I_1}{1 - \gamma_1}, \qquad +++\gamma_1 \in [0,\ 1[, \tag{126}$$

- for parabolic models it follows $l = 0$ and
- for hyperbolic meridians $\gamma_2 \in]0,\ \gamma_1[$; the second node does not belong to the relevant region of the surface and has no physical meaning, cf. [220]; due to this fact the hyperbolic surfaces are not recommended for applications.

For materials, which fail under hydrostatic compression (hard foams, ceramics, sintered and granular materials, etc.) the additional hydrostatic node A_D is needed. The parameters in (124) are then bounded as follows

$$\gamma_1 \in]0,\ 1[, \qquad \gamma_2 < 0. \tag{127}$$

For instance the closed surface with the substitution

$$\sigma_{\text{eq}} \to \sqrt[3]{\frac{\sigma_{\text{eq}} - \gamma_1 I_1}{1 - \gamma_1} \left(\frac{\sigma_{\text{eq}} - \gamma_2 I_1}{1 - \gamma_2}\right)^2} \tag{128}$$

and the shape b of the cross-section in the π-plane (Fig. 4) can be considered. The properties of the surface with $\gamma_1 = 1/3, \gamma_2 = -1/3$ are shown in Figs. 27, 28 and 26.

The closed surfaces with $j = l$ possess a symmetry plane orthogonal to the hydrostatic axis

$$\frac{I_1}{\sigma_+} = \frac{1}{2}\left(\frac{1}{\gamma_1} + \frac{1}{\gamma_2}\right). \tag{129}$$

The ellipsoid of Schleicher (Sect. 6) with this property is widely applied in modeling [114].

There is no method known, which allows to choose the powers in (124) analytically. Rational substitution, e. g. such transform where the root in (124) spared, is a simple possibility. For example a quadratic substitution

$$\sigma_{\text{eq}}^2 \to \frac{\sigma_{\text{eq}} - \gamma_1 I_1}{1 - \gamma_1} \frac{\sigma_{\text{eq}} - \gamma_2 I_1}{1 - \gamma_2}, \qquad \gamma_1 \in [0,\ 1[\tag{130}$$

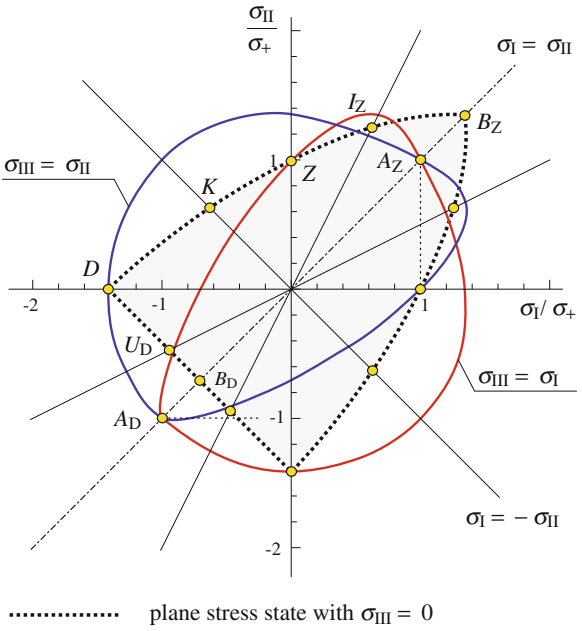

Fig. 26 Model of Sayir I (87) with $c_3 = 3^2/2$ and the substitution (128) with $\gamma_1 = 1/3$, $\gamma_2 = -1/3$ in the $\sigma_\mathrm{I}-\sigma_\mathrm{II}$-plane (s. Burzyński-plane (Fig. 27) and π-plane (Fig. 28)). The meridians with $\sigma_\mathrm{III} = \sigma_\mathrm{II}$ and $\sigma_\mathrm{III} = \sigma_\mathrm{I}$ are shown for clarity (spatial image)

can be applied for the model of von Mises (16), see rotationally symmetric model (51), and the models of hexagonal symmetry (Sect. 9.2) for fitting the available measured data.

The nonconvex surfaces in the meridian section are obtained with (124), if among the parameters γ_i there are two complex conjugated values. Figure 29 represents, as an example, a hyperboloid [63]. Such surfaces can be used as parts of combined models (Sect. 11.2).

10.2 Unified Strength Theory of Yu

The Unified Strength Theory (UST) is built up from two six-edge pyramids in the principal stress space [105, 228, 229]

$$\begin{cases} \sigma_\mathrm{I} - \dfrac{1}{d\,(1+b)}\,(b\,\sigma_\mathrm{II} + \sigma_\mathrm{III}) - \sigma_\mathrm{eq} = 0, \\ \dfrac{1}{d}\,\sigma_\mathrm{I} - \dfrac{1}{1+b}\,(b\,\sigma_\mathrm{II} + \sigma_\mathrm{III}) + \sigma_\mathrm{eq} = 0. \end{cases} \tag{131}$$

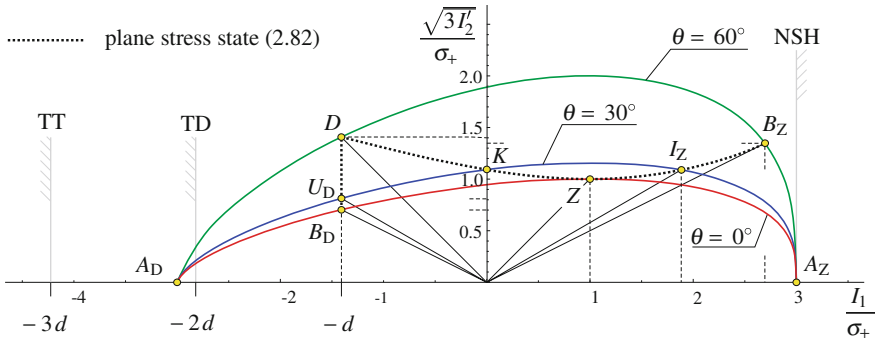

Fig. 27 Model of Sayir I (87) with $c_3 = 3^2/2$ and the substitution (128) with $\gamma_1 = 1/3, \gamma_2 = -1/3$ in the Burzyński-plane. Properties: $d = 1.41$, $k = 1.09$, $i_Z = 1.09$, $u_D = 0.81$, $b_Z = 1.35$, $b_D = 0.70$, $a_+^{hyd} = 1$, $a_-^{hyd} = 1$, $v_+^{in} = 1/2$, $v_-^{in} = -0.05$. The reference values for the hydrostatic nodes A_Z and A_D are: NSH—upper bound due to the normal stress hypothesis $a_+^{hyd} = 1$, (41), TT—lower bound for the point A_D with respect to the normal stress hypothesis as trigonal trapezohedron, $a_-^{hyd} = d$, TD—lower bound for the point A_D with respect to the normal stress hypothesis as triangular dipyramid, $a_-^{hyd} = 2d/3$

The faces of the first pyramid are obtained from the first equation with the cyclic permutations of indices. The faces of the second one are obtained in the same manner from the second equation.

The model (131) describes the compressible material behavior with the properties (22) using two parameters $d \geq 1$ and $b \in [0, 1]$. The value d corresponds to the relation d (Table 1)

$$d = \frac{|\sigma_-|}{\sigma_+}, \tag{132}$$

which simplifies the application of the model.

The analysis of the UST leads to the following special cases (Figs. 5 and 30):

- $b = 1$ results in the Twin-Shear Theory (TST) of Yu,
- with

$$b = \frac{\sqrt{3} - 1}{2} \tag{133}$$

  follows a continuous analogy of the model of Pisarenko-Lebedev (48),
- with $b = 0$ the model of Mohr-Coulomb (Single-Shear Theory of Yu), Eq. (45), is obtained,
- with $d \to \infty$, $b \in [0, 1]$ absolutely brittle materials can be described (normal stress hypothesis), Eq. (8),
- the Unified Yield Criterion (111) results from the UST with $d = 1$ and $b \in [0, 1]$.

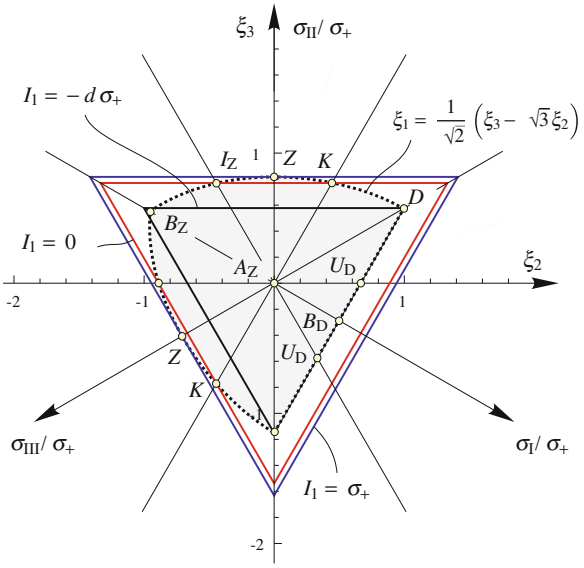

Fig. 28 Cross-sections $I_1 = \sigma_+$, $I_1 = 0$, $I_1 = -d\,\sigma_+$ and the line of the plane stress state of the model of Sayir I (87) with $c_3 = 3^2/2$ and the substitution (128) with $\gamma_1 = 1/3$, $\gamma_2 = -1/3$ in the π-plane, see Fig. 27

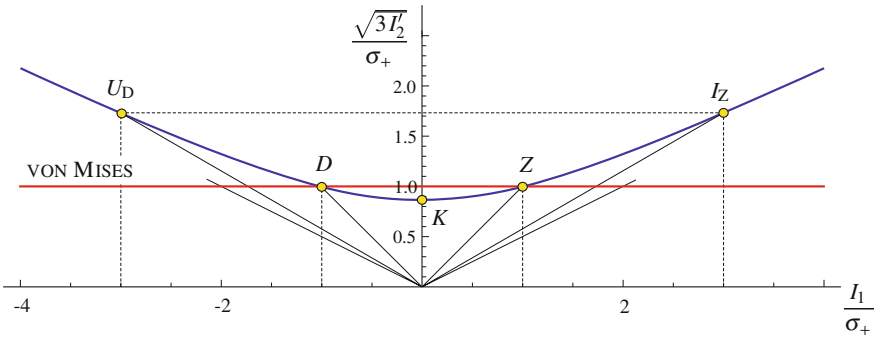

Fig. 29 Model of von Mises and the hyperboloid of one sheet (51) with $\gamma_1 = -\gamma_2 = 1/\sqrt{3}\,i$ in the Burzyński-plane with the properties: $d = 1$, $k = \sqrt{3}/2$, $i_Z = u_D = \sqrt{3}$, $\nu_+^{in} = \nu_-^{in} = 1$

The hydrostatic tensile stress computes to

$$a_+^{hyd} = \frac{1}{1 - \dfrac{1}{d}} = \frac{1}{1 - 2\,\nu_+^{in}}. \tag{134}$$

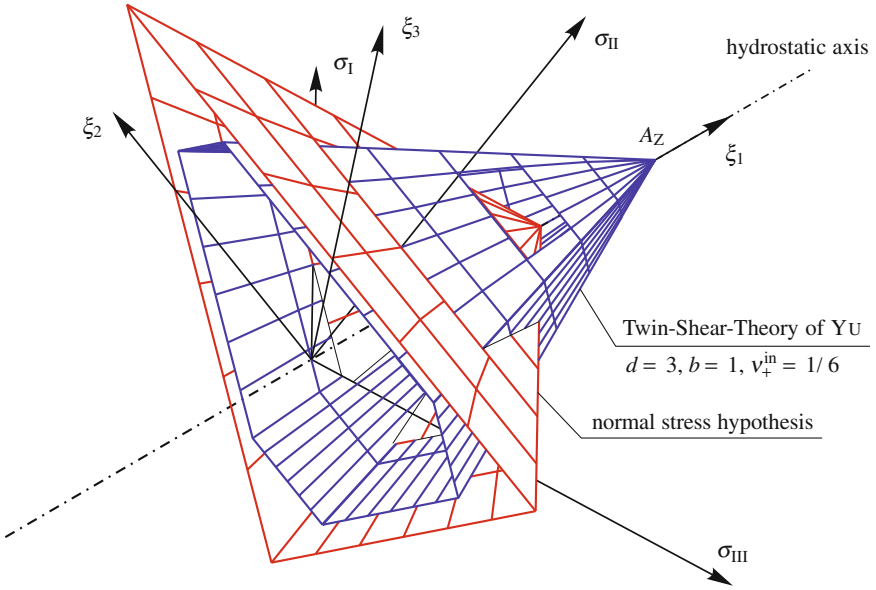

Fig. 30 Twin-Shear Theory ($d = 3, b = 1, \nu_+^{\text{in}} = 1/6$) and the normal stress hypothesis ($d \to \infty$, $b = 0 \ldots 1, \nu_+^{\text{in}} = 0$) in the principal stress space. The point A_Z of the normal stress hypothesis is shown for better understanding

The surface Φ of the UST is open in the hydrostatic compression direction ($I_1 < 0$):

$$a_-^{\text{hyd}} \to \infty. \tag{135}$$

The relation k equals to

$$k = \sqrt{3}\,\frac{1+b}{1+b+\dfrac{1}{d}} = \sqrt{3}\,\frac{1+b}{1+b+2\,\nu_+^{\text{in}}}. \tag{136}$$

For i_Z and u_D it follows

$$i_Z = \frac{\sqrt{3}\,(1+b)}{2-b\,(1/d-2)}, \qquad u_D = \frac{\sqrt{3}\,(1+b)}{(2+b)\,1/d}. \tag{137}$$

The relations b_Z and b_D are given by (22). The Poisson's ratios at tension and compression are

$$\nu_+^{\text{in}} = \frac{1}{2\,d}, \qquad \nu_-^{\text{in}} = \frac{d}{2}. \tag{138}$$

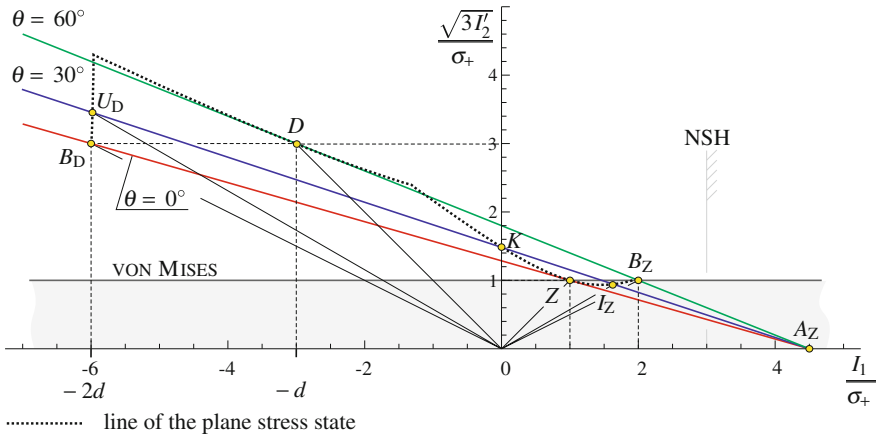

Fig. 31 UST with $d = 3$ and $b = 1$ with the properties $k = 6\sqrt{3}/7$, $i_Z = 6\sqrt{3}/11$, $u_D = 2\sqrt{3}$, $b_D = 3$, $b_Z = 1$, $a_+^{hyd} = 3/2$, $\nu_+^{in} = 1/6$, $\nu_-^{in} = 3/2$ and the model of von Mises in the Burzyński-plane, cf. [105]. NSH—reference value $a_+^{hyd} = 1$ from the normal stress hypothesis

The invariant representation of the UST (131) is given in [105, 115]. It results from the Radcig model (102) by the linear transform (126) and the parameters

$$\gamma_1 = \frac{1 - 1/d}{3}, \qquad \eta = \frac{2 + 1/d}{1 + 2/d}, \tag{139}$$

$$b_1 = \frac{1 + b - 1/d + 2\,b/d}{1 + b + 2/d - b/d}, \qquad b_2 = \frac{3(1 - b)}{b\,(1 - 1/d) - 2 - 1/d} + 1. \tag{140}$$

The meridians with $\theta = 0$, $\pi/6$ and $\pi/3$ of the UST are represented in the Burzyński-plane by straight lines through the point $A_Z(3\,a_+^{hyd},\ 0)$ and the points $Z\ (1,\ 1)$, $K\ (0,\ k)$ and $D\ (-d,\ d)$, respectively. The Twin Stress Theory (TST) with the parameter values $d = 3$ and $b = 1$ is shown in Figs. 30, 31 and 32.

10.3 Models for Applications

Because of their simplicity and versatility the following models can be recommended for various classes of isotropic materials.

10.3.1 Unified Strength Theory of Yu

The UST (131) is well-accepted and often used in computations and theoretical investigations. The linear relations of the model result in low computational complexity.

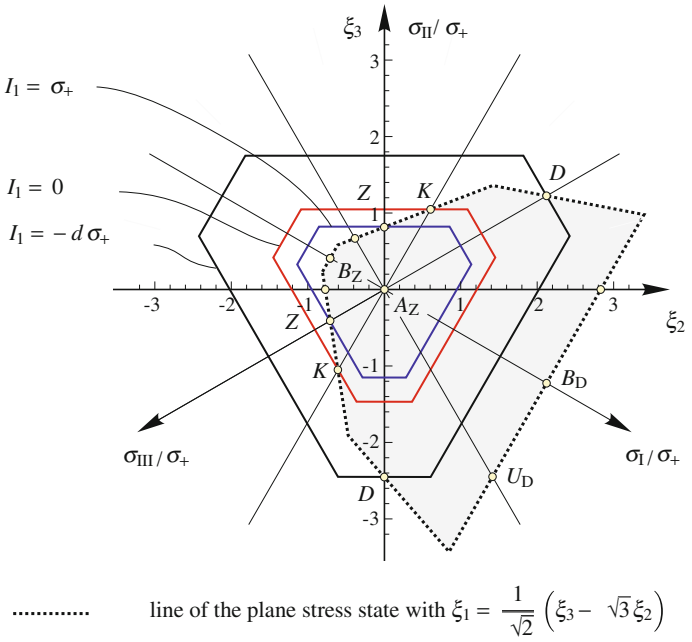

Fig. 32 UST with $d = 3$ and $b = 1$: cross-sections $I_1 = \sigma_+$, $I_1 = 0$, $I_1 = -d\,\sigma_+$ and the line of the plane stress state in the π-plane, see principal stress space (Fig. 30) and Burzyński-plane (Fig. 31)

The model is restricted to materials with $a_-^{\text{hyd}} \to \infty$ (the hydrostatic compression is unbounded). The straight lines of the meridians of this model simplify the description of the material behavior, however they have no theoretical foundation. The model can be modified near the hydrostatic tension (Sect. 11.1) in order to reduce the relation a_+^{hyd} [229].

The UYC (UST with $d = 1$) cannot describe the SD-effect (no strength differential effect) and the Poynting-Swift-effect for incompressible material [105]. Because the intersections of the planes (131) with each other lie outside of the closed region, where the model is valid (Fig. 33), the approximation of the measurements using different optimization criteria (Sect. 12) becomes difficult.

If the UST is used as a plastic potential these intersections lead to singularities in the strain field.

10.3.2 Rotationally Symmetric Models

Depending on the number of experiments, the quality of the measurements and the required modeling precision, the function Φ can be simplified, if the influence

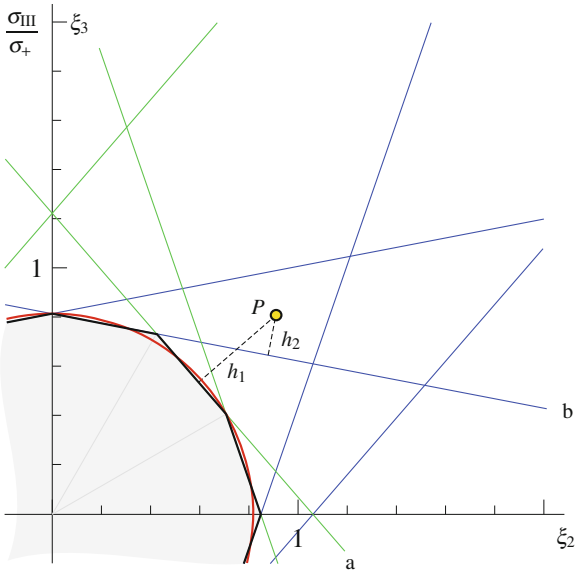

Fig. 33 UYC with $b = 1/2$ in the π-plane. P—measurement (schematic); h_1, h_2—normals to some planes of the model: $a\,\sigma_{\mathrm{eq}} = \dfrac{1}{1+b}\,(\sigma_{\mathrm{II}} + b\,\sigma_{\mathrm{III}}) - \sigma_{\mathrm{I}}$, $b\,\sigma_{\mathrm{eq}} = \sigma_{\mathrm{II}} - \dfrac{1}{1+b}\,(\sigma_{\mathrm{I}} + b\,\sigma_{\mathrm{III}})$. The model of von Mises is presented for comparison

of the third deviatoric invariant is neglected. These models contains the quadratic rotationally symmetric model (51), Figs. 11, 12 and 34.

Using the substitution (124) the rotationally symmetric model of the form

$$(3I_2')^3 = \left(\frac{\sigma_{\mathrm{eq}} - \gamma_1\, I_1}{1-\gamma_1}\right)^j \left(\frac{\sigma_{\mathrm{eq}} - \gamma_2\, I_1}{1-\gamma_2}\right)^l \sigma_{\mathrm{eq}}^m, \quad \gamma_1 \in [0,\ 1[\tag{141}$$

with

$$j + l + m = 6 \tag{142}$$

can be introduced. The following combination of the parameters γ_i for materials with $a_-^{\mathrm{hyd}} \to \infty$ can be used

- for a cone with $\gamma_1 = \gamma_2$, $m = 0$ and
- for a paraboloid with $l = 0$, $m = 1 \ldots 5$.

For closed criteria, which restrict in addition to the hydrostatic tension the hydrostatic compression, the following values of parameters γ_i should be considered

- $\gamma_2 < 0, m = 0 \ldots 3,\ j \neq l$ (Fig. 35) or
- $\gamma_2 < 0, m = 0,\ 2,\ 4,\ j = l$ a surface similar to the ellipsoid of Schleicher (Fig. 34) with the symmetry plane orthogonal to the hydrostatic axis with (129).

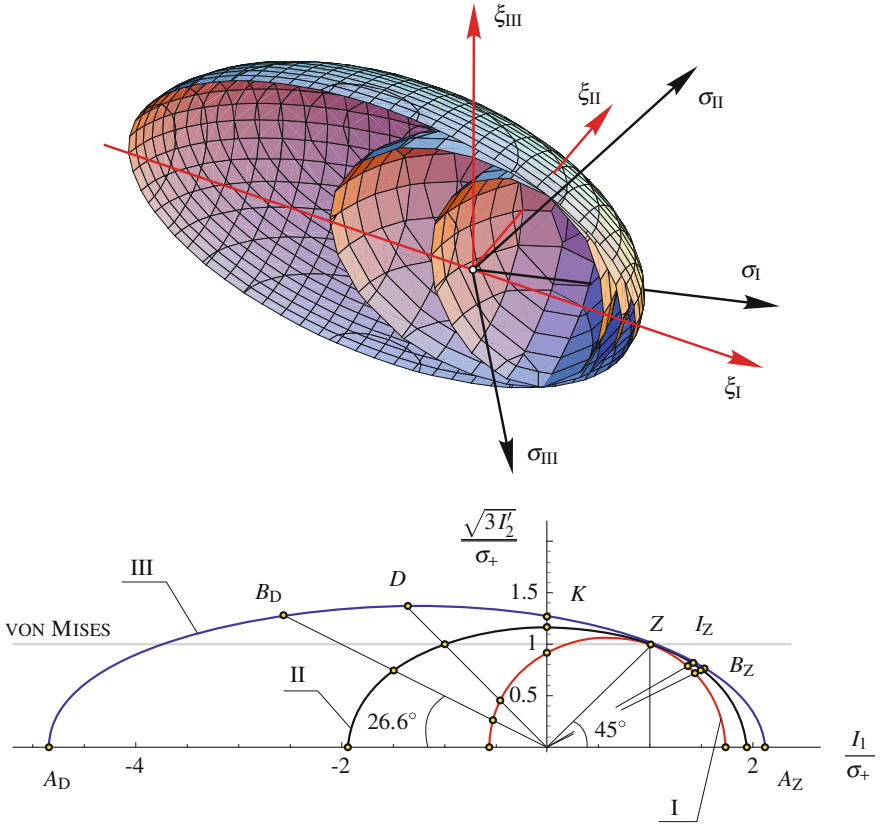

Fig. 34 Model of Schleicher (51) with the Poisson's ratio $\nu_+^{\text{in}} = \frac{1}{10}$, [103]: *top* in the principal stress space $\sigma_{\text{I}}, \sigma_{\text{II}}, \sigma_{\text{III}}$ (for clarity the surfaces *I, II* and *III* are cut $\xi_{\text{II}} \geq 0$) *bottom* in the Burzyński-plane *I* $\nu_-^{\text{in}} = -\frac{1}{2}$, $\gamma_1 = \frac{1}{15}(-9 + 2\sqrt{78})$, $\gamma_2 = \frac{1}{15}(-9 - 2\sqrt{78})$, $d = 0.45$, $k = 0.92$; *II* $\nu_-^{\text{in}} = \frac{1}{10}$, $\gamma_1 = \gamma_2 = \frac{2}{\sqrt{15}}$, $d = 1$, $k = 1.17$ (ellipsoid of Beltrami); *III* $\nu_-^{\text{in}} = \frac{1}{2}$, $\gamma_1 = \frac{1}{15}(2 + \sqrt{26})$, $\gamma_2 = \frac{1}{15}(2 - \sqrt{26})$, $d = 1.36$, $k = 1.25$

This model yields more possibilities for approximations in comparison to (51). If an analytical solution of the equation with respect to σ_{eq} is required, the model

$$(3I_2')^{3/2} = \left(\frac{\sigma_{\text{eq}} - \gamma_1 I_1}{1 - \gamma_1}\right)^j \left(\frac{\sigma_{\text{eq}} - \gamma_2 I_1}{1 - \gamma_2}\right)^l \sigma_{\text{eq}}^m, \quad \gamma_1 \in [0,\ 1[\tag{143}$$

with

$$j + l + m = 3 \tag{144}$$

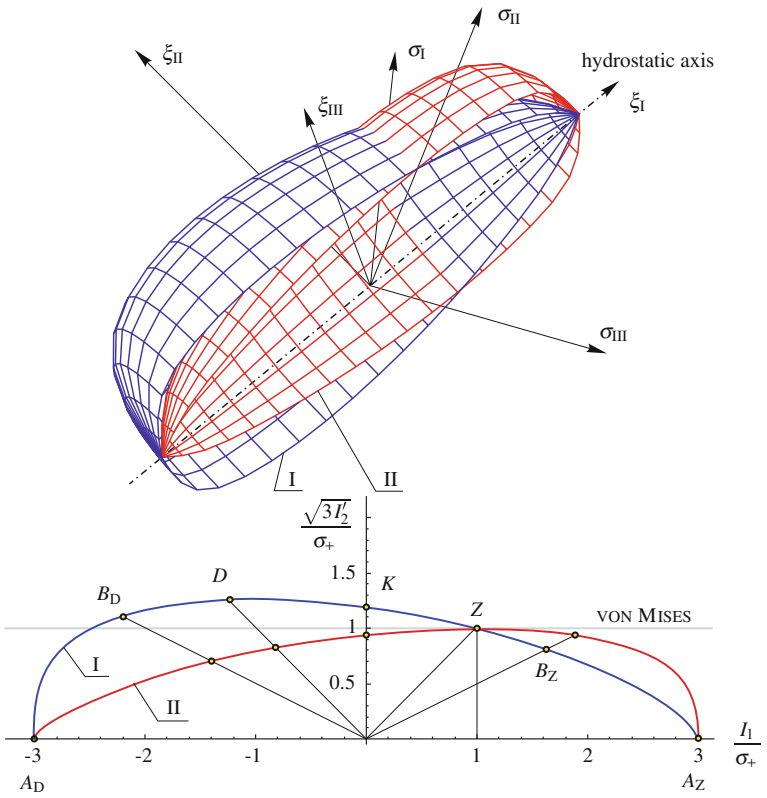

Fig. 35 Rotationally symmetric model (141) with $\gamma_1 = 1/3$, $\gamma_2 = -1/3$ or $a_+^{\text{hyd}} = 1$, $a_-^{\text{hyd}} = 1$ *I.* $j = 4$, $l = 2$, $d = 1.25$, $k = 1.19$, $b_Z = 0.82$, $b_D = 1.10$, $\nu_+^{\text{in}} = \frac{1}{5}$, $\nu_-^{\text{in}} = 0.44$; *II.* $j = 2$, $l = 4$, $d = 0.83$, $k = 0.94$, $b_Z = 0.94$, $b_D = 0.70$, $\nu_+^{\text{in}} = \frac{1}{2}$, $\nu_-^{\text{in}} = 0.27$ in the principal stress space and in the Burzyński-plane

can be used too. The number of the possible meridian shapes is lower in comparison with (141).

10.3.3 Geometrical-Mechanical Model

The model

$$3\,I_2' \,\frac{1 + c_3\,\cos 3\theta + c_6\,\cos^2 3\theta}{1 + c_3 + c_6} = \frac{\sigma_{\text{eq}} - \gamma_1\,I_1}{1 - \gamma_1}\,\frac{\sigma_{\text{eq}} - \gamma_2\,I_1}{1 - \gamma_2} \tag{145}$$

is a generalization of the rotationally symmetric model (51). The equivalent stress σ_{eq} can be computed analytically. The model can be used for describing of the multi-modular theory of elasticity.[7]

The relations compute to

$$d^2 \frac{1 - c_3 + c_6}{1 + c_3 + c_6} = \frac{(1 + d\,\gamma_1)\,(1 + d\,\gamma_2)}{(1 - \gamma_1)\,(1 - \gamma_2)}, \tag{146}$$

$$k^2 = \frac{1 + c_3 + c_6}{(1 - \gamma_1)\,(1 - \gamma_2)}. \tag{147}$$

The Poisson's ratio at tension ν_+^{in} is the same as in (54). The Poisson's ratio at compression ν_-^{in} is not provided because of its complexity.

The model

$$(3I_2')^{3/2} \frac{1 + c_3 \cos 3\theta + c_6 \cos^2 3\theta}{1 + c_3 + c_6} = \left(\frac{\sigma_{\text{eq}} - \gamma_1 I_1}{1 - \gamma_1}\right)^{3-l-m} \left(\frac{\sigma_{\text{eq}} - \gamma_2 I_1}{1 - \gamma_2}\right)^{l} \sigma_{\text{eq}}^{m} \tag{148}$$

with the substitution (124) and the adjustment (144) allows the analytical computation of the equivalent stress σ_{eq}. The number of possible shapes of the meridian line is however still not sufficient for a fitting of measurements. The relations compute to

$$d^3 \frac{1 - c_3 + c_6}{1 + c_3 + c_6} = \left[\frac{1 + d\,\gamma_1}{1 - \gamma_1}\right]^{3-l-m} \left[\frac{1 + d\,\gamma_2}{1 - \gamma_2}\right]^{l}, \tag{149}$$

$$k^3 = \frac{1 + c_3 + c_6}{(1 - \gamma_1)^{3-l-m}\,(1 - \gamma_2)^{l}}. \tag{150}$$

As strength hypothesis it can be recommended to use the geometrical-mechanical model (105) with the substitution (124) and the adjustment (142)

$$(3I_2')^3 \frac{1 + c_3 \cos 3\theta + c_6 \cos^2 3\theta}{1 + c_3 + c_6} = \left(\frac{\sigma_{\text{eq}} - \gamma_1 I_1}{1 - \gamma_1}\right)^{6-l-m} \left(\frac{\sigma_{\text{eq}} - \gamma_2 I_1}{1 - \gamma_2}\right)^{l} \sigma_{\text{eq}}^{m}. \tag{151}$$

This model has a large region of convex forms in the π-plane and various settings for the meridian. The relations are obtained analogous to (149) and (150)

$$d^6 \frac{1 - c_3 + c_6}{1 + c_3 + c_6} = \left[\frac{1 + d\,\gamma_1}{1 - \gamma_1}\right]^{6-l-m} \left[\frac{1 + d\,\gamma_2}{1 - \gamma_2}\right]^{l}, \tag{152}$$

$$k^6 = \frac{1 + c_3 + c_6}{(1 - \gamma_1)^{6-l-m}\,(1 - \gamma_2)^{l}}. \tag{153}$$

[7] Theory of elasticity with different Young's moduli $E_+ \neq E_-$ and elastic Posisson's ratios $\nu_+^{\text{el}} \neq \nu_-^{\text{el}}$ at tension and compression [9, 212]

The models (145), (148) and (151) describe incompressible material behavior with $\gamma_1 = \gamma_2 = 0$ and for $c_3 = c_6 = 0$ become rotationally symmetric model (141). With $c_3 = 0$ one obtains the models of hexagonal symmetry. The convexity conditions in the parameter space $c_3 - c_6$ must be taken into account for these models.

10.3.4 Convex π-Plane Model

The model (99) with the substitution (124) and the adjustment (142) can be used for analysis in certain special situations. For instance, in order to check if the given measurements can be described by a convex model. The number of measurements must be sufficient in order to obtain reasonable approximations. This model contains applying the linear substitution (126) the pyramids of Sayir II [178] and due to Haythornthwaite. The model of Drucker II [55] and due to Schmidt-Ishlinsky are special cases of these models. This model incorporate various conditions, e.g. $\xi = 0$, $b_Z = 1$, $a_+^{\text{hyd}} = 1$, to obtain special theories.

11 Combined Criteria

The mechanical behavior of modern materials can seldom be represented by a single surface Φ [157]. The extrapolated behavior at a hydrostatic tension (point A_Z) is in this case frequently overestimated. It occurs also that the Poisson's ratio at compression can admit incorrect values with $\nu_-^{\text{in}} > 1/2$ for yield criteria (Sect. 4).

For a reliable description of the measured data a number of combined models is proposed: the standard hypotheses (strain hypothesis (41), Mohr-Coulomb model (45) and Burzyński-Yagn model (51)) are combined in a different manner. Further reasons for the development of the combined models are:

- a small number of well-recognized models (Sect. 2, 6),
- simple interpretation of the measurements, which for instance can be separated in the regions of the brittle and of the ductile failure based on the hydrostatic stress with e. g. $I_1 < \sigma_+$ and $I_1 \geq \sigma_+$. In this case the surfaces with hexagonal symmetry in the π-plane are often used for ductile material behavior (Tresca and Schmidt-Ishlinsky models) and the surfaces with the trigonal symmetry (Fig. 4, cross section b) for the brittle one (normal stress hypothesis),
- taking into account the incompressibility $\nu_-^{\text{in}} = 1/2$ for loadings with $I_1 < 0$,
- the restriction of the hydrostatic stresses with, e. g., $a_+{}^{\text{hyd}} \in \left[1/3,\ 1\right]$ (Fig. 7),
- decrease of the power of the stresses in each part of the combined surface Φ to $n \leq 6$, which simplifies the analysis of the measurements and results in an increased computational stability.

Combined models containing a "cap" (cut-off), which bounds the hydrostatic stress at the point A_Z, and a "body". Models for incompressible material behavior (e. g. Schmidt-Ishlinsky, von Mises or Tresca) are usually chosen as the "body" in

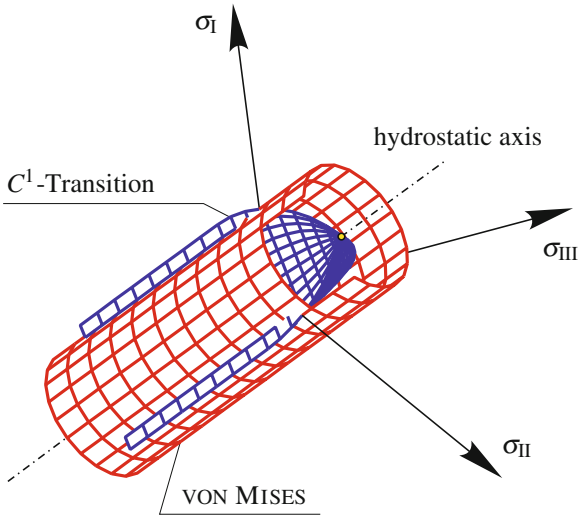

Fig. 36 Combined model with a C^1-transition in the cross-section $I_1 = 0$ built up from the model with the cross-section a in the π-plane (Fig. 4) in the principal stress space. The *cylinder* of von Mises is shown for comparison

the compression region ($I_1 < 0$). The influence of the first invariant in the model Φ changes with the transition from the "body" to the "cap" [107].

In order to reduce the number of possible combinations of surfaces additional plausibility conditions [105] are introduced

- the C^0-transition (continuous, not differentiable transition) follows for polyhedral surfaces (Sect. 11.1),
- for combinations of continuously differentiable surfaces it is a natural requirement the C^1-transition (Sect. 11.2),
- for combinations of surfaces, which have the same shape in the π-plane and are continuous, the C^1-transition in the meridian sections is recommended (Fig. 36).

The above mentioned conditions prohibit for instance the use of the model of Pelczyński [155, 234], which is built up from the normal stress hypothesis (8) and the model of von Mises (Figs. 2 and 37), some modifications, see [43, 45, 55, 173, 197, 217, 232]. The complicated shapes of the lines, resulting from the combination of the two surfaces, have no physical meaning.

11.1 Criteria with C^0-Transition

These models are built up from the Unified Strength Theory of Yu (Sect. 10.2) and the strain hypothesis (41). The normal stress hypothesis (8) is usually used as cut-off

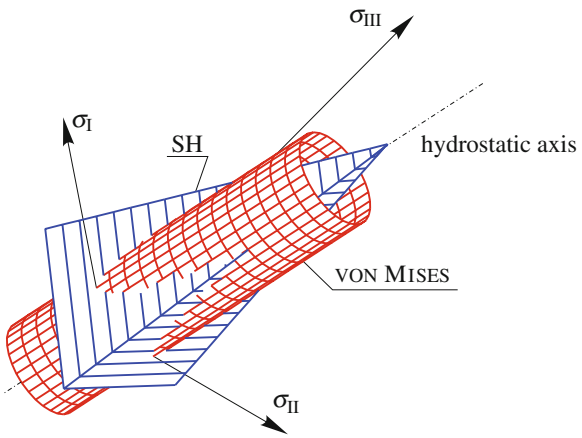

Fig. 37 "Pencil" of Pelczyński in the principal stress space with a C^0-transition between the surface of the strain hypothesis (SH), (41) and the *cylinder* of von Mises [107], cf. [234]

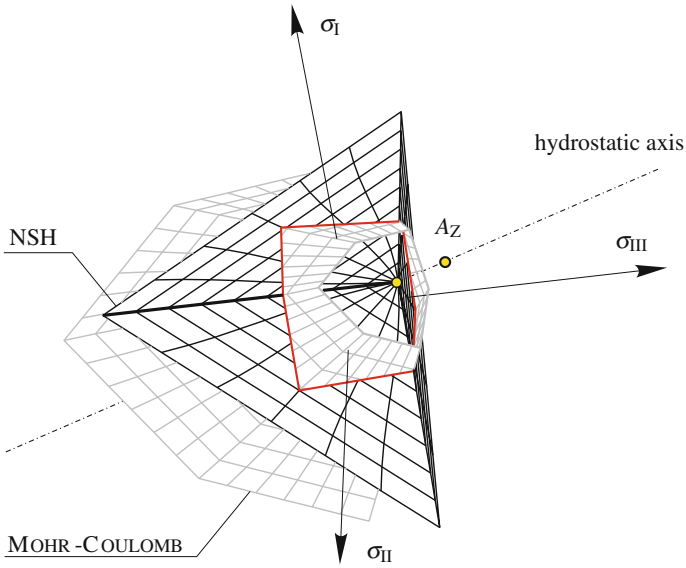

Fig. 38 Combined model with a C^0-transition in the principal stress space (model of Mohr-Coulomb with $d = 3$, $\nu_+^{\text{in}} = 1/6$ and the normal stress hypothesis $\nu_+^{\text{in}} = 0$ as a cut-off) [107]

(Figs. 30 and 38) instead of the strain hypothesis in order to reduce the number of parameters in the model [49, 70, 153, 154, 229].

The inclination of the meridian line of the angle $\theta = 0$ of the combined model, defined by the Poisson's ratio ν_+^{in}, has a jump at the point Z (Figs. 39 and 40)

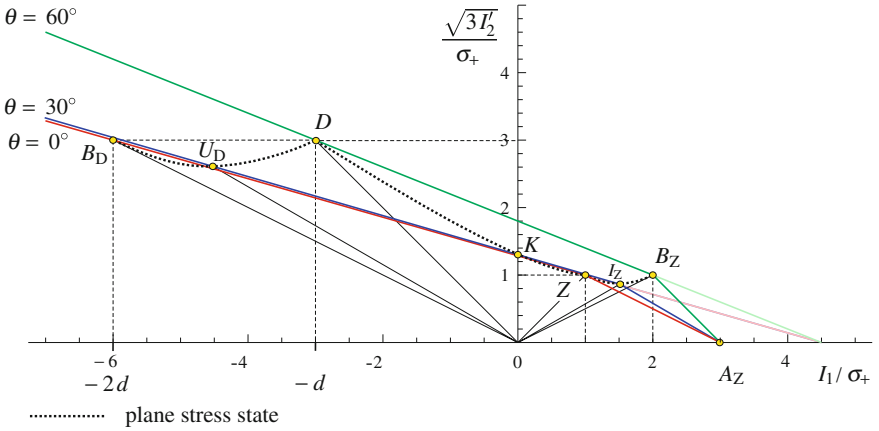

Fig. 39 Pyramid of the UST (131) with $b = 0$, $d = 3$, $k = 1.30$, $b_Z = 1$,$i_Z = 0.87$, $a_+^{\text{hyd}} = 3/2$, $\nu_+^{\text{in}} = 1/6$, $\nu_-^{\text{in}} = 3/2$ in the Burzyński-plane with the normal stress hypothesis as cut-off, $i_Z = 0.87$, $a_+^{\text{hyd}} = 1$, $\nu_+^{\text{in}} = 0$ (Fig. 38)

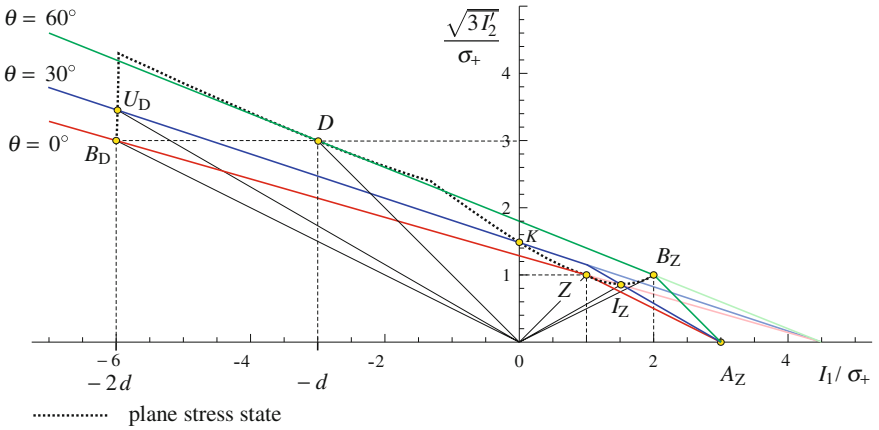

Fig. 40 Pyramid of the UST (131) with $b = 1$, $d = 3$, $k = 1.48$, $b_Z = 1$,$i_Z = 0.94$, $a_+^{\text{hyd}} = \frac{3}{2}$, $\nu_+^{\text{in}} = \frac{1}{6}$, $\nu_-^{\text{in}} = \frac{3}{2}$ in the Burzyński-plane with the normal stress hypothesis as cut-off, $i_Z = 0.87$, $a_+^{\text{hyd}} = 1$, $\nu_+^{\text{in}} = 0$ (Fig. 30), cf. [105]

$$\nu_+^{\text{in}} = \begin{cases} 0, & I_1 > \sigma_+, \text{ NSH as cut-off;} \\ 0 \ldots \dfrac{1}{2}, & I_1 \leq \sigma_+, \text{ UST of Yuas body.} \end{cases} \tag{154}$$

It is possible to combine two surfaces of UST with different parameter sets $(d,\ b)$ under the constraint

$$\nu_+^{\text{cut-off}} \in \left[0,\ \nu_+^{\text{body}}\right] \tag{155}$$

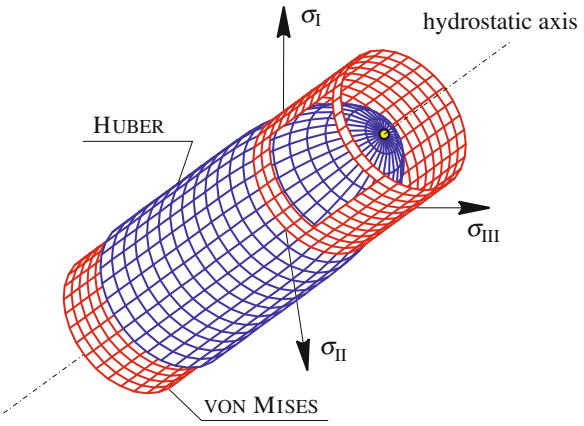

Fig. 41 Model of Huber with the C^1-transition in the cross section $I_1 = 0$ and the cylinder of von Mises in the principal stress space [107]

However, the resulting surface is too complex for applications. The existing information on the material behavior, which allow to deduce two different parameter sets $(d,\ b)$ of the UST, can be as usual better taken into account with the help of C^1-criteria.

11.2 Criteria with C^1-Transition

Combined surfaces with C^1-transitions have the following advantages:

- unique computation of the strain rates for the yield surface Φ with the flow rule, e. g. with (27) and
- lower number of parameters compared to C^0-criteria.

11.2.1 Model of Huber

The first combined hypothesis was proposed in 1904 by Huber [36, 37, 67, 91, 103, 118]. The model consists of the ellipsoid of Beltrami (Sect. 6.4) and of a cylinder with the transition at the cross-section $I_1 = 0$ (Figs. 41 and 42)

$$3\,I_2' = \begin{cases} \dfrac{\sigma_{\mathrm{eq}} - \gamma_1\,I_1}{1-\gamma_1}\,\dfrac{\sigma_{\mathrm{eq}} + \gamma_1\,I_1}{1+\gamma_1}, & I_1 > 0,\ \text{cap;} \\ \dfrac{\sigma_{\mathrm{eq}}}{1-\gamma_1}\,\dfrac{\sigma_{\mathrm{eq}}}{1+\gamma_1}, & I_1 \le 0,\ \text{body.} \end{cases} \tag{156}$$

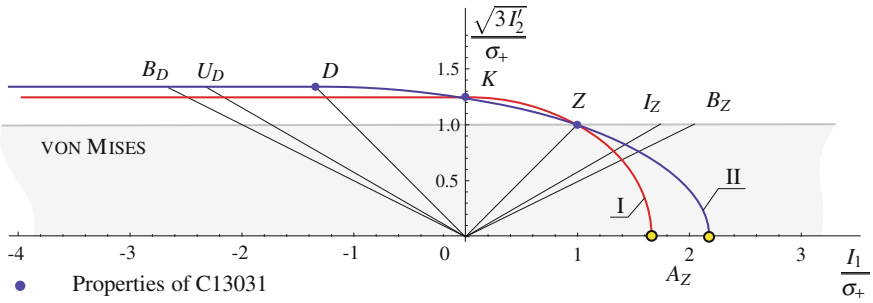

Fig. 42 Models fitted to the measured data for polyoxymethylene (POM) Hostaform C13031, Ticona GmbH, Sulzbach in the Burzyński-plane [113]: *I* model of Huber (156) with $k = 1.25$, ($d = 1.25$, $\nu_+^{\text{in}} = -0.04$, $\nu_-^{\text{in}} = 1/2$, $3\,a_+^{\text{hyd}} = 1.67$), *II* modified model of Huber (163) with $d = 1.34$, ($k = 1.24$, $\nu_+^{\text{in}} = 0,20$, $\nu_-^{\text{in}} = 12$, $3\,a_+^{\text{hyd}} = 2.18$)

The transition between the surfaces in the cross-section $I_1 = 0$ is continuously differentiable. The model has the property $k = d \geq 1$. The parameter $\gamma_1 \in [0,\ 1[$ results from the relation (52)

$$k^2 = \frac{1}{(1-\gamma_1)(1+\gamma_1)}. \tag{157}$$

The Poisson's ratio at tension can be computed using (54) as follows

$$\nu_+^{\text{in}} = \frac{3}{2\,k^2} - 1. \tag{158}$$

Further values are

$$b_Z = \frac{1}{\sqrt{2\,\left(1-\nu_+^{\text{in}}\right)}}, \qquad a_+^{\text{hyd}} = \frac{1}{\sqrt{3\,\left(1-2\,\nu_+^{\text{in}}\right)}}. \tag{159}$$

The model is simple and represents the "classical view" with respect to the inelastic material behavior, cf. [140]:

- compressible properties for $I_1 > 0$ with $\nu_+{}^{\text{in}} \in]-1,\ 1/2]$ and
- incompressible properties for $I_1 < 0$, $\nu_-^{\text{in}} = 1/2$.

The model can be used as a yield surface with the empirical restriction (34), which leads to the relation $d = k \in [1,\ 1.007]$. The latter condition is rather restrictive, which makes the fitting of the model to the measurements harder. However, the model should be preferred to the von Mises-model (16), since one obtains safer results in the region $I_1 > \sigma_+$ with $b_Z \in [0.98,\ 1]$ and $a_+^{\text{hyd}} \geq 2.89$ in regions, where the information on these loading cases are missing.

The model of Huber (156) can be extended (Fig. 43).

The new model reflects the observation, that "the hydrostatic pressure improves the material strength" [118]. This model consists of the ellipsoid of Beltrami with $\gamma_1 \in [0,\ 1[$ for $I_1 > 0$ and of the hyperboloid (Sect. 10.1) for $I_1 \le 0$:

$$3\,I_2' = \begin{cases} \dfrac{\sigma_{\text{eq}} - \gamma_1\,I_1}{1-\gamma_1}\,\dfrac{\sigma_{\text{eq}} + \gamma_1\,I_1}{1+\gamma_1}, & I_1 > 0,\ \text{ellipsoid of Beltrami;} \\ \dfrac{\sigma_{\text{eq}} - \gamma_0\,I_1\,i}{1-\gamma_1}\,\dfrac{\sigma_{\text{eq}} + \gamma_0\,I_1\,i}{1+\gamma_1}, & I_1 \le 0,\ \text{hyperboloid of one sheet.} \end{cases} \tag{160}$$

The transition at the cross-section $I_1 = 0$ is continuously differentiable. The values compute to

$$\nu_+^{\text{in}} = \frac{1}{2}\left(1 - 3\,\gamma_1^2\right), \qquad \nu_-^{\text{in}} = \frac{1}{2} + \frac{3\,\gamma_0^2}{2\left(1 - \gamma_0^2 - \gamma_1^2\right)}, \tag{161}$$

$$k^2 = \frac{1}{(1-\gamma_1)\,(1+\gamma_1)}, \qquad d = \frac{1}{\sqrt{1 - \gamma_0^2 - \gamma_1^2}}, \qquad a_+^{\text{hyd}} = \frac{1}{3\,\gamma_1}. \tag{162}$$

With $\gamma_0 = 0$ the model of Huber (156) is obtained. The value $\gamma_0 \neq 0$ results in a non-convex model, cf. [144, 221, 231]. With the setting $\gamma_0 = \gamma_1$ the model of Kuhn [118] is obtained. A model built up of two ellipsoids with the transition at the point K results for purely complex γ_0. The tangent line at the point K is parallel to the hydrostatic axis, cf. [212].

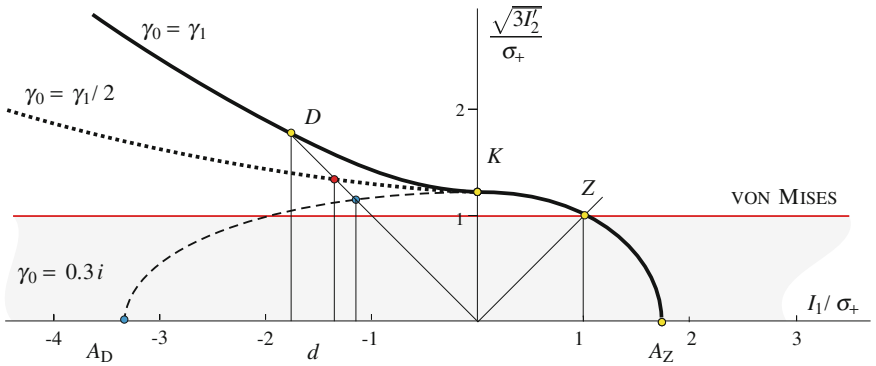

Fig. 43 Model of Kuhn with the C^1-transition at $I_1 = 0$ [107]: $\gamma_1 = 1/\sqrt{3}$, $\nu_+^{in} = 0$, $k = \sqrt{3/2}$, $a_+^{\text{hyd}} = 1/\sqrt{3}$ with; $\gamma_0 = \gamma_1$ ($d = \sqrt{3}$, $\nu_-^{\text{in}} = 2$), modification with $\gamma_0 = \gamma_1/2$ ($d = 2\sqrt{3/7}$, $\nu_-^{\text{in}} = 5/7$), combination of two ellipsoids with $\gamma_0 = 0.3\,i$ ($d = 1.1496$, $\nu_-^{in} = 0.32$, $a_-^{\text{hyd}} = -10/9$)

11.2.2 Modification of the Model of Huber

An analogous approach results in the modified model of Huber (Fig. 42) for the materials with the relation $d \geq k \geq 1$ and incompressibility in the region $I_1 \leq -d\,\sigma_+$ [103, 107, 113]

$$3\,I_2' = \begin{cases} \dfrac{\sigma_{\text{eq}} - \gamma_1\,I_1}{1-\gamma_1}\dfrac{\sigma_{\text{eq}} - \gamma_2\,I_1}{1-\gamma_2}, & I_1 > -d\,\sigma_+, \text{ ellipsoid;} \\ \dfrac{\sigma_{\text{eq}}}{1-\gamma_1}\dfrac{\sigma_{\text{eq}}}{1-\gamma_2}, & I_1 \leq -d\,\sigma_+, \text{ cylinder.} \end{cases} \tag{163}$$

In contrast to the model of Huber (156) the C^1-transition between two surfaces at the cross-section $I_1 = -d\,\sigma_+$ is defined by the point D (compression). The model can be better fitted to the measurements, that belong to the region $I_1 \in \left[-d\,\sigma_+,\ \sigma_+\right]$, it means in the region $D - K - Z$.

Further we obtain with (52)

$$k = \frac{\sqrt{2}\,d}{\sqrt{1+d}} \qquad \text{or} \qquad d = \frac{2\,k}{\sqrt{2^3 + k^2} - k} \tag{164}$$

based on the relation

$$d + \frac{1}{\gamma_1} = -\left(d + \frac{1}{\gamma_2}\right). \tag{165}$$

This relation sets the symmetry plane of the ellipsoid in the cross-section with $I_1 = -d\,\sigma_+$, see (129). There are three equations: for d and k and the constraint ν_-^{in}. The parameters of the model $\gamma_1 \in [0,\ 1[$ and $\gamma_2 < 0$ are unknown and should be determined. There are two solutions

$$\begin{cases} \nu_-^{\text{in}} = -\dfrac{-1 + \gamma_1^2 + \gamma_2^2 - \gamma_1\,\gamma_2}{(-2 + \gamma_1 + \gamma_2)\,(-1 + \gamma_1 + \gamma_2)}, \\ d = \dfrac{1}{1 - \gamma_1 - \gamma_2} \end{cases} \tag{166}$$

and

$$\begin{cases} \nu_-^{\text{in}} = -\dfrac{-1 + \gamma_1^2 + \gamma_2^2 - \gamma_1\,\gamma_2}{(-2 + \gamma_1 + \gamma_2)\,(-1 + \gamma_1 + \gamma_2)}, \\ k^2 = \dfrac{1}{(1 - \gamma_1)\,(1 - \gamma_2)}, \end{cases} \tag{167}$$

which should be compared. The conservative solution will be chosen. The solution of the above equations with $\nu_-^{\text{in}} = 1/2$ defined through (165) leads to

$$\begin{cases} \gamma_1 = \dfrac{1}{2\,d}\left(d - 1 + \sqrt{d^2 - 1}\right), \\ \gamma_2 = \dfrac{1}{2\,d}\left(d - 1 - \sqrt{d^2 - 1}\right) \end{cases} \tag{168}$$

or

$$\begin{cases} \gamma_1 = \dfrac{1}{4\,k}\left(3\,k - \sqrt{2^3 + k^2} + \sqrt{2}\sqrt{k\,(k + \sqrt{2^3 + k^2}) - 4}\right), \\ \gamma_2 = \dfrac{1}{4\,k}\left(3\,k - \sqrt{2^3 + k^2} - \sqrt{2}\sqrt{k\,(k + \sqrt{2^3 + k^2}) - 4}\right), \end{cases} \tag{169}$$

respectively.

The setting $d = k = 1$, which yields $\gamma_1 = \gamma_2 = 0$, results in the model of von Mises. With $d = 3\left(\sqrt{17} - 1\right)/8 \approx 1.17$ or $k = \sqrt{\left(9\sqrt{17} - 27\right)/8} \approx 1.12$ the value $\gamma_1 = 1/3$ is obtained. This corresponds to the value $a_+^{\mathrm{hyd}} = 1$ of the normal stress hypotheses. The Poisson's ratio at tension is computed as follows:

$$\nu_+^{\mathrm{in}} = \frac{3}{2\,d} - 1 = \frac{3\sqrt{8 + k^2}}{4\,k} - \frac{7}{4}. \tag{170}$$

For this model the yield condition should be restricted by (34). This results in restrictions for the parameters $d \in [1,\ 1.014]$ and $k \in [1,\ 1.010]$. With

$$a_+^{\mathrm{hyd}} = \frac{2}{3}\,\frac{d}{d - 1 + \sqrt{d^2 - 1}} \tag{171}$$

one gets $a_+^{\mathrm{hyd}} \geq 3.79$. This model is more suitable than the model of von Mises (16), which results in underpredictions in the region $I_1 > \sigma_+$.

The model can be applied instead of the paraboloid of Balandin (51). In this case incompressible yielding at compression can be obtained without the use of a non-associated flow rule (Sect. 4).

11.2.3 Combined Geometrical-Mechanical Model

A combined model can be built up based on the geometrical-mechanical model (105) with the transition at the cross-section $I_1 = 0$ (Fig. 44)

$$(3\,I_2')^3\,\frac{1 + c_3\cos 3\theta + c_6\cos^2 3\theta}{1 + c_3 + c_6} = \begin{cases} \left(\dfrac{\sigma_{\mathrm{eq}} - \gamma_1\,I_1}{1 - \gamma_1}\,\dfrac{\sigma_{\mathrm{eq}} + \gamma_1\,I_1}{1 + \gamma_1}\right)^3, & I_1 > 0; \\ \left(\dfrac{\sigma_{\mathrm{eq}}}{1 - \gamma_1}\,\dfrac{\sigma_{\mathrm{eq}}}{1 + \gamma_1}\right)^3, & I_1 \leq 0. \end{cases} \tag{172}$$

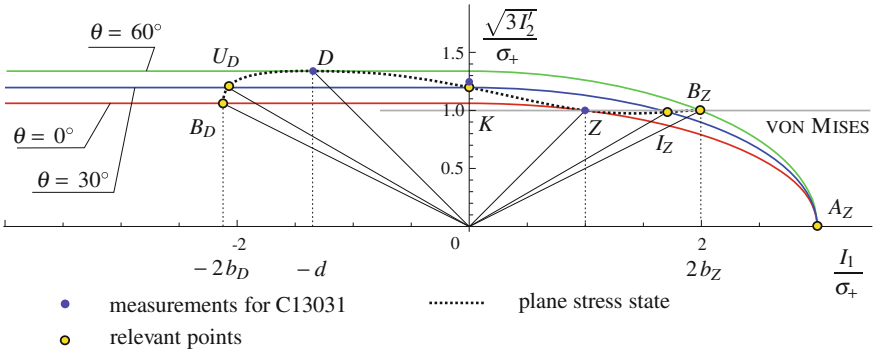

Fig. 44 Combined geometric mechanical model (172) for the polyoxymethylene (POM) Hostaform C13031, Ticona GmbH, Sulzbach, fitting starts from the values $d = 1.34$, $k = 1.25$ in the Burzyński-plane [113]: $k = 1.20$, $b_Z = 0.999$, $b_D = 1.06$, $\nu_+^{in} = 1/3$, $\nu_-^{in} = 1/2$, $a_+^{hyd} = 1$, $c_3 = 0.7885$, $c_6 = 0.3029$, $\gamma_1 = 1/3$

Since the necessary information on the material behavior under the hydrostatic tension (point A_Z) is almost always missing, the response under the hydrostatic tension can be defined by setting $\gamma_1 = 1/3$, which is based on the normal stress hypothesis (Sect. 2.1). It leads to the Poisson's ratio at tension with

$$\nu_+^{in} = \frac{1}{2}\left(1 - 3\,\gamma_1^2\right) \tag{173}$$

to $\nu_+^{in} = 1/3$. This setting can be corrected in dependence on the Poisson's ratio ν_+^{in}. For $\nu_+^{in} = 0.48$ one gets $\gamma_1 = 1/5\sqrt{3} \approx 0.1155$.

The values c_3 and c_6 can be computed from relations d and k, if the convexity restrictions (Fig. 20) are taken into account. These values result from the equations

$$k^6 = \frac{1 + c_3 + c_6}{(1 - \gamma_1^2)^3}, \qquad d^6 = \frac{1 + c_3 + c_6}{1 - c_3 + c_6}\,\frac{1}{(1 - \gamma_1)^3\,(1 + \gamma_1)^3}. \tag{174}$$

The model (172) can be recommended for many applications (Fig. 44).

A similar model with the C^1-transition at the cross-section $I_1 = -d\,\sigma_+$, cf. the modified model of Huber (163), can be formulated (Fig. 45).

The parameters c_3, c_6 and γ_2 of the model result from the formulas for d, k and $\nu_-^{in} = 1/2$. The last condition leads to the geometric relation (165)

$$\frac{1}{\gamma_2} = -\left(2\,d + \frac{1}{\gamma_1}\right). \tag{175}$$

This model has additional fitting possibilities in comparison to (172). Whether the model can be preferred over the model (172) it can be determined if further measurements, for instance at the points B_Z or B_D, are available. If only three measurements

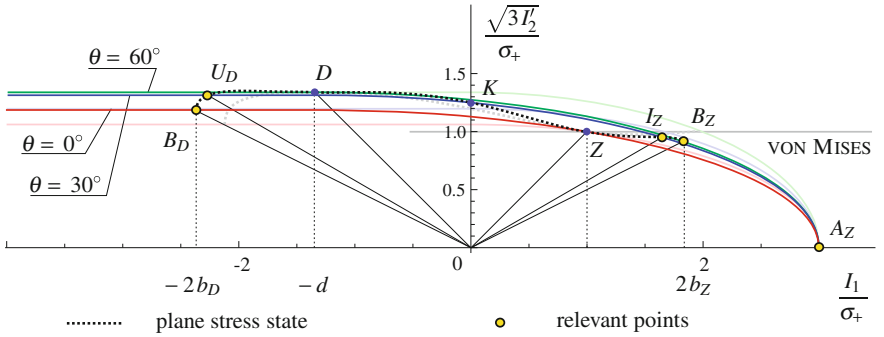

Fig. 45 Combined geometrical-mechanical model with the transition at $I_1 = -d\,\sigma_{\text{eq}}$ for the polyoxymethylene (POM) Hostaform C13031, Ticona GmbH, Sulzbach, with the values $d = 1.34$, $k = 1.25$ in the Burzyński-plane: $c_3 = 0.4743, c_6 = 0.3642, \gamma_2 = -0.1761, b_Z = 0.92, b_D = 1.19$, $\nu_+^{\text{in}} = 0.28$, $\nu_-^{\text{in}} = 1/2$, $a_+^{\text{hyd}} = 1$. The lines from Fig. 44 are shown for comparison [113]

at tension, compression and torsion (Z, K and D) exist, the application of the model with C^1-transition at $I_1 = -d\sigma_+$ is not meaningful.

12 Fitting

The objective function for fitting of the model to the measurements can be formulated in many ways, which lead to different results. The following three kinds of objective functions

- mathematical,
- physical and
- geometrical

can be considered [111, 114].

The mathematical objective functions are derived in a purely formal way, so that the fast convergence of the optimization routine can be achieved. Physical objective functions are based on a measurable value, which can be "related to mechanics". These conditions usually lead to complex implementations and slow computations. Geometrical criteria are based on the properties of the surface Φ.

12.1 Mathematical Criteria

This kind of objective functions will be presented using the geometrical-mechanical model (151) with the restriction (142) and the powers $j = 4$, $l = 2$, $m = 0$. The function Φ is rewritten in the form

$$\Omega = (3\,I_2^{'})^3\,\frac{1 + c_3\,\cos 3\theta + c_6\,\cos^2 3\theta}{1 + c_3 + c_6} - \left(\frac{\sigma_{\text{eq}} - \gamma_1\,I_1}{1 - \gamma_1}\right)^4 \left(\frac{\sigma_{\text{eq}} - \gamma_2\,I_1}{1 - \gamma_2}\right)^2, \tag{176}$$

so that the surface is given by the equation $\Omega = 0$.

The n measurements are given e. g. in the principal stress space σ_{I}^i, σ_{II}^i, σ_{III}^i, $i = 1 \ldots n$. The objective functions can be formulated as follows

$$f = \frac{1}{n-1} \sum_{i=1}^{n} \left| \Omega(c_3, c_6, \gamma_1, \gamma_2, \sigma_{\text{I}}^i,\, \sigma_{\text{II}}^i,\, \sigma_{\text{III}}^i) \right|^{m_1} \tag{177}$$

with $m_1 = 1,\ 2$ or

$$f_\infty = \max_{i=1\ldots n} \left| \Omega(c_3, c_6, \gamma_1, \gamma_2, \sigma_{\text{I}}^i,\, \sigma_{\text{II}}^i,\, \sigma_{\text{III}}^i) \right|. \tag{178}$$

Other exponents m_1 can be used, however they do not lead to any significantly different results. In order to compare various fitting results the following value is considered

$$f_{m_1} = (f)^{1/m_1}\,. \tag{179}$$

The optimization problem is formulated as

$$\text{minimize}\ f(c_3, c_6, \gamma_1, \gamma_2) \tag{180}$$

for the chosen meridian shape through j, l and m. The solution is obtained in the form of the parameters of the models c_3, c_6, γ_1 and γ_2. Using these parameters the measurements σ_{I}^i, σ_{II}^i, σ_{III}^i, $i = 1 \ldots n$ are approximated. This optimization problem contains the constraints for the parameters of meridians γ_1, γ_2, parameters of the cross-section c_3, c_6 and for the Poisson's ratios ν_+^{in}, ν_-^{in} (Sect. 4).

The function Ω (176) can be modified, so that additional solutions of the optimization for comparisons become possible, e. g.:

$$\left[(3\,I_2^{'})^3\,\frac{1 + c_3\,\cos 3\theta + c_6\,\cos^2 3\theta}{1 + c_3 + c_6}\right]^{l_1} - \left[\left(\frac{\sigma_{\text{eq}} - \gamma_1\,I_1}{1 - \gamma_1}\right)^4 \left(\frac{\sigma_{\text{eq}} - \gamma_2\,I_1}{1 - \gamma_2}\right)^2\right]^{l_1} = 0 \tag{181}$$

with the integer exponent $l_1 \geq 1$.

The formulation (176) is derived with $\sigma_+ = \sigma_{\text{eq}}$. If there are "enough" measurements the equivalent stress σ_{eq} can also be seen as a parameter subject to optimization.

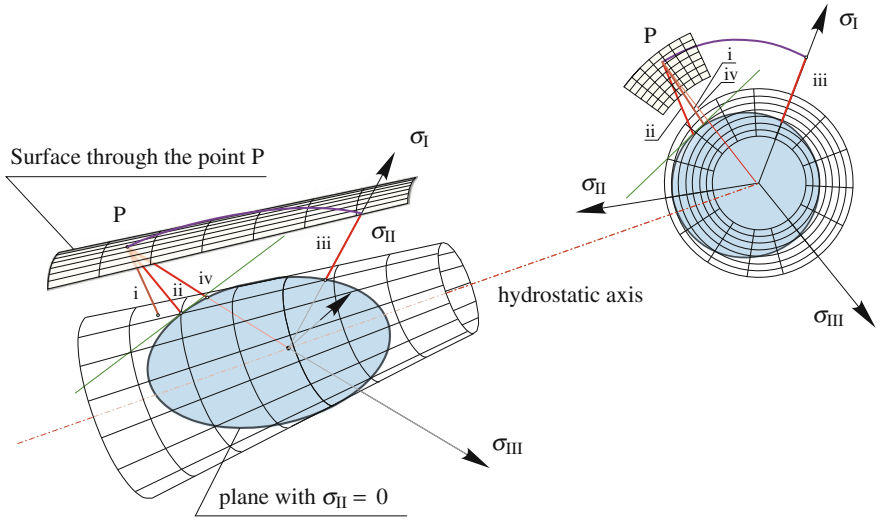

Fig. 46 Cone of Drucker-Prager (51) in the principal stress state (*left*) and in the π-plane (*right*). Comparison of the *four* physical optimization criteria

12.2 Physical Criteria

For a limit surface, which is defined implicitly in the form (5) or (6) and available measurements it is required to estimate the quality of fitting. Four physical criteria for estimation of the optimization quality are discussed (Fig. 46). In order to apply the criteria the measurements must be transformed into a principal stress state $(\sigma_{\mathrm{I}}^i, \sigma_{\mathrm{II}}^i, \sigma_{\mathrm{III}}^i)$ for $i = 1 \ldots n$. The four criteria can hardly be used in order to obtain the parameters of a model because of the high computational complexity. However, they can be used for comparison of different optimization results.

The criteria can be formulated as follows:

1. The regression quality in the principal stress space is evaluated, that is for each measurement the distance from the limit surface in the principal stress space $(\sigma_{\mathrm{I}}, \sigma_{\mathrm{II}}, \sigma_{\mathrm{III}})$ is computed and then averaged over all measurements. Formally that means, we start with a set of measurements $(\sigma_{\mathrm{I}}^i, \sigma_{\mathrm{II}}^i, \sigma_{\mathrm{III}}^i)$ and solve for each measurement the optimization problem

$$\begin{aligned} &\min\ (\sigma_{\mathrm{I}} - \sigma_{\mathrm{I}}^i)^2 + (\sigma_{\mathrm{II}} - \sigma_{\mathrm{II}}^i)^2 + (\sigma_{\mathrm{III}} - \sigma_{\mathrm{III}}^i)^2 \\ &\text{subject to } \Phi(\sigma_{\mathrm{I}}, \sigma_{\mathrm{II}}, \sigma_{\mathrm{III}}) = 0. \end{aligned} \tag{182}$$

The solution is obtained using a Lagrange multiplier. For example the function

$$F(\sigma_{\mathrm{I}}, \sigma_{\mathrm{II}}, \sigma_{\mathrm{III}}, \lambda) = (\sigma_{\mathrm{I}} - \sigma_{\mathrm{I}}^i)^2 + (\sigma_{\mathrm{II}} - \sigma_{\mathrm{II}}^i)^2 + (\sigma_{\mathrm{III}} - \sigma_{\mathrm{III}}^i)^2 - \lambda\, \Phi(\sigma_{\mathrm{I}}, \sigma_{\mathrm{II}}, \sigma_{\mathrm{III}}) \tag{183}$$

is defined and the stationary points are obtained from the equation

$$\nabla F = 0. \tag{184}$$

Generally this equation has more than one solution, however a single point $(z^i_{\mathrm{I}},\ z^i_{\mathrm{II}},\ z^i_{\mathrm{III}})$ of minimal distance on the limit surface is to be determined. Since the number of solutions is small, the correct one can be chosen by trial-and-error. Finally, the value of the objective function $f_{3\mathrm{D}}$ computes to

$$f_{3\mathrm{D}} := \frac{1}{n-1}\sum_{i=1}^{n}\sqrt{(\sigma^i_{\mathrm{I}} - z^i_{\mathrm{I}})^2 + (\sigma^i_{\mathrm{II}} - z^i_{\mathrm{II}})^2 + (\sigma^i_{\mathrm{III}} - z^i_{\mathrm{III}})^2}. \tag{185}$$

2. The minimal distance can be computed not in the principal stress space but for a plane stress state. For example we put $\sigma_{\mathrm{III}} = 0$ and hence simplify the optimization problem (182)

$$\begin{aligned} &\min\ (\sigma^i_{\mathrm{I}} - \sigma_{\mathrm{I}})^2 + (\sigma^i_{\mathrm{II}} - \sigma_{\mathrm{II}})^2 \\ &\text{subject to } \Phi(\sigma_{\mathrm{I}}, \sigma_{\mathrm{II}}, 0) = 0. \end{aligned} \tag{186}$$

A further computation is performed in analogy to the previous case. For each point $(\sigma^i_{\mathrm{I}},\ \sigma^i_{\mathrm{II}},\ 0)$ the point of minimal distance $(z^i_{\mathrm{I}},\ z^i_{\mathrm{II}},\ 0)$ on the curve

$$\Phi(\sigma_{\mathrm{I}},\ \sigma_{\mathrm{II}},\ 0) = 0 \tag{187}$$

is determined and the value of the objective function $f_{2\mathrm{D}}$ is estimated as follows

$$f_{2\mathrm{D}} := \frac{1}{n-1}\sum_{i=1}^{n}\sqrt{(\sigma^i_{\mathrm{I}} - z^i_{\mathrm{I}})^2 + (\sigma^i_{\mathrm{II}} - z^i_{\mathrm{II}})^2}. \tag{188}$$

3. If the model is based on the equivalent stress concept, that is

$$\Phi(\sigma_{\mathrm{I}},\ \sigma_{\mathrm{II}},\ \sigma_{\mathrm{III}},\ \sigma_{\mathrm{eq}}) = 0, \tag{189}$$

whereas $\sigma_{\mathrm{eq}} = \sigma_+$, a simple estimation for the quality of fitting can be proposed. The equivalent stress σ_{eq} is considered as a parameter as fitting is performed. The fitted equivalent stress is denoted by σ^*_{eq}. In order to estimate the quality of fitting for each point $(\sigma^i_{\mathrm{I}},\ \sigma^i_{\mathrm{II}},\ \sigma^i_{\mathrm{III}})$, $i = 1 \ldots n$ the value $\sigma_{\mathrm{eq}} = \sigma^i_{\mathrm{eq}}$ is computed so, that the point lies on the surface

$$\Phi(\sigma_{\mathrm{I}},\ \sigma_{\mathrm{II}},\ \sigma_{\mathrm{III}},\ \sigma^i_{\mathrm{eq}}) = 0, \tag{190}$$

i. e. the equation

$$\Phi(\sigma^i_{\mathrm{I}},\ \sigma^i_{\mathrm{II}},\ \sigma^i_{\mathrm{III}},\ \sigma^i_{\mathrm{eq}}) = 0 \tag{191}$$

must be solved for each $i = 1 \ldots n$ with respect to σ_{eq}^{i}. The estimated value f_{eq} computes to

$$f_{\mathrm{eq}} := \frac{1}{n-1} \sum_{i=1}^{n} \left| \frac{\sigma_{\mathrm{eq}}^{i} - \sigma_{\mathrm{eq}}^{*}}{\sigma_{\mathrm{eq}}^{*}} \right|. \tag{192}$$

4. The distance between the experimental point and the surface of model is measured along the line connecting the point with the origin. The sum of all the distances normalized by $n - 1$ computes to the value f_{ray}.

The criterion 1 is ubiquitous and can be used for an arbitrary set of measurements and an arbitrary surface. Often the measurements belong to a plane stress state, in this case the criterion 2 is of stronger physical relevance. Since it is a plausible assumption, that a measurement corresponding to a plane stress state is approximated by a point of the model, which also belong to a plane stress state. The criterion 3 is only suitable for the models based on the equivalent stress concept (2). It can be used too, if for instance torsion τ_* or compression σ_- are taken as the equivalent stress. An advantage of the criterion 4 is that it has a "mechanical background": Each measurement (e. g. torsion) is compared to the corresponding point on the surface (point K for torsion). It is clear that it can be easily applied and leads to relatively fast convergence of the optimization routine.

12.3 Geometrical Criteria

The principle of the conservative modeling can be stated as follows: among all best possible solutions the one is preferred, which represents the most conservative assumption about the material behavior [103]. Geometrical criteria allow to compare different optimal solutions. These criteria are listed below [108]:

- linear criteria:
  - the shortest length of the line in the meridian section of the closed surface Φ with the plane $\xi_2 = 0$ (Fig. 13, coordinates $(\xi_1,\ \xi_2,\ \xi_3)$, Figs. 34 and 35),
  - the minimal length of the line of the plane stress state,
  - the distance between the hydrostatic nodes A_{Z} and A_{D} for foams, ceramics, etc.,

$$\text{minimize} \left(\chi\, a_{-}^{\mathrm{hyd}} + (1-\chi)\, a_{+}^{\mathrm{hyd}} \right), \qquad \chi \in [0,\ 1] \tag{193}$$

and for materials with $a_{-}^{\mathrm{hyd}} \to \infty$

$$\text{minimize} \left(a_{+}^{\mathrm{hyd}} \right), \tag{194}$$

  - relation k: minimize (k),
  - relation d: minimize (d),

- square criteria:
  - the minimal area of the closed surface Φ in the principal stress space,
  - minimal area of the closed surface Φ in the meridian cross-section with the plane $\xi_2 = 0$,
  - minimal area circumscribed by the line of the plane stress state,
- cubic criteria, for instance the minimal volume circumscribed by the closed surface Φ in the principal stress space.

These criteria can be chosen in dependence on the measurements and the requirements imposed upon the model. A comparison of the criteria can be performed in the Pareto-diagram [44, 61, 152, 196]. The geometrical criteria allow to select a single point from the Pareto-solutions [114].

13 Applications

In order to illustrate the application of the models and fitting of the parameter, some measurements from the literature are analyzed. The stages of the analysis are visualized. The experimental data are normalized with respect to σ_+ for better comparison of the surfaces Φ.

13.1 Measurements of Coffin for Gray Cast Iron

29 measurements for the plane stress state for gray cast iron[8] are shown in Coffin-Schenectady [47] and approximated as follows:

- region Tension-Tension

$$\sigma_{\text{eq}} = \sigma_{\text{I}}, \qquad \sigma_{\text{eq}} = \sigma_{\text{II}} \tag{195}$$

  with $\sigma_{\text{eq}} = 33 \times 10^3$ psi.
- region Tension-Compression

$$\begin{aligned} (\kappa\, \sigma_{\text{eq}} + \sigma_0)^2 &= (k\, \sigma_{\text{I}} + \sigma_0)^2 - \sigma_{\text{II}}\, (k\, \sigma_{\text{I}} + \sigma_0) + \sigma_{\text{II}}^2, \\ (\kappa\, \sigma_{\text{eq}} + \sigma_0)^2 &= (k\, \sigma_{\text{II}} + \sigma_0)^2 - \sigma_{\text{I}}\, (k\, \sigma_{\text{II}} + \sigma_0) + \sigma_{\text{I}}^2 \end{aligned} \tag{196}$$

  with $\kappa = 3$ and $\sigma_0 = 30$ psi.
- region Compression-Compression

$$\sqrt{\frac{1}{2}\left[(\sigma_{\text{I}} - \sigma_{\text{II}})^2 + \sigma_{\text{I}}^2 + \sigma_{\text{II}}^2\right]} + \frac{1}{3}\,\mu\,(\sigma_{\text{I}} + \sigma_{\text{II}}) = \vartheta \tag{197}$$

[8] 3.08 % total C, 2.04 % Si, 0.56 % Mn, 0.112 % S, 0.33 % P

with $\mu = 0.51$ and $\vartheta = 88 \times 10^3$ psi.

The measurements were digitalized from the diagram $\sigma_{\mathrm{I}} - \sigma_{\mathrm{II}}$ [47] . The agreement with the approximation presented in the paper results for $\kappa = 2.9050$, $\mu = 0.5307$ and $\vartheta = 89.0202 \times 10^3$ psi and is to be ascribed to the precision of the digitalization and the rounding error. The computation of stresses leads to $\sigma_{\mathrm{BD}} = 137.76 \times 10^3$ psi, $\sigma_{\mathrm{UD}} = 148.20 \times 10^3$ psi, $\sigma_{-} = 108.15 \cdot 10^3$ psi, $\tau_{*} = 27.49 \times 10^3$ psi and $\sigma_{\mathrm{AZ}} = 33 \cdot 10^3$ psi.

For further evaluations the measurements are normalized with respect to $\sigma_{+} = 33 \times 10^3$ psi (Table 7). The relations of the evaluations are summarized in Table 8. The relations a_{Z} and b_{D} result from the extrapolations. The smallest value

$$b_{\mathrm{D}} = \frac{103.35}{33} = 3.13 \tag{198}$$

is obtained from the results of the test 11 with the convexity requirement

$$\frac{\sigma_{\mathrm{I}} - (-69.4)}{(-137.3) - (-69.4)} = \frac{\sigma_{\mathrm{II}} - (-137.3)}{(-69.4) - (-137.3)} \tag{199}$$

for $\sigma_{\mathrm{I}} = \sigma_{\mathrm{II}}$. If the classical material behavior (22) with $b_{\mathrm{D}} = d$ is assumed, the estimate

$$b_{\mathrm{D}} \in [3,\ 3.29] \tag{200}$$

is obtained from the measurements at axial compression.

The value b_{Z} can be estimated

$$b_{\mathrm{Z}} = \frac{28.52}{33} \ldots \frac{30.22}{33} = 0.86 \ldots 0.92. \tag{201}$$

The lower bound for a_{Z} is defined using the stress value $\sigma_{\mathrm{BZ}} = 30.22 \times 10^3$ psi and the convexity condition

$$2\sigma_{\mathrm{BZ}} < 3\sigma_{\mathrm{AZ}}. \tag{202}$$

It follows

$$a_{+}^{\mathrm{hyd}} > \frac{2}{3} \cdot \frac{30.22}{33} = 0.61. \tag{203}$$

13.1.1 Strain Hypothesis

In the first quadrant of the $\sigma_{\mathrm{I}} - \sigma_{\mathrm{II}}$-diagramm (region Tension-Tension, Fig. 47) the strain hypothesis (41) can be used instead of the normal stress hypothesis (8) in order to estimate relations in this region. For fitting of parameters and computation of the relations i_{Z}, b_{Z} and a_{Z} the model is used in the form (10) with (42). The Poisson's ratio computes to $\nu_{+}^{\mathrm{in}} \in [-0.0870,\ -0.0521]$ which is equivalent to $\gamma_{\mathrm{I}} \in [0.3681,\ 0.3913]$. Relations i_{Z}, b_{Z} and a_{Z} are specified in Table 8.

Table 7 Measurements by Coffin-Schenectady and their normalized values with respect to $\sigma_+ = 33 \cdot 10^3$ psi, the axiatoric-deviatoric invariants and the stress angle, plane stress state $\sigma_{III} = 0$

Test number	σ_I 10^3 [psi]	σ_{II} 10^3 [psi]	σ_I [-]	σ_{II} [-]	I_1 [-]	I_2' [-]	I_3' [-]	$\cos 3\theta$ [-]	θ [grad]
7	−77.60	−151.45	−2.35	−4.59	−6.94	5.2667	0.199442	0.0429	29. 2
11	−69.40	−137.30	−2.10	−4.16	−6.26	4.3278	0.065570	0.0189	29.6
12	−30.00	−116.95	−0.91	−3.54	−4.45	3.3881	−1.758632	−0.7327	45.7
23	−24.45	−120.52	−0.74	−3.65	−4.39	3.7268	−2.317541	−08369	48.9
	0	−108.67	0	−3.29	−3.29	3.6147	−2.645169	−1	60
	0	−101.78	0	−3.08	−3.08	3.1709	−2.173324	−1	60
46	0	−98.90	0	−3.00	−3.00	2.9939	−1.993946	−1	60
19	17.03	−67.68	0.52	−2.05	−1.53	1.8434	−0.809151	−0.8399	49.0
	23.28	−52.79	0.71	−1.60	−0.89	1.3948	−0.389280	−0.6140	42.6
18	25.35	−50.85	0.77	−1.54	−0.77	1.3827	−0.339070	−0.5418	40.9
	23.67	−47.65	0.72	−1.44	−0.73	1.2117	−0.279228	−0.5439	41.0
	32.60	−32.51	0.99	−0.99	0	0.9733	0.000814	0.0022	30
17	27.60	−27.47	0.84	−0.83	0	0.6962	0.000914	0.0041	29.9
	26.49	−26.49	0.80	−0.80	0	0.6442	−0.000002	0	30
	28.36	−14.52	0.86	−0.44	0.42	0.4368	0.058351	0.5251	19.4
9	30.25	−13.38	0.92	−0.41	0.51	0.4587	0.073234	0.6125	17.4
	30.58	0	0.93	0	0.93	0.2862	0.058921	1	0
6	32.55	0	0.99	0	0.99	0.3243	0.071085	1	0
	29.47	13.67	0.89	0.41	1.31	0.1997	0.004307	0.1254	27.6
	29.68	15.21	0.90	0.46	1.36	0.2023	−0.001518	−0.0434	30.8
	35.18	17.62	1.07	0.53	1.60	0.2841	−0.000188	−0.0032	30.1
	28.64	28.52	0.87	0.86	1.73	0.2501	−0.048125	−0.9999	59.8
	29.59	29.80	0.90	0.90	1.80	0.2699	−0.053974	−0.9998	59.7
4	30.22	30.22	0.92	0.92	1.83	0.2795	−0.056886	−1	60
	15.90	31.57	0.48	0.96	1.44	0.2288	−0.000551	−0.0131	30.3
	16.32	32.91	0.49	1	1.49	0.2487	0.000710	0.0149	29.7
	0	30.66	0	0.93	0.93	0.2877	0.059381	1	0
	0	33.28	0	1.01	1.01	0.3390	0.075957	1	0
1	0	34.18	0	1.04	1.04	0.3576	0.082308	1	0

The measurement number and the respective values for σ_I, σ_{II} are shown in Figs. 6, 7 and 8 in [47] The values for the measurement 23 with $\sigma_I = -42.900 \times 10^3$ psi, $\sigma_{II} = -104,000 \times 10^3$ psi (Fig. 8 in [47]) are different from the digitalized values, which are used for evaluation

13.1.2 Burzyński-Yagn Model

The measurements can be described using the rotationally symmetric model (51). The best approximation is obtained with the hyperboloid (Table 9).

The position of the measurements in the Burzynski-plane suggests that a rotationally symmetric model is not suitable in this case. The material behavior in the region Tension-Tension is underestimated and overestimated near the point B_D (Table 8).

Table 8 Relations for the evaluations of the measurements by Coffin-Schenectady, $\sigma_+ = 33 \times 10^3$ psi with different models

Approximation	b_D	u_D	d	k	i_Z	b_Z	a_+^{hyd}	ν_+^{in}	ν_-^{in}
Coffin	4.17	3.89	3.38	1.44	0.87	1	1	≥ 0	–
SH in the region TT	–	–	–	–	0.84	0.95	0.91	−0.05	–
SH in the region TT	–	–	–	–	0.82	0.92	0.85	−0.09	–
Eq. (51), hyperboloid	4.39	3.91	2.79	1.66	0.73	0.66	0.53	−0.20	1.24
Eq. (51), cone	7.15	4.61	2.34	1.40	0.83	0.78	1.62	0.07	1.51
Eq. (51), paraboloid	4.29	3.88	2.82	1.68	0.73	0.66	0.52	−0.21	1.21
UST by Yu, $b = 0.35$ with cut-off	3.05	3.03	3.05	1.39	0.87	1	1	0…0.16	1.53
UST by Yu, $b = 1$ with cut-off	3.05	3.52	3.05	1.49	0.87	1	1	0…0.16	1.53
Bigoni-Piccolroaz GMM (for Bigoni), $l = 3, m = 1$	3.58	3.71	3.04	1.50	0.88	0.89	0.92	0.09	1.51
GMM, straight line $l = m = 0$	3.48	3.85	2.92	1.49	0.92	0.94	1.40	0.14	1.54
GMM, parabola $l = 0, m = 1$	3.48	3.84	2.94	1.53	0.90	0.90	1.10	0.10	1.47
CPM: straight line $l = m = 0$	3.31	3.82	2.50	1.50	0.94	0.91	1.43	0.15	1.37
CPM: straight line $l = m = 0$	3.34	3.82	3.00	1.50	0.93	0.97	1.43	0.15	1.55
CPM: parabola $l = 0, m = 1$	3.41	3.80	3.00	1.53	0.90	0.91	1.11	0.10	1.48

13.1.3 Unified Strength Theory of Yu

The values b_D (198) and d are similar. It follows that UST (Sect. 10.2) with the relationship $b_D = d$ can be used. In [230] Yu puts $d = 3.05$, in order to describe the Tension-Compression region. In the Tension-Tension region the normal stress hypothesis is used as a cut-off (Sect. 11.1) [228, 229]. In Table 8 the relations for the parameters $b = 0.35$ und $b = 1$ are presented. In the third quadrant of the $\sigma_I - \sigma_{II}$-diagramm (Compression-Compression region) the UST is not sufficient.

Table 9 Parameters of the models for the approximation of the measurements by Coffin-Schenectady, $\sigma_+ = 33 \times 10^3$ psi

Model	Eq.	Meridian	f_2	γ_1	γ_2	c_3	c_6
		straight line	1.1935	0.2867		–	–
Burzyński-Yagn	(51)	hyperbola	0.7763	0.6345	0.0073	–	–
		parabola	0.7800	0.6451	0	–	–
GMM, $l = m = 0$		straight line	53.7926	0.2376		0.8671	0.2832
GMM, $l = 0, m = 1$	(152)	parabola	62.6810	0.3033	0	0.8161	0.2960
(for Bigoni), $l = 3, m = 1$		hyperbola	84.6122	0.3617	0.2721	0.6969	0.0805

Values of the objective function f_2 (179) are to be compared for respective models only
(for Bigoni)—approximation by Bigoni-Piccolroaz reformulated using GMM

13.1.4 Geometrical-Mechanical Model

The best approximation for GMM (151) is obtained with a straight meridian (Figs. 47, 48, 49, 50). The value $b_D = 3.48$ lies outside of the bounds given by (200).

These approximations with GMM can be compared to the approach by Bigoni-Piccolroaz [26] with seven parameters (Table 8). This approximation can be obtained using GMM with $l = 3$, $m = 1$ (Table 9).

The experimental results with $\sigma_I = \sigma_{II}/4$ cannot be represented by GMM. A precise approximation is however possible using the continuously differentiable GMM (Sect. 11.2.3) . The switching occurs in the plane $I_1 = -d\,\sigma_+$ with $d = 3 \ldots 3.29$.

13.1.5 Convex π-Plane Model

The results of fitting using GMM (105) with $n = 6$ can be also represented by CPM (99). The parameter γ_1 of the linear substitution (126) is the same (Table 9): $\gamma_1 = 0.2376$. With the parameters $c_3 = 0.8672$ and $c_6 = 0.2832$ the relations (106) are computed to

$$d_{\text{inc}} = \sqrt[6]{\frac{1 + c_3 + c_6}{1 - c_3 + c_6}}, \qquad k_{\text{inc}} = \sqrt[6]{1 + c_3 + c_6}. \tag{204}$$

The parameter $d_{\text{inc}} = 1.3149$ corresponds to the same parameter of CPM and with $d_{\text{inc}} = 1.3149, k_{\text{inc}} = 1.1361$ the bridge-parameter $\xi = 0.8766$ is computed. These values can be used as a starting point for optimization:

$$f_2 = 7.6597: \qquad d_{\text{inc}} = 1.3149, \qquad \xi = 0.8766, \qquad \gamma_1 = 0.2376. \tag{205}$$

The optimization results

$$f_2 = 6.0831: \qquad d_{\text{inc}} = 1.2122, \qquad \xi = 1, \qquad \gamma_1 = 0.2325 \tag{206}$$

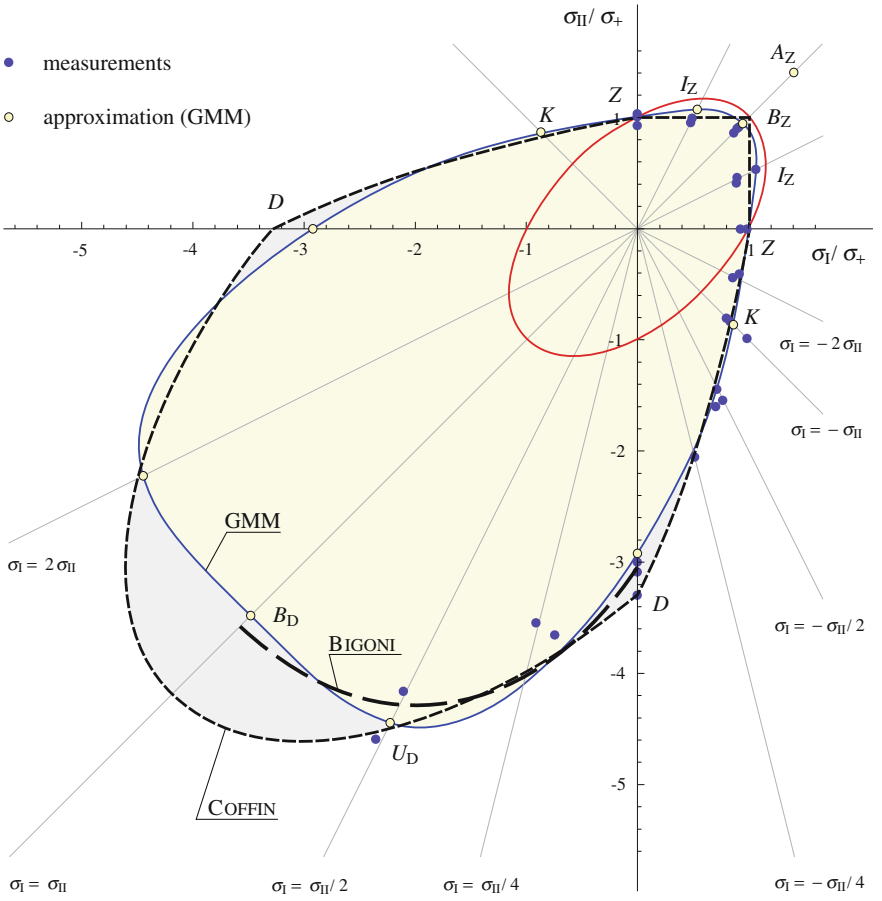

Fig. 47 Plane stress state $\sigma_{\mathrm{III}} = 0$: geometrical-mechanical model ($\sigma_+ = 33 \times 10^3$ psi, $\gamma_1 = \gamma_2 = 0.2375$, $c_3 = 0.8672$, $c_6 = 0.2832$, $l = m = 0$) with the values $b_{\mathrm{D}} = 3.48$, $d = 2.92$, $k = 1.49$ for gray cast iron (Table 8). The models of von Mises and the approximations of Coffin-Schenectady and Bigoni-Piccolroaz (between the points B_{D} and D) are shown for comparison

lead to the pyramid due to Haythornthwaite, which follows from the prism of Haythornthwaite (94) with the substitution (126) [107]. This approximation (Fig. 48, Model 1) underestimates the value at compression, it yields $d = 2.50$.

Additionally, it can be required, that the curve of the plane stress state contains the point D with the coordinates $\sigma_{\mathrm{I}} = 0$, $\sigma_{\mathrm{II}} = -98.90/33$ (relation $d = 3$), it follows (Fig. 48, Model 2)

$$f_2 = 8.1939: \qquad d_{\mathrm{inc}} = 1.3522, \qquad \xi = 0.9662, \qquad \gamma_1 = 0.2335. \tag{207}$$

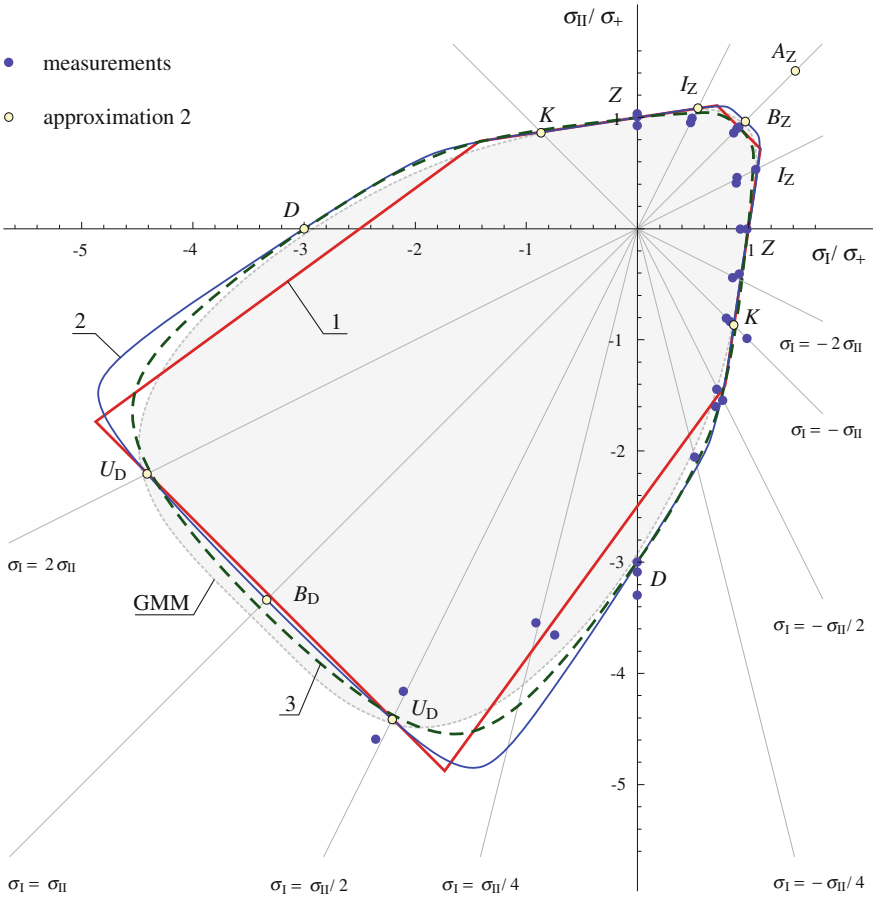

Fig. 48 Plane stress state $\sigma_{III} = 0$: CPM ($\sigma_+ = 33 \times 10^3$ psi) for gray cast iron (Table 8): *1* CPM with $l = m = 0$, $f_2 = 6.0831$: $d_{inc} = 1.2122$, $\xi = 1$, $\gamma_1 = 0.2325$, *2* CPM with $l = m = 0$ and $d \geq 3$, $f_2 = 8.1939$: $d_{inc} = 1.3522$, $\xi = 0.9662$, $\gamma_1 = 0.2335$, *3* CPM with $l = 0$, $m = 1$ and $d \geq 3$, $f_2 = 8.8342$: $d_{inc} = 1.3028$, $\xi = 0.8868$, $\gamma_1 = 0.3003$. The GMM (Fig. 47) is shown for comparison

Similar approximation (Fig. 48, Model 3) is obtained with the paraboloid $l = 0$, $m = 1$ using the substitution (124) and the restriction $d \geq 3$

$$f_2 = 8.8342: \qquad d_{inc} = 1.3028, \qquad \xi = 0.8868, \qquad \gamma_1 = 0.3003. \tag{208}$$

The models with a straight meridian fitted with the parameters (206), (207) should be preferred here because of their simplicity. The setting (208) with the parabolic meridian $l = 0$, $m = 1$ yields a lower value $a_Z = 1.11$. For further approximations see [1, 14, 34, 202].

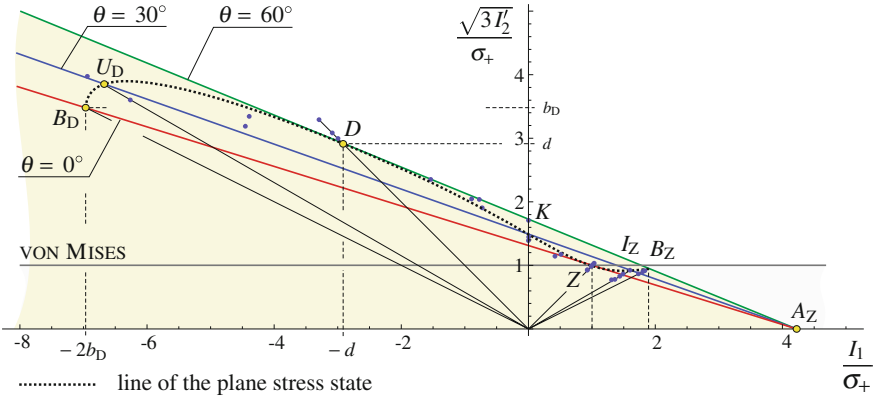

Fig. 49 Geometric-mechanical model ($\sigma_+ = 33 \cdot 10^3$ psi, $\gamma_1 = \gamma_2 = 0.2375$, $c_3 = 0.8672$, $c_6 = 0.2832$, $l = m = 0$) with the values $b_D = 3.48$, $d = 2.92$, $k = 1.49$ for gray cast iron (Table 8) in the Burzyński-plane. The models of von Mises is shown for comparison, s. (Fig. 47)

13.2 Measurements by Pae for Poly(oxymethylene) (POM)

The measurements for POM, du Pont Delrin 500, $\rho = 1.425\,\mathrm{g/cm^3}$ are provided in [151]. The following inaccuracies were found out after the analysis of the measurements from [151]:

- Molar mass and crystallinity were not specified;
- Table 1, hydrostatic pressure, $(\mathrm{psi}) \times 10^{-3}$;
- Table 1, average experimental yield stresses, the meausrement 10.5 is shifted from the column "Shear" in to the column "Tension";
- Figure 3 (a), hydrostatic axis, the factor $1/\sqrt{3}$ for the first invariant I_1 was not taken into account as the measurements were represented in the principal stress space: $p = 7.3\,\mathrm{kbar}$, $I_1 = 3 \cdot 7.3 \cdot 14503.8 = 317.63 \times 10^3$ psi. From the normalization with respect to σ_+ it follows $\frac{I_1}{\sigma_+} = \frac{317.63 \times 10^3}{10.6 \cdot 10^3} = 29.97\,[-]$. The hydrostatic node A_Z should lie at $29.97/\sqrt{3} = 17.3\,[-]$, (or with $\frac{7.25 \cdot 10^3}{0.0230} \frac{1}{10.6 \times 10^3} \frac{1}{\sqrt{3}} = 17.2\,[-]$, cf. Eq. (3) with $I_2' = 0$ and Table III in [151]). The difference results from the rounding error;
- Figures 3 (a) and (b), representation of the model in the π-plane, additionally to the cross-sections $I_1 = \text{const.}$ of the models of von Mises and Tresca a model with trigonal symmetry is shown, which is however not defined;
- The units in the Table III, [151] are not provided.

These measurements are visualized in the Burzyński-plane and approximated with a quadratic rotationally symmetric model (51), Fig. 51.

It can be seen in Fig. 51 that the points on the meridian $\theta = \pi/3$ are separated from the points on the meridians with $\theta = 0$ and $\theta = \pi/6$. So the trigonal symmetry of the surface can be assumed. The application of the geometrical-mechanical model

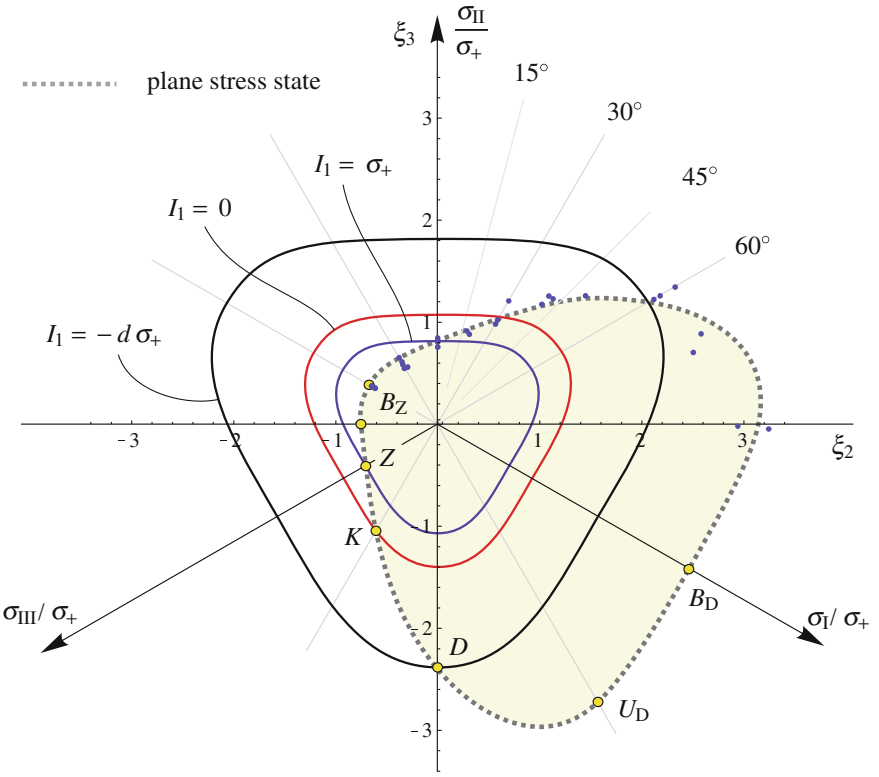

Fig. 50 Measurements by Coffin-Schenectady [47] in the π-plane approximated with the geometrical-mechanical model (151), s. Fig. 49, $d = 2.92$; line of the plane stress state with $\sigma_I = 0$. The cross-sections orthogonal to the hydrostatic axis with $I_1 = \text{const.}$ through the points Z, K and D are shown

(151) with the compressible substitution (146) can be recommended in this case. A possible approximation is shown in the Burzyński-plane (Fig. 52), in the plane $\sigma_I - \sigma_{II}$ (Fig. 53) and in the π-plane (Fig. 54). Further applications to POM can be found in [113].

13.3 Measurements of Cristensen for PVC Hard Foam

Closed-cell PVC (polyvinyl chloride) foam Divinycell H200 (DIAB International AB, Schweden) with the density $\rho = 200\,\text{kg/m}^3$ was tested in the region $D-K-Z$ (compression-torsion-tension) [46]. 25 measurements presented in the diagram σ_{11}-τ_{12} in [46] were digitalized (Fig. 55). The stresses at tension σ_+ corresponds to the data provided by the manufacturer [52] and indirectly to the measurements by

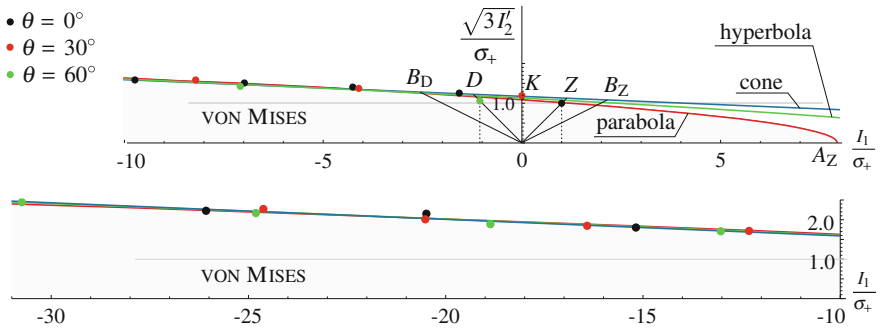

Fig. 51 Approximation of the measurements by Pae for POM in the Burzyński-plane with the quadratic rotationally symmetric model (51) with $\sigma_+ = 10.6 \times 10^3$ psi and σ_{eq} as a parameter: cone of Drucker-Prager (Mirolyubov): $\gamma_1 = \gamma_2 = 0.0403$, $\sigma_{eq} = 1.12$; $d = 1.09$, $k = 1.04$, $\nu_+^{in} = 0.44$, $\nu_-^{in} = 0.57$, paraboloid of Balandin: $\gamma_1 = 0.1277$, $\gamma_2 = 0$, $\sigma_{eq} = 1.01$; $d = 1.14$, $k = 1.07$, $\nu_+^{in} = 0.40$, $\nu_-^{in} = 0.60$, hyperboloid of Burzyński-Yagn: $\gamma_1 = 0.089$, $\gamma_2 = 0.0107$, $\sigma_{eq} = 1.07$; $d = 1.11$, $k = 1.05$, $\nu_+^{in} = 0.42$, $\nu_-^{in} = 0.58$. The diagram is divided in two regions $I_1 \in [-10,\ 8]$ and $I_1 \in [-31,\ -10]$ for clarity

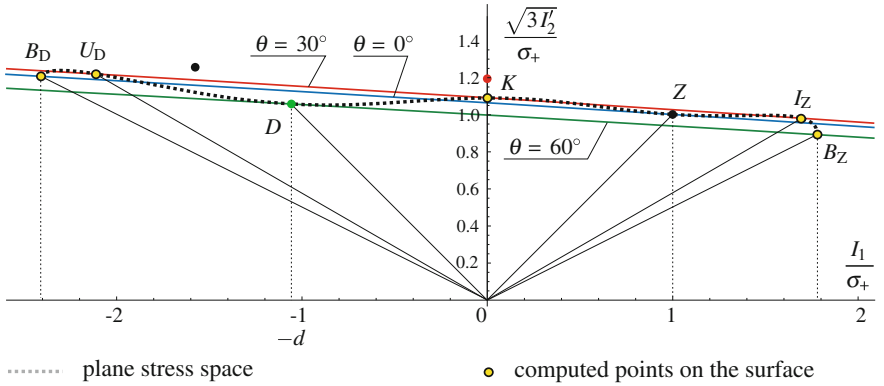

Fig. 52 POM-measurements by Pae in the Burzyński-plane approximated using the geometrical-mechanical model (151) with the parameters $\gamma_1 = 0.0869$, $\gamma_2 = 0$, $j = 4$, $l = 2$, $m = 0$, $c_3 = -0.2717$, $c_6 = 0.4314$ and $\sigma_{eq} = 1$: $d = \frac{11.2}{10.6} = 1.06$, $k = \sqrt{3}\,\frac{6.67}{10.6} = 1.09$, $\nu_+^{in} = 0.41$, $\nu_-^{in} = 0.63$. The region $I_1 \in [-2.5,\ 2]$ is shown for clarity

Gdoutos for the PVC-foam H 250 [72]. The stresses at compression σ_- are significantly lower compared to the data in [52, 72]. The value for torsion is also lower than the manufacturer's data and the measurements by Deshpande-Fleck and Gdoutos.

In order to present the models in the diagram σ_{11}–τ_{12} (Fig. 55) the invariants (Appendix 15) were reduced with $\sigma_{22} = \sigma_{33} = \tau_{13} = \tau_{23} = 0$ as follows

$$I_1 = \sigma_{11}, \qquad I_2' = \frac{1}{3}\,(\sigma_{11}^2 + 3\,\tau_{12}^2), \qquad I_3' = \frac{2}{3^3}\,\sigma_{11}^3 + \frac{1}{3}\,\sigma_{11}\,\tau_{12}^2. \tag{209}$$

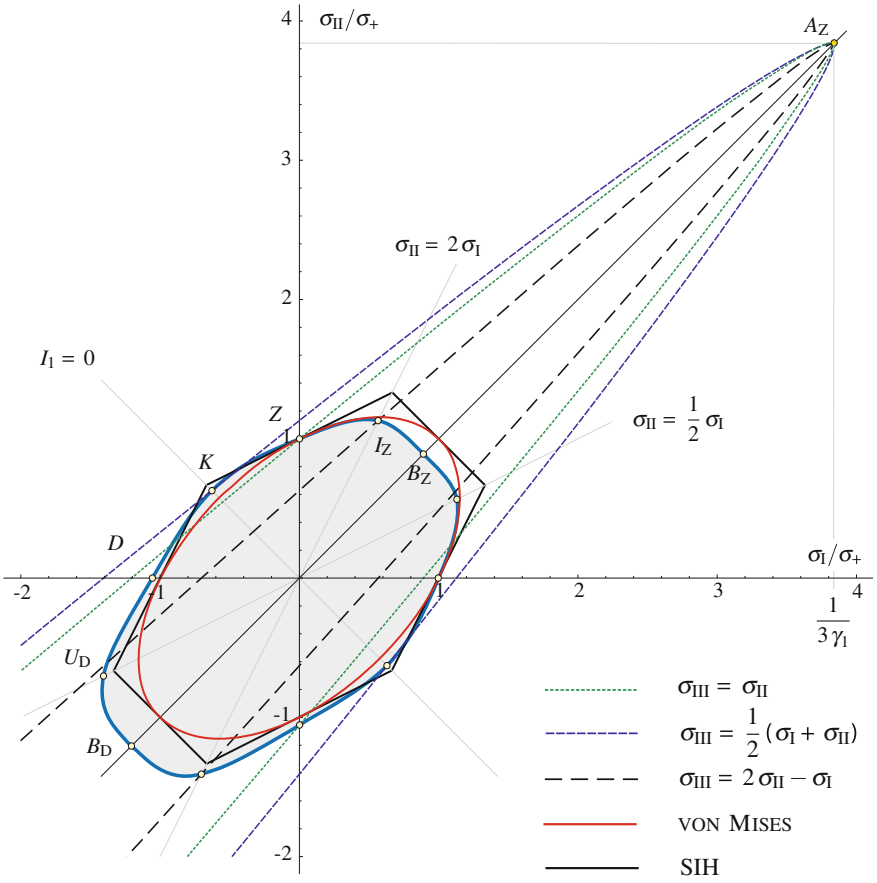

Fig. 53 Plane stress state $\sigma_{III} = 0$: geometrical-mechanical model for POM with the values $d = 1.06$, $k = 1.09$ (Fig. 52). The models of von Mises and Schmidt-Ishlinsky are shown for comparison

The restriction of the hydrostatic tension was set by Christensen according to the normal stress hypothesis ($a_+^{hyd} = 1$, $\gamma_1 = 1/3$) in order to obtain a closed limit surface in the tension region for the approximation with the paraboloid (open in the region $I_1 > 0$).

The combined model (paraboloid bounded by the normal stress hypothesis) presented by Christensen has singularities. A similar approximation can be obtained with the hyperboloid and the cone (51), Figs. 55 and 56. Further measurements can be described using the ellipsoid of Schleicher (51). These approximations are shown in the Burzyński-plane (Fig. 57), however they are not optimal:

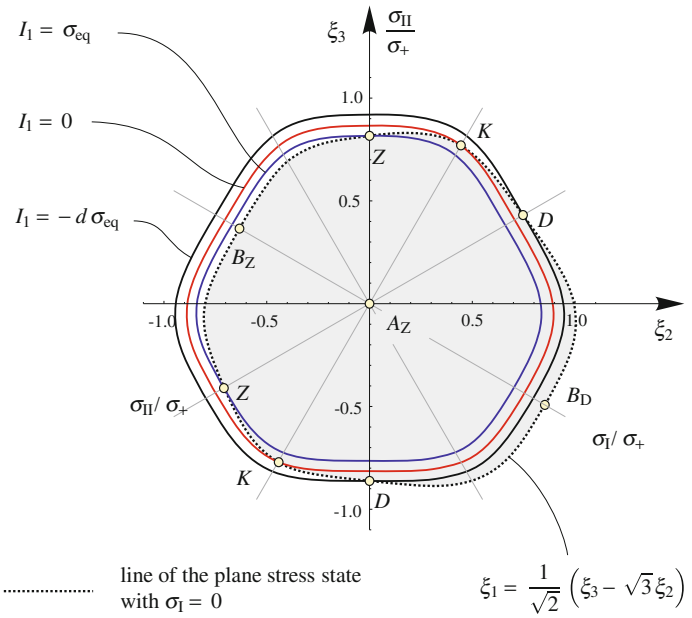

Fig. 54 Cross-sections $I_1 = \sigma_+$, $I_1 = 0$ and $I_1 = -d\,\sigma_+$ of the geometrical-mechanical model for POM with the values $d = 1.06$, $k = 1.09$ in the π-plane; see Figs. 52, 53 (for clarity only one section of the plane stress state with $\sigma_I = 0$ is shown)

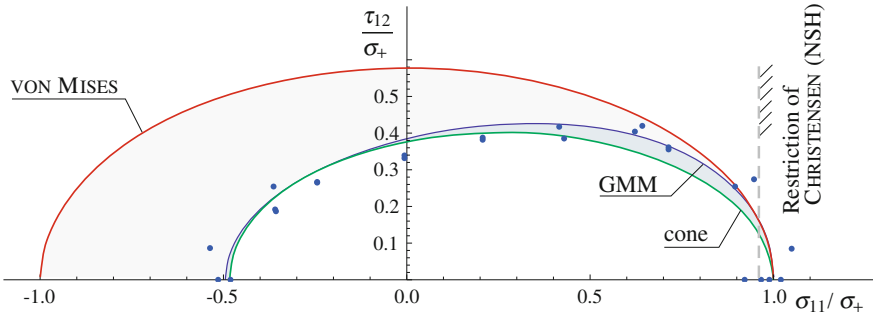

Fig. 55 Measurements by Christensen [46] in the diagram $\sigma_{11} - \tau_{12}$ with the normalization by $\sigma_+ = 7.12\,\text{MPa}$ and the models: cylinder of von Mises, Eq. (16); cone of Drucker-Prager, Eq. (51): $\gamma_1 = \gamma_2 = -0.5325$, $\nu_+^{in} = 1.30$, $\nu_-^{in} = 0.11$, $d = 0.48$, $k = 0.65$; GMM Eq. (151), $j = 2$, $l = 4$, $m = 0$ with $c_3 = -1.0585$, $c_6 = 0.2354$, $\gamma_1 = 0.4219$, $\gamma_2 = -0.5747$, $\nu_+^{in} = 1/2$, $\nu_+^{in} = -0.24$, $d = 0.49$, $k = 0.66$

- The cone, the paraboloid and the hyperboloid are in this case open in the direction $I_1 > 0$. The hydrostatic tension is not constrained, however such constraint is required.

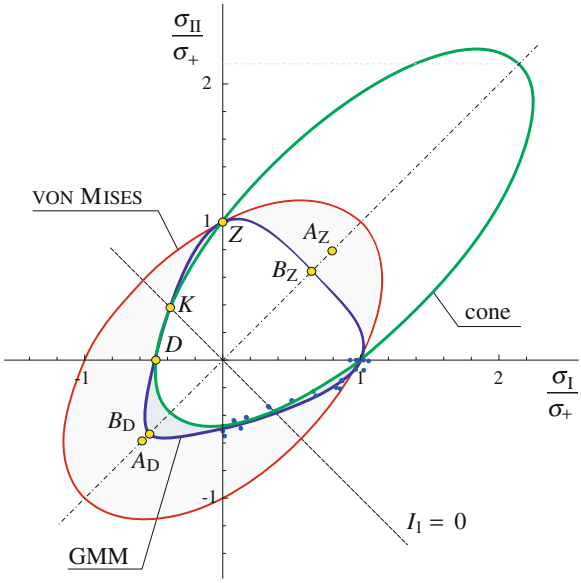

Fig. 56 Measurements by Christensen [46] in the diagram $\sigma_{\mathrm{I}}-\sigma_{\mathrm{II}}$, $\sigma_{\mathrm{III}}=0$ with the normalization by $\sigma_+ = 7.12\,\mathrm{MPa}$ with the models from Fig. 55. The points A_{Z} and A_{D} of the GMM are shown for clarity

- The ellipsoid of Schleicher is fitted under the constraint $\nu_+^{\mathrm{in}} \le 1/2$. The quality of this approximation is not sufficient, the material strength in the region $D-K-Z$ is overestimated.
- All the approximations with the rotationally symmetric models can not describe the typical $\backsim$-form of the curve of the plane stress state in the Burzyński-plane for the materials with $d < 1$ (cf. Figs. 58, 59 and 62).

In Figs. 57, 58 and 59 on the left and on the right hand side the constraints for the hydrostatic stresses at tension and compression are shown. These constraints result from the normal stress hypothesis and lead to a bounded region on the hydrostatic axis for approximation of hard foams.

13.3.1 Geometrical-Mechanical Model

In the first step the optimization $f_2 \to \min$ is performed for the geometric-mechanical model (151), (Fig. 58). Here the constraints are applied:

- $\gamma_1 = 1/3$ from the normal stress hypothesis and
- $\nu_+^{\mathrm{in}} \le 1/2$ as plausibility condition.

The line of the plane stress state approximates the measurements with a good quality, however the resulting extrapolation in the region $I_1 > \sigma_+$ is unconvincing:

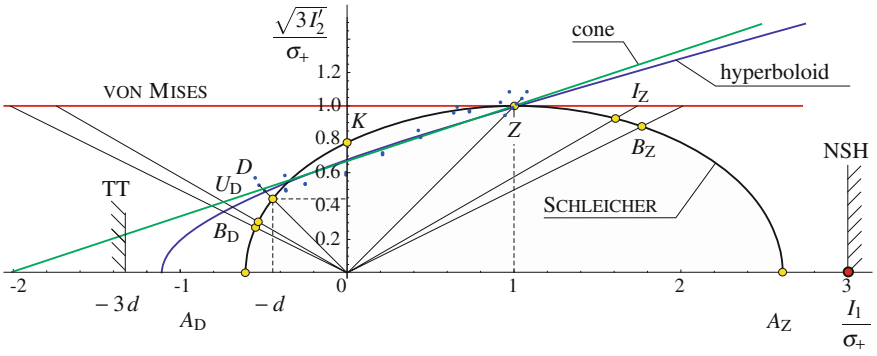

Fig. 57 Measurements by Christensen [46] in the Burzyński-plane approximated with the quadratic rotationally symmetric model (51), $\sigma_+ = 6.94$: ellipsoid of Schleicher with the constraints $\nu_+^{\text{in}} \leq 1/2$: $\gamma_1 = -1.6389$, $\gamma_2 = 0.3831$: $\nu_+^{\text{in}} = 1/2$, $\nu_-^{\text{in}} = -0.34$, $d = 0.44$, $k = 0.78$, $b_Z = 0.88$, $b_D = 0.27$; hyperboloid: $\gamma_1 = -0.9001$, $\gamma_2 = -0.1473$: $\nu_+^{\text{in}} = 1.14$, $\nu_-^{\text{in}} = 0.05$, $d = 0.49$, $k = 0.68$, $b_Z = 1.64$, $b_D = 0.37$; cone of Drucker-Prager: $\gamma_1 = \gamma_2 = -0.4956$: $\nu_+^{\text{in}} = 1.24$, $\nu_-^{\text{in}} = 0.13$, $d = 0.50$, $k = 0.67$, $b_Z = 1.98$, $b_D = 0.40$; NSH: Restriction from the normal stress hypothesis $\gamma_1 = 1/3$; TT: Restriction from the normal stress hypothesis as trigonal trapezohedron $3\,a_-^{\text{hyd}} = 3\,d$

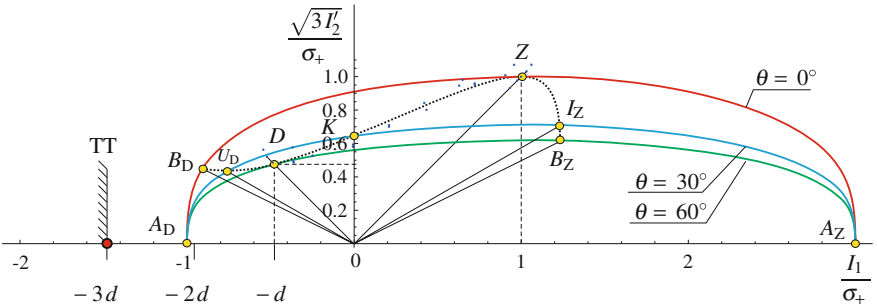

Fig. 58 Measurements by Christensen [46] in the Burzyński-plane approximated with the geometrical-mechanical model (151), $j = 1, l = 1, m = 4$ with $f_2 \rightarrow \min$, ($f_2 = 0.321$): $c_3 = -1.0950$, $c_6 = 0.2263$, $\gamma_1 = 1/3$, $\gamma_2 = -1$, $\gamma_3 == 0$, $\sigma_+ = 7.04$: $\nu_+^{\text{in}} = 1/2$, $\nu_-^{\text{in}} = 0.29$, $d = 0.53$, $k = 0.68$, $b_Z = 0.62$, $b_D = 0.49$; the optimization constraints $\gamma = 1/3$ and $\nu_+^{\text{in}} \leq 1/2$

- the surface Φ has a symmetry plane $I_1 = \sigma_+$ and
- there are no measurements available in the region $I_1 > \sigma_+$, which confirm the setting $\gamma_1 = 1/3$.

In Figs. 59, 60 and 61 a further approximation with the GMM (151) and setting for the meridian $j = 2, l = 4, m = 0$ is presented. This representation shows that the restriction obtained from the normal stress hypothesis $-\frac{1}{\gamma_2} > 3\,d$ does not hold in this case. A further approximation can be obtained with the GMM (151), $j = 1$, $l = 5, m = 0, \gamma_1 \in [0,\ 1[, \gamma_2 < 0$ (Fig. 62). The point A_D is shifted to the left.

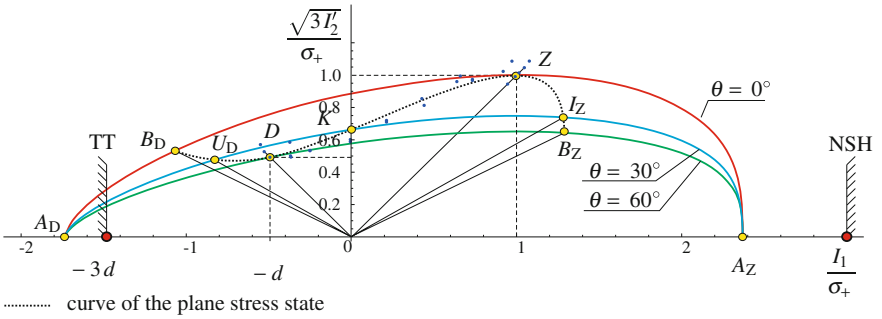

Fig. 59 Measurements by Christensen [46] in the Burzyński-plane approximated with the geometrical-mechanical model (151), $j = 2$, $l = 4$, $m = 0$, $f_2 \rightarrow \min$, ($f_2 = 0.229$): $c_3 = -1.0585$, $c_6 = 0.2354$, $\gamma_1 = 0.4219$, $\gamma_2 = -0.5747$, $\gamma_3 = 0$, $\sigma_+ = 7.12$: $\nu_+^{\text{in}} = 1/2$, $\nu_-^{\text{in}} = -0.24$, $d = 0.49$, $k = 0.66$, $b_Z = 0.64$, $b_D = 0.53$; the optimization constraints $d \geq 0.49$ and $\nu_+^{\text{in}} \leq 1/2$

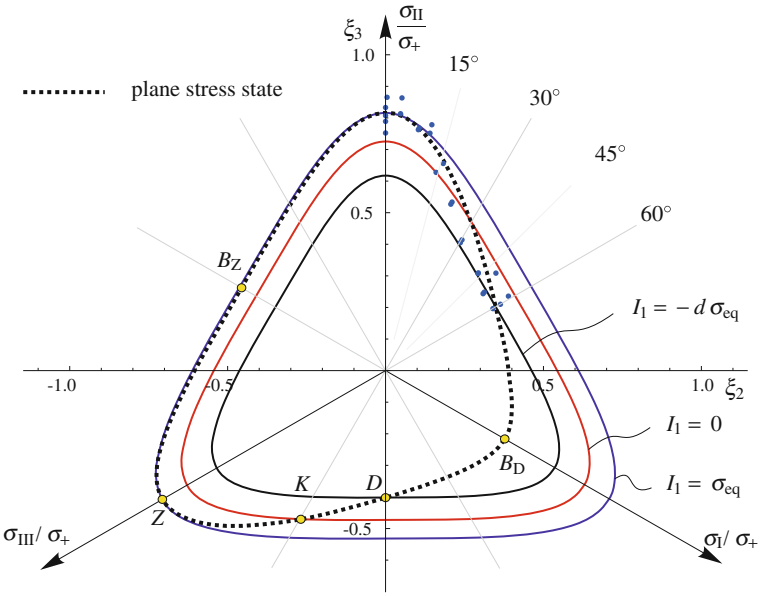

Fig. 60 Measurements by Christensen [46] in the π-plane approximated with the geometrical-mechanical model (151), see Fig. 59. The cross-sections orthogonal to the hydrostatic axis with $I_1 = \text{const.}$ through the points Z, K and D are shown

Both approximations with the constraints $d \geq 0.49$ and $\nu_+^{\text{in}} \leq 1/2$ lead to similar results for the points B_Z and B_D. A comparison of the Figs. 57, 58, 59 and 62 shows the differences of the approximations. For a more precise description of the plane stress state the loading points B_D and B_Z are necessary. The respective testing

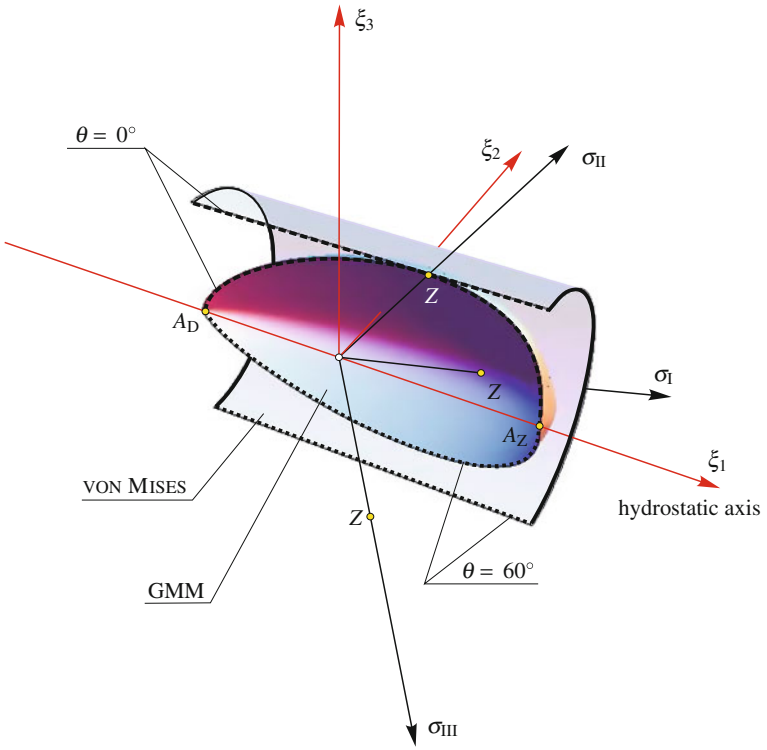

Fig. 61 Geometric-mechanical model (151) with the parameters from Fig. 59 and the model of von Mises in the principal stress space (σ_I, σ_{II}, σ_{III}), (the surfaces are cut for clarity; with $\theta = 0°$ and $\theta = 60°$ the meridians are labeled)

procedures for hard foams are described in [112]. The value at the point B_Z reduces the interval $a_+{}^{\text{hyd}} \in \left]\frac{1}{3},\ 1\right]$ to $a_+{}^{\text{hyd}} \in \left]\frac{2}{3}\, b_Z,\ 1\right]$ because of the convexity condition.

The optimization constraint $\nu_+^{\text{in}} \leq 1/2$ allows to obtain plausible approximations as in Figs. 57, 58, 59 and 62 with $\nu_+^{\text{in}} = 1/2$. In order to justify this constraint the test B_Z is required as well.

13.3.2 Linear Geometrical Criterion

A further criterion based on a simple approach (Sect. 12.3) can be applied in order to compare the available approximations, e. g. the geometric criterion (193) with the equally weighted nodes $\chi = 1/2$. For the approximation in Fig. 62 it can be obtained:

$$\frac{1}{2}\left(\frac{1}{\gamma_1} - \frac{1}{\gamma_2}\right) = \frac{1}{2}\left(\frac{1}{0.6050} - \frac{1}{0.4415}\right) = 1.96. \tag{210}$$

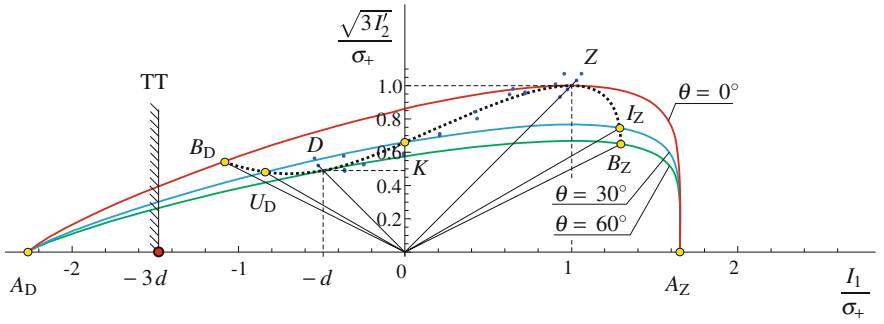

Fig. 62 Measurements by Christensen [46] in the Burzyński-plane approximated with the geometrical-mechanical model (151), $j = 1$, $l = 5$, $m = 0$, $f_2 \to \min$, ($f_2 = 0.226$): $c_3 = -1.0380$, $c_6 = 0.2405$, $\gamma_1 = 0.6050$, $\gamma_2 = -0.4415$, $\sigma_+ = 7.22$: $\nu_+^{\text{in}} = 1/2$, $\nu_-^{\text{in}} = 0.26$, $d = 0.49$, $k = 0.66$, $b_Z = 0.65$, $b_D = 0.54$; the optimization constraints $d \geq 0.49$ and $\nu_+^{\text{in}} \leq 1/2$

The criterion leads to the values 2 and 2.06 for Figs. 58 and 59, respectively. It follows, that the approximation (Fig. 62) is to be preferred according to the criterion (210). The same result is obtained for $\chi = 0$.

13.3.3 Combined Geometrical-Mechanical Criterion

The position of the hydrostatic nodes A_D and A_Z can be adjusted, if the combined models (Sect. 11.2) are used and so a more conservative solution can be obtained. For this approximation of the measurements by Christensen a C^1-combination of two surfaces can be used. The surfaces are connected in the cross-section $I_1 = \sigma_+$, so that $\nu_+^{\text{in}} = 1/2$ holds. The second surface in the region $I_1 > \sigma_+$ with the same values of the parameters c_3, c_6 is continuously differentiable coupled with the first one.

The parameter $\gamma_1 \in [1/3,\ 1\ [$ of the right surface in the Burzyński-plane can be fitted according to the assumption regarding the position of the point A_Z, for instance based on the normal stress hypothesis ($a_+^{\text{hyd}} = 1$):

- $\gamma_1 = \dfrac{1}{3}$, $\gamma_2 = -1$, $j = 1$, $l = 1$, $m = 4$, cf. Fig. 58;
- $\gamma_1 = \dfrac{1}{3}$, $\gamma_2 = -\dfrac{1}{3}$, $j = 2$, $l = 4$, $m = 0$, cf. Fig. 59;
- $\gamma_1 = \dfrac{1}{3}$, $\gamma_2 = -\dfrac{1}{9}$, $j = 1$, $l = 5$, $m = 0$, cf. Fig. 62, etc.

These approximations result in similar values of b_Z. Contrary to $a_+^{\text{hyd}} = 1$ a more conservative value, for instance with $a_+^{\text{hyd}} = 1/2$ and $\nu_+^{\text{in}} = 1/2$ can be obtained. It follows then $\gamma_1 = 2/3$ (Fig. 63).

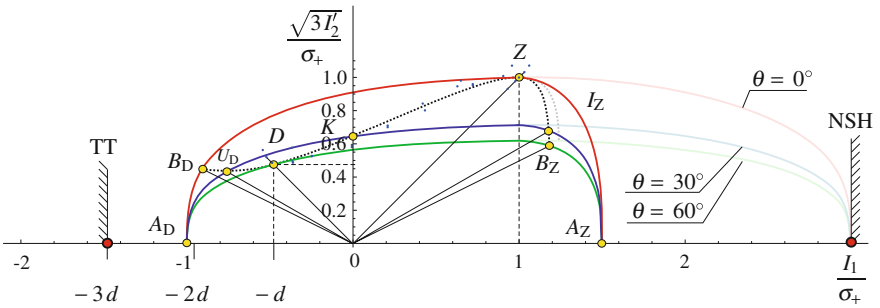

Fig. 63 Measurements by Christensen [46] in the Burzyński-plane approximated with the combined geometrical-mechanical model (151) with $j = l = 1, m = 4, c_3 = -1.0950, c_6 = 0.2263$: Region $I_1 \leq \sigma_{eq}$: $\gamma_1 = 1/3, \gamma_2 = -1, \nu_+^{in} = 1/2, \nu_-^{in} = 0.29, d = 0.53, k = 0.68, b_D = 0.49$ (Fig. 58), Region $I_1 > \sigma_+$: $\gamma_1 = 2/3, \gamma_2 = 2, \nu_+^{in} = 1/2, b_Z = 0.60$

14 Summary and Outlook

The modeling of the deformation and limit behavior of real materials is influenced by many phenomena. In the case of traditional materials and applications the number of influence factors taken into account is reduced. The corresponding models are simple and easy manageable. As usual they are based on a small number of material parameters. The experimental identification of the parameters and verification of the models is often simple. In many situations one needs only one basic test [8].

For high tech materials or applications with increasing safety requirements it is necessary to take into account non-classical effects since they have a significant influence on the deformation and limit behavior. Such phenomena are the different behavior at tension and compression—strength differential effect (SD-effect), the influence of the hydrostatic pressure, the Poynting-Swift-effect, the Kelvin-effect, etc. [8, 16, 229]. In contrast to the classical material behavior, which can be described by tensorial linear equations only, non-classical behavior partly should be presented by tensorial non-linear equations. The effects related to these equations are sometimes named second order effects [169]. They can be observed for elastic, plastic, creep behavior and in fluid mechanics [8, 169]. Therefore in this chapter several models allowing the description of complex material behavior are presented.

The models discussed in this chapter are limited by the assumption of isotropic material behavior. Further investigation should be directed on extension of these models to the case of anisotropic materials. In addition, the application of the suggested models to coated materials is not clear.

The concept of the equivalent stress is a simple and traditional engineering way to solve problems related to the strength prediction or material behavior modeling. The formulation and investigation of limit criteria will be in the focus of the scientific community in the future. The reason ist that one has new materials and particular application field [4].

The development of the concept of the equivalent stress is considered in conjunction with:

- materials science,
- thermo-dynamics,
- morphology, and
- advanced measurement programs.

This results in verification of new effects that result from the model, in the precise description of the failure with the consideration of the physical processes, taken into account the phase transitions for the definition of the limits of the parameters.

15 Invariants

Assuming isotropic material behavior the invariants of the stress tensor play an important role in the formulation of the equivalent stress expression. Here we define several sets of invariants mostly used in practical situations [8, 234].

15.1 Principal Invariants

Let us postulate that the stress state is defined by the stress tensor $\boldsymbol{\sigma}$. This tensor is a symmetric second rank tensor. The principal invariants are the solution of the eigenvalue problem

$$(\boldsymbol{\sigma} - \lambda \boldsymbol{I}) \cdot \boldsymbol{n} = \boldsymbol{0}. \tag{211}$$

$\boldsymbol{I}$ is the unit second rank tensor, $\boldsymbol{n}$ denotes the eigendirections and λ the eigenvalues of the problem. In our case the eigenvalues are named principal values or principal stresses. For the stress tensor it can be shown that the principal stresses are real-valued. Three different cases should be distinguished:

- three different solutions,
- one single and one double solution, and
- one triple solution

The necessary conditions for the solution of the problem (211) results in

$$\boldsymbol{n} = \boldsymbol{0} \quad \text{or} \quad |\boldsymbol{\sigma} - \lambda \boldsymbol{I}| = \det(\boldsymbol{\sigma} - \lambda \boldsymbol{I}) = 0. \tag{212}$$

The first Eq. (212) is a trivial solution. The second equation (212) is of greater importance since the principal stresses can be computed with help of this condition. The solution can be obtained from

$$\lambda^3 - I_1(\boldsymbol{\sigma})\lambda^2 + I_2(\boldsymbol{\sigma})\lambda - I_3(\boldsymbol{\sigma}) = 0, \tag{213}$$

where $I_i(\boldsymbol{\sigma})$, $(i = 1, 2, 3)$ are the invariants of the stress tensor

$$\begin{aligned} I_1(\boldsymbol{\sigma}) &= \boldsymbol{I} \cdot\cdot\, \boldsymbol{\sigma}, \\ I_2(\boldsymbol{\sigma}) &= \frac{1}{2}\left[I_1^2(\boldsymbol{\sigma}) - I_1\left(\boldsymbol{\sigma}^2\right)\right], \\ I_3(\boldsymbol{\sigma}) &= |\boldsymbol{\sigma}| = \det \boldsymbol{\sigma} = \frac{1}{3}\left[I_1\left(\boldsymbol{\sigma}^3\right) + 3I_1(\boldsymbol{\sigma})I_2(\boldsymbol{\sigma}) - I_1^3(\boldsymbol{\sigma})\right]. \end{aligned} \tag{214}$$

The solutions of Eq. (213) are named principal invariants or principal stresses λ_i, $i = 1, 2, 3$. The following relations are valid after ordering the λ_i-values

$$\sigma_{\mathrm{I}} \geq \sigma_{\mathrm{II}} \geq \sigma_{\mathrm{III}}. \tag{215}$$

If the principal stresses are distinguished that means

$$\sigma_{\mathrm{I}} \neq \sigma_{\mathrm{II}} \neq \sigma_{\mathrm{III}}, \tag{216}$$

the following spectral decomposition holds

$$\boldsymbol{\sigma} = \sigma_{\mathrm{I}} \boldsymbol{n}_{\mathrm{I}} \boldsymbol{n}_{\mathrm{I}} + \sigma_{\mathrm{II}} \boldsymbol{n}_{\mathrm{II}} \boldsymbol{n}_{\mathrm{II}} + \sigma_{\mathrm{III}} \boldsymbol{n}_{\mathrm{III}} \boldsymbol{n}_{\mathrm{III}}, \tag{217}$$

where $\boldsymbol{n}_{\mathrm{I}}, \boldsymbol{n}_{\mathrm{II}}, \boldsymbol{n}_{\mathrm{III}}$ are the eigendirections (principal directions), which can be obtained from the solution of

$$(\boldsymbol{\sigma} - \sigma_i \boldsymbol{I}) \cdot \boldsymbol{n}_i = \boldsymbol{0}, \quad \boldsymbol{n}_i \cdot \boldsymbol{n}_j = \delta_{ij}. \tag{218}$$

δ_{ij} is the Kronecker symbol. The last equation in (218) is the orthogonality condition for the principal directions.

15.2 Irreducible Invariants

The stress tensor has three irreducible invariants:

- the linear invariant $J_1(\boldsymbol{\sigma}) = I_1(\boldsymbol{\sigma}) = \boldsymbol{I} \cdot\cdot\, \boldsymbol{\sigma}$,
- the quadratic invariant $J_2(\boldsymbol{\sigma}) = \boldsymbol{\sigma} \cdot\cdot\, \boldsymbol{\sigma}$,
- the cubic invariant $J_3(\boldsymbol{\sigma}) = (\boldsymbol{\sigma} \cdot \boldsymbol{\sigma}) \cdot\cdot\, \boldsymbol{\sigma}$.

The following representation is also possible

- the linear invariant $J_1(\boldsymbol{\sigma}) = I_1(\boldsymbol{\sigma}) = \boldsymbol{I} \cdot\cdot\, \boldsymbol{\sigma}$,
- the quadratic invariant $J_2(\boldsymbol{\sigma}) = \frac{1}{2}\boldsymbol{\sigma} \cdot\cdot\, \boldsymbol{\sigma}$,
- the cubic invariant $J_3(\boldsymbol{\sigma}) = \frac{1}{3}(\boldsymbol{\sigma} \cdot \boldsymbol{\sigma}) \cdot\cdot\, \boldsymbol{\sigma}$.

15.3 Axiatoric-Deviatoric Invariants

The axiatoric-deviatoric invariants are based on the principal invariants of the stress deviator, which can be computed from the eigenvalue problem for the deviator

$$\boldsymbol{s} = \boldsymbol{\sigma} - \frac{1}{3}\boldsymbol{\sigma} \cdot\cdot \boldsymbol{I} = \boldsymbol{\sigma} - \frac{1}{3} I_1(\boldsymbol{\sigma})\boldsymbol{I} \tag{219}$$

Principal deviatoric stresses follow from

$$|\boldsymbol{s} - \lambda \boldsymbol{I}| = \det(\boldsymbol{s} - \lambda \boldsymbol{I}) = 0 \tag{220}$$

or

$$\lambda^3 - I_1(\boldsymbol{s})\lambda^2 + I_2(\boldsymbol{s})\lambda - I_3(\boldsymbol{s}) = 0, \tag{221}$$

which can be simplified with respect to $I_1(\boldsymbol{s}) = 0$

$$\lambda^3 + I_2(\boldsymbol{s})\lambda - I_3(\boldsymbol{s}) = 0.$$

Here the second and the third invariants are equal to

$$I_2(\boldsymbol{s}) = -\frac{1}{2} J_2\left(\boldsymbol{\sigma}^2\right), \qquad I_3(\boldsymbol{s}) = |\boldsymbol{s}| = \det \boldsymbol{s} = \frac{1}{3} J_3\left(\boldsymbol{s}^3\right). \tag{222}$$

For a better distinguishing incompressible and compressible material behavior the second, the third deviatoric and the axiatoric invariant will be used

$$I_1(\boldsymbol{\sigma}) = \boldsymbol{\sigma} \cdot\cdot \boldsymbol{I}. \tag{223}$$

15.4 Cylindrical Invariants

There are other sets of invariants, for example, Novozhilov's invariants [148], which are defined as it follows

- the axiatoric invariant (223)
- the second invariant of the stress deviator (222)

$$I_2(\boldsymbol{s}) = -\frac{1}{2} J_2\left(\boldsymbol{s}\right),$$

- and the stress angle

Table 10 Main criteria

Abbrev.	Name	Reference	Section	Equation	BP	3D	π
Classical Strength Theories							
NSH	Normal Stress Hypothesis (Rankine)	[166, 175]	2.1	8	14	2	
	Tresca	[209]	2.2	13	15		22
	von Mises	[85, 91, 139]	2.3	16	14	2	22
SI	Schmidt-Ishlinsky	[92, 182]	2.4	17	15		22
Standard Models (Pressure-Sensitive Criteria)							
SH	Strain Hypothesis	[8, 174]	6.1	41			
MSH	Maximum Strain Hypothesis	[134]	6.1				
MC	Mohr-Coulomb	[141]	6.2	45			
PL	Pisarenko-Lebedev	[121]	6.3	48		38	
SD	Sdobirev	[191]	6.3				
	Burzyński-Yagn	[36, 220]	6.4	51	17		
	Drucker-Prager, Mirolyubov	[56, 138]	6.4		17	6	
	Balandin, Burzyński-Torre	[17, 36, 207]	6.4		17	11	
	Beltrami	[21]	6.4		17	12	
	Schleicher	[179]	6.4			34	
Mathematical Formulations (Pressure-Sensitive Criteria)							
	Altenbach-Zolochevsky I	[7]	7.1	56			
	Altenbach-Zolochevsky II	[8]	7.2	63			
Pressure-Insensitive Criteria with Trigonal Symmetry							
	Sayir I	[178]	9.1.1	87		18	
	Sayir II	[178]	9.1.2	89			
	Haythornthwaite	[83]	9.1.3	94			
CPM	Convex π-plane model	[33]	9.1.4	99			
	Radcig model	[105]	9.1.5	100			
GMM	Geometrical-Mechanical Model	[107]	9.1.6	105			
TQM	Triquadratic model	[103]	9.1.7	108			
Pressure-Insensitive Criteria with Hexagonal Symmetry							
UYC	Unified Yield Criterion of Yu	[222, 229]	9.2.1	111			22
	Sokolovsky	[157]	9.2.1				
BCM	Bicubic model	[103]	9.2.2	113			
MAC	Multiplicative Ansatz Criterion	[116]	9.2.3	116			
	Ishlinsky-Ivlev	[93, 98]	9.2.3				
	Universal model with hexagonal symmetry	[116]	9.2.4	121			
	Model based on the stress angle	[33]	9.2.5	122			
	Dodd-Naruse	[53]	9.2.5				
	Drucker I	[54]	9.2.5				
Pyramidal Criteria (Pressure-Sensitive Criteria)							
UST	Unified Strength Theory of Yu	[228]	10.2	131			
SST	Single-Shear-Theory of Yu	[228]	10.2				
TST	Twin-Shear-Theory of Yu	[228]	10.2			30	
	Drucker II	[55]	10.3.4				
	Haythornthwaite	[107]	10.3.4				
Combined Criteria							
	Pelczyński	[155]	11			37	
	Huber	[36, 91]	11.2.1	156	42	41	
	Kuhn	[118]	11.2.1	160	43		
	Modification of the model of Huber	[103]	11.2.2	163	42		
	Combined Geometrical-Mechanical Model	[103]	11.2.3	172	44		

$$\cos 3\theta = \frac{3\sqrt{3}}{2}\frac{\det \boldsymbol{s}}{(I_2'(\boldsymbol{s}))^{3/2}}, \qquad \theta \in \left[0, \frac{\pi}{3}\right], \tag{224}$$

see [43, 150, 234] among others.

16 Criteria of this Chapter 2

In Table 10 many of the discussed in this chapter criteria are summarized. The table is organized as it follows:

- In the first column (Abbrev.) some abbreviations are presented.
- The main name of the criteria is presented in column 2.
- The third column indicates the main reference(s).
- Column 4 presents the section, where the given criterion is discussed.
- In the column 5 the relevant equation is presented.
- In the last three columns are given the references to the figures (in the Burzyński-plane (BP), in the principal stress space (3D) and in the π-plane (π)).

References

1. Alpa, G.: On a statistical approach to brittle rupture for multiaxial states of stress. Eng. Fract. Mech. **19**(5), 881–901 (1984)
2. Altenbach, H.: Criterion with application to strength, yielding, and damage of isotropic materials. In: Lemaitre, J. (ed.) Handbook of Materials Behavior Models, pp. 175–186. Academic Press, San Diego (2001a)
3. Altenbach, H.: A nonclassical model for creep-damage processes. Mater. Phys. Mech. **3**, 25–35 (2001b)
4. Altenbach, H.: Strength hypotheses—a never ending story. Czasopismo Techniczne (Techn Trans) Politechniki Krakowkiej **107**(20), 5–15 (2010)
5. Altenbach, H.: Kontinuumsmechanik - Eine elementare Einführung in die materialunabhängigen und materialabhängigen Gleichungen. Springer Vieweg, Heidelberg (2012)
6. Altenbach, H., Kolupaev, V.A.: Fundamental forms of strength hypotheses. In: Indeitcev, D.A., Krivtsov, A.M. (eds.) Proceedings of XXXVI Summer School Advanced Problems in Mechanics, Institute for Problems in Mechanical Engineering, pp. 32–45. RAS, St. Petersburg (2009)
7. Altenbach, H., Lauschke, U., Zolochevsky, A.: Ein verallgemeinertes Versagenskriterium und seine Gegenüberstellung mit Versuchsergebnissen. ZAMM **73**(4–5), T 372-T 375 (1993)
8. Altenbach, H., Altenbach, J., Zolochevsky, A.: Erweiterte Deformationsmodelle und Versagenskriterien der Werkstoffmechanik. Deutscher Verlag für Grundstoffindustrie, Stuttgart (1995)
9. Ambarcumyan, S.A.: Multimodulus Elasticity Theory (in Russ.: Raznomodul'naja teorija uprugosti). Nauka, Moscow (1982)
10. Andrew, W.: The effect of creep and other time related factors on plastics and elastomers, vol. I. Book B, New York (1991)
11. Annin, B.D.: Theory of ideal plasticity with a singular yield surface. J. Appl. Mech. Tech. Phys. **40**(2), 347–353 (1999)

12. de Araújo, F.C.: Elasticidade e plasticidade. Imprensa Portuguesa, Porto (1961)
13. Argon, A., Andrews, R., Godrick, J., Whitney, W.: Plastic deformation bands in glassy polystyrene. J. Appl. Phys. **39**(3), 1899–1906 (1968)
14. Aubertin, M., Simon, R.: Un critère de rupture multiaxial pour matériaux fragiles. Can. J. Civ. Eng. **25**(2), 277–290 (1998)
15. Bach, C.: Elastizität und Festigkeit. Springer, New York (1902)
16. Backhaus, G.: Deformationsgesetze. Akademie-Verlag, Berlin (1983)
17. Balandin, P.P.: On the strength hypotheses (in Russ.: K voprosu o gipotezakh prochnosti). Vestnik inzhenerov i tekhnikov **1**, 19–24 (1937)
18. Bardenheier, R.: Mechanisches Versagen von Polymerwerkstoffen: Anstrengungsbewertung mehrachsialer Spannungszustände. Hanser, München (1982)
19. Bauwens, J.: Yield condition and propagation of Lüders' lines in tension-torsion experiments on poly (vinyl chloride). J. Polym. Sci., Part A-2: Polym. Phys. **8**(6), 893–901 (1970)
20. Becker, W., Gross, D.: Mechanik elastischer Körper und Strukturen. Springer, Berlin (2002)
21. Beltrami, E.: Sulle condizioni di resistenza dei corpi elastici. Il Nuovo Cimento **18**(1), 145–155 (1885)
22. Belyaev, N.M.: Strength of Materials. Mir Publ, Moscow (1979)
23. Betten, J.: Kontinuumsmechanik, 2nd edn. Springer, Berlin (2001)
24. Betten, J.: Creep Mechanics. Springer Verlag, Berlin (2008)
25. Betten, J., Borrmann, M.: Der Poynting-Effekt als Ursache einer werkstoffbedingten Anisotropie. Forsch. Ingenieurwes. **54**(1), 16–18 (1988)
26. Bigoni, D., Piccolroaz, A.: Yield criteria for quasibrittle and frictional materials. Int. J. Solids Struct. **41**(11), 2855–2878 (2004)
27. Billington, E.W.: The Poynting-Swift effect in relation to initial and post-yield deformation. Int. J. Solids Struct. **21**(4), 355–371 (1985)
28. Billington, E.W.: Introduction to the Mechanics and Physics of Solids. Adam Hilger Ltd., Bristol (1986a)
29. Billington, E.W.: The Poynting-Swift effect. Acta Mech. **58**, 19–31 (1986b)
30. Birger, I.A.: On a criterion for fracture and plasticity (in Russ.: Ob odnom kriterii razrushenija i plastichnosti). Mechanika tverdogo tela, Izvestija Akademii Nauk SSSR **4**, 143–150 (1977)
31. Birger, I.A., Shopp, B.F., Iosilevich, G.B.: Strength Computations for Machine Components (in Russ.: Raschet na prochnost' detalej mashin, Spravochnik). Mashinostroenie, Moscow (1993)
32. Blumenauer, H.: Werkstoffprüfung. Dt. Verl. für Grundstoffindustrie, Leipzig (1996)
33. Bolchoun, A., Kolupaev, V.A., Altenbach, H.: Convex and non-convex flow surfaces (in German: Konvexe und nichtkonvexe Fließflächen). Forsch. Ingenieurwes. **75**(2), 73–92 (2011)
34. Brencich, A., Gambarotta, L.: Isotropic damage model with different tensile-compressive response for brittle materials. Int. J. Solids Struct. **38**(34), 5865–5892 (2001)
35. Burzyński, W.: Studjum nad hipotezami wytężenia. Akademia Nauk Technicznych, Lwów (1928)
36. Burzyński, W.: Über die Anstrengungshypothesen. Schweizerische Bauzeitung **94**(21), 259–262 (1929a)
37. Burzyński, W.: Über die Anstrengungshypothesen. Schweizerische Bauzeitung **95**(7), 87–88 (1929b)
38. Burzyński, W.: Theoretical foundations of the hypotheses of material effort. Eng. Trans. Pol. Acad. Sci. **56**(Special Issue), 9–45 (2008)
39. Burzyński, W.: Selected passages from Włodzimierz Burzyński's doctoral dissertation "Study on material effort hypotheses" printed in Polish by the Academy of Technical Sciences, Lwów, 1928, 1–192. Eng. Trans. Pol. Acad. Sci. **57**(3–4), 127–157 (2009)
40. Candland, C.T.: Implications of macroscopic failure criteria which are independent of hydrostatic stress. Int. J. Fract. **11**(3), 540–543 (1975)
41. Cardarelli, F.: Materials Handbook: A Concise Desktop Reference, 2nd edn. Springer, London (2008)
42. Chen, W.F., Han, D.J.: Plasticity for Structural Engineers. Springer, New York (1988)

43. Chen, W.F., Zhang, H.: Structural Plasticity—Theory, Problems, and CAE Software. Springer, New York (1991)
44. Chong, E.K.P., Zak, S.H.: An Introduction to Optimization. Wiley, Hoboken, NJ (2008)
45. Christensen, R.M.: The Theory of Materials Failure. University Press, Oxford (2013)
46. Christensen, R.M., Freeman, D.C., DeTeresa, S.J.: Failure criteria for isotropic materials, applications to low-density types. Int. J. Solids Struct. **39**(4), 973–982 (2002)
47. Coffin, L., Schenectady, N.: The flow and fracture of a brittle material. J. Appl. Mech. **17**, 233–248 (1950)
48. Coulomb, C.A.: Essai sur une application des regles des maximis et minimis a quelquels problemes de statique relatifs, a la architecture. Mem. Acad. Roy. Div. Sav. **7**, 343–387 (1776)
49. Cowan, H.J.: The strength of plain, reinforced and prestressed concrete under the action of combined stresses, with particular reference to the combined bending and torsion of rectangular sections. Mag. Concr. Res. **5**(14), 75–86 (1953)
50. Darkov, A., Shpiro, G.: Strength of Materials (in Russ.: Soprotivlenie materialov). Visshaja Shkola, Moscow (1965)
51. Desai, C.S.: A general basis for yield, failure and potential functions in plasticity. Int. J. Numer. Anal. Meth. Geomech. **4**(4), 361–375 (1980)
52. Diabgroup (2011) Technical manual, divinicell h. Tech. rep., www.diabgroup.com, Hemmingen
53. Dodd, B., Naruse, K.: Limitation on isotropic yield criteria. Int. J. Mech. Sci. **31**(7), 511–519 (1989)
54. Drucker, D.C.: Stress-strain relations for strain hardening materials: Discussion and proposed experiments. In: Reissner E., Prager W., Stoker R.R. (eds.) Non-Linear Problems in Mechanics of Continua. Brown University. Proceedings of the First Symposium in Applied Mathematics, American Mathematical Society, vol. 1, PP. 181–187. New York (1949)
55. Drucker, D.C.: Limit analysis of two and three dimensional soil mechanics problems. J. Mech. Phys. Solids **1**(4), 217–226 (1953)
56. Drucker, D.C., Prager, W.: Soil mechanics and plastic analysis or limit design. Q. Appl. Math. **10**, 157–165 (1952)
57. Edelman, F., Drucker, D.C.: Some extensions of elementary plasticity theory. J. Franklin Inst. **251**(6), 581–605 (1951)
58. Ehrenstein, G.W.: Mit Kunststoffen konstruieren. Hanser, München (1995)
59. Elias, H.G.: Makromoleküle: Physikalische Strukturen und Eigenschaften, vol. 2. Wiley-VCH, Weinheim (2001)
60. Ely, R.: Biaxial stress testing of acrylic tube specimens. Polym. Eng. Sci. **7**(1), 40–44 (1967)
61. Eschenauer, H., Olhoff, N., Schnell, W.: Applied Structural Mechanics: Fundamentals of Elasticity, Load-bearing Structures, Structural Optimization. Springer, Berlin (1997)
62. Feodosiev, V.I.: Ten Lectures-Discussions of the Strength Theory (in Russ.: Desjat' lekzijbesed po soprotivleniju materialov). Nauka, Moscow (1975)
63. Filin, A.P.: Applied Mechanics of Solid Deformable Bodies (in Russ.: Prikladnaja mechanika tverdogo deformiruemogo tela), vol. 1. Nauka, Moscow (1975)
64. Filonenko-Borodich, M.M.: Theory of Elasticity. P. Noordhoff W. N, Groningen (1960)
65. Filonenko-Boroditsch, M.M.: Festigkeitslehre, vol. 1. Technik, Berlin (1960)
66. Finnie, I., Heller, W.R.: Creep of Engineering Materials. McGraw-Hill, New York (1959)
67. Föppl, A., Föppl, L.: Drang und Zwang: Eine höhrere Festigkeitslehre für Ingenieure. R. Oldenbourg, München (1920)
68. Freudenthal, A., Gou, R.: Second order effects in the theory of plasticity. Acta Mech. **8**(1), 34–52 (1969)
69. Freudenthal, A.M.: Constitutive equations of rock with shear dilatancy. Tech. Rep. AD-AOll 402, DTIC Document (1975)
70. Fridman, Y.B.: Unified Theory of Strength (in Russ.: Edinaya teorija prochnosti). Oborongiz, Moscow (1943)

71. Fromm, H.: Grenzen des elastischen Verhaltens beanspruchter Stoffe. In: Auerbach F, Hort W. (eds.) Statik und Dynamik elastischer Körper nebst Anwendungsgebieten. II. Teil. Zum Gebrauch für Ingenieure, Physiker und Mathematiker, vol. 4, pp. 359–435. Verlag von Barth, J.A., Leipzig (1931)
72. Gdoutos, E.E.: Failure of cellular foams under multiaxial loading. Compos. A **33**, 163–176 (2002)
73. Geniev, G.A., Kissjuk, V.N., Tjupin, G.A.: Plasticity Theory for Concrete and Reinforced Concrete (in Russ.: Teorija plastichnosti betona i zhelezhobetona). Strojizdat, Moscow (1974)
74. Gol'denblat, I.I., Kopnov, V.A.: Yield and Strength Criteria for Structural Materials (in Russ.: Kriterii prochnosti i plastichnosti konstrukzionnych materialov). Mashinostroenie, Moscow (1968)
75. Göldner, H., Holzweißig, F.: Leitfaden der Technischen Mechanik: Statik, Festigkeitslehre, Kinematik. Dynamik, Fachbuchverlag, Leipzig (1989)
76. Gollub, W.: Grenzen und Möglichkeiten der Mohr-Coulombschen Bruchbedingung, 18: Mechanik/Bruchmechanik, vol. 68. VDI, Düsseldorf (1989)
77. Grashof, F.: Theorie der Elasticität und Festigkeit. Gaertner, Berlin (1878)
78. Gross, D., Seelig, T.: Fracture Mechanics: with an Introduction to Micromechanics. Springer, Berlin (2011)
79. Gummert, P., Reckling. K.A.: Computation of the Bearing Capacity of Structures by the Method of Limiting Equilibrium (in Russ.: Raschet nesushej sposobnosti konstrukzij po metody predel'nogo ravnovesija). Strohizdat, Moscow (1949)
80. Haigh, B.P.: The strain-energy function and the elastic limit. Engineering **109**, 158–160 (1920)
81. Häusler, O., Tsakmakis, C.: Torsion eines Kreiszylinders bei großen Deformationen und inkompressiblem Materialverhalten. Forschungszentrum Karlsruhe GmbH, Karlsruhe (1995)
82. Hayhurst, D.R.: Creep rupture under multi-axial states of stress. J. Mech. Phys. Solids **20**(6), 381–390 (1972)
83. Haythornthwaite, R.M.: Mechanics of triaxial tests for soil. Proc. ASCE J. Soil Mech. Found. Div. **86**(SM5), 35–62 (1960)
84. Haythornthwaite, R.M.: Range of yield condition in ideal plasticity. Proc. ASCE J. Eng. Mech. Div. **87**(EM6), 117–133 (1961)
85. Hencky, H.: Zur Theorie plastischer Deformationen und der hierdurch im Material hervorgerufenen Nachspannungen. ZAMM **4**(4), 323–334 (1924)
86. Hencky, H.: Ermüdung, Bruch, Plastizität. Stahlbau **16**(23/24), 95–97 (1943)
87. Hill, R.: On the inhomogeneous deformation of a plastic lamina in a compression test. Phil. Mag. Series 7 **41**(319), 733–744 (1950)
88. Hoffman, O., Sachs, G.: Introduction to the Theory of Plasticity for Engineers. McGraw-Hill, New York (1953)
89. Holzmann, G., Meyer, H., Schumpich, G.: Technische Mechanik Festigkeitslehre. Springer, Vieweg, Wiesbaden (2012)
90. Hu, W., Wang, Z.R.: Multiple-factor dependence of the yielding behavior to isotropic ductile materials. Comput. Mater. Sci. **32**(1), 31–46 (2005)
91. Huber, M.T.: Specific strain work as a measurment of material effort (in Polish: Właściwa praca odkształcenia jako miara wytężenia materyału). Czasopismo Techniczne **22**, 34–40, 49–50, 61–62, 80–81 (1904)
92. Ishlinsky, A.Y.: Hypothesis of strength of shape change (in Russ.: Gipoteza prochnosti formoizmenenija). Uchebnye Zapiski Moskovskogo Universiteta, Mekhanika **46**, 104–114 (1940)
93. Ishlinsky, A.Y., Ivlev, D.D.: Mathematical Theory of Plasticity (in Russ.: Matematicheskaja teorija plastichnosti). Fizmatlit, Moscow (2003)
94. Ismar, H., Mahrenholtz, O.: Über Beanspruchungshypothesen für metallische Werkstoffe. Konstruktion **34**, 305–310 (1982)
95. Issler, L., Ruoß, H., Häfele, P.: Festigkeitslehre - Grundlagen. Springer, Berlin (2006)
96. Ivlev, D.D.: On the development of a theory of ideal plasticity. J. Appl. Math. Mech. **22**(6), 1221–1230 (1958)

97. Ivlev, D.D.: The theory of fracture of solids. J. Appl. Math. Mech. **23**(3), 884–895 (1959)
98. Ivlev, D.D.: On extremal properties of the yield criteria (in Russ.: Ob ekstremal'nych svojstvach uslovij plastichnosti). J. Appl. Math. Mech. **5**, 1439–1446 (1960)
99. Ivlev, D.D.: Theory of Ideal Plasticity (in Russ.: Teorija idealnoj plastichnosti). Nauka, Moscow (1966)
100. Ivlev, D.D.: Theory of Limit State and Ideal Plasticity (in Russ.: Teorija predel'nogo sostojanija i ideal'noj plastichnosti). Voronezhskij Gosudarstvennyj Universitet, Voronezh (2005)
101. Kłębowski, Z.: Obecny stan wytrzymałościowego obliczenia materiałów o własnościach uogólnionych; uogólnione obliczenie osiowo symetrycznego cienkościennego naczynia pod ciśnieniem. Przegląd Techniczny **11**, 7–31 (1934)
102. Ko, W.L.: Application of the finite elastic theory to the behavior of rubberlike materials. Ph.D. thesis, California Institute of Technology, Pasadena (1963)
103. Kolupaev, V.A.: 3D-Creep Behaviour of Parts Made of Non-Reinforced Thermoplastics (in German: Dreidimensionales Kriechverhalten von Bauteilen aus unverstärkten Thermoplasten). Ph.D. thesis, Martin-Luther-Universität Halle-Wittenberg, Halle (2006)
104. Kolupaev, V.A., Altenbach, H.: Application of the generalized model of Mao-Hong Yu to plastics (in German: Anwendung der Unified Strength Theory (UST) von Mao-Hong Yu auf unverstärkte Kunststoffe. In: Grellmann, W. (ed.) Martin-Luther-Universität Halle-Wittenberg, vol. 12, pp. 320–339. Merseburg, Tagung Deformations- und Bruchverhalten von Kunststoffen (2009)
105. Kolupaev, V.A., Altenbach, H.: Considerations on the unified strength theory due to Mao-Hong Yu (in German: Einige Überlegungen zur Unified Strength Theory von Mao-Hong Yu). Forsch. Ingenieurwes. **74**(3), 135–166 (2010)
106. Kolupaev, V.A., Altenbach, H.: Consistent view of generalised yield surfaces. In: Khan, A.S. (ed.) 18th International Symposium on Plasticity & Its Current Applications—Non-linear Response of Conventional & Advanced Materials, and Multi-scale Modeling, pp. 76–78. Neat Press, Fulton MD (2011)
107. Kolupaev, V.A., Bolchoun, A.: Combined yield and fracture criteria (in German: Kombinierte Fließ- und Grenzbedingungen). Forsch. Ingenieurwes. **72**(4), 209–232 (2008)
108. Kolupaev, V.A., Kraatz, A., Moneke, M., Bolchoun, A.: Description of the multiaxial creep for hard foams (in German: Beschreibung der mehraxialen Kriechphänomene bei Hartschaumstoffen). Kautschuk, Gummi, Kunststoffe **59**(1–2), 17–27 (2006)
109. Kolupaev, V.A., Bolchoun, A., Moneke, M.: Computation of the Poisson's ratio for the hardening of thermoplastics (in German: Ermittlung der Querkontraktionszahl bei der Verfestigung von Thermoplasten). In: Grellmann, W. (ed.) Martin-Luther-Universität Halle-Wittenberg, vol. 11, pp. 375–385. Merseburg, Tagung Deformations- und Bruchverhalten von Kunststoffen (2007)
110. Kolupaev, V.A., Bolchoun, A., Altenbach, H.: New trends in application of strength hypotheses (in German: Aktuelle Trends beim Einsatz von Festigkeitshypothesen). Konstruktion **5**, 59–66 (2009a)
111. Kolupaev, V.A., Bolchoun, A., Altenbach, H.: Unified representation and evaluation of the strength hypotheses. In: Elboujdaini M., Tyson B., Patnaik P. (eds.) 12th International Conference on Fracture ICF 12, p. 10. Ottawa (2009b)
112. Kolupaev, V.A., Bolchoun, A., Altenbach, H.: Testing of multi-axial strength behavior of hard foams. In: Brémand, F. (ed.) ICEM 14–14th International Conference on Experimental Mechanics, 4–9 July, EPJ Web of Conferences 6, 16003 (2010), 8 p. Poitiers, France (2010)
113. Kolupaev, V.A., Mohr-Matuschek, U., Altenbach. H.: Application of strength hypotheses for POM (in German: Anwendung von Festigkeitshypothesen an POM). In: Radusch H.J., Fiedler L. (eds.) 14. International Scientific Conference on Polymeric Materials P.2010, 15. - 17. September, Martin-Luther-Universität Halle-Wittenberg, p. 12. Halle (Saale) (2010b)
114. Kolupaev, V.A., Bolchoun, A., Altenbach. H.: Strength hypothesis applied to hard foams. Appl. Mech. Mater. (Advances in Experimental Mechanics VIII) **70**, 99–104 (2011)
115. Kolupaev, V.A., Yu, M.H., Altenbach, H.: Visualisation of the unified strength theory. Arch. Appl. Mech. (2013a). doi:10.1007/s00419-013-0735-8

116. Kolupaev, V.A., Yu, M.H., Altenbach, H.: Yield criteria of hexagonal symmetry in the π-plane. Acta Mech. (2013b). doi:10.1007/s00707-013-0830-5
117. Koval'chuk, B.I.: On the criterion for limit state of some hull steels under complex loading states at normal and above-normal temperatures (in Russ.: O kriterii predel'nogo sostojanija nekotorich korpusnich stalej v uslovijach slozhnogo naprjazhennogo sostojanija pri kompatnoj i povishennich temperaturach). Problemi Prochnosti **5**, 10–15 (1981)
118. Kuhn, P.: Grundzüge einer allgemeinen Festigkeitshypothese, Auszug aus Antrittsvorlesung des Verfassers vom 11. Juli, : Vom Konstrukteur und den Festigkeitshypothesen. Inst. für Maschinenkonstruktionslehre, Karlsruhe (1980)
119. Kunz, J., Michaeli, W., Herrlich, N., Land, W.: Kunststoffpraxis: Konstruktion. WEKA Media GmbH & Co, KG, Kissing (2002)
120. Lebedev, A.A.: Experimental study of long-term strength of chromium-nickel steel in biaxial tension (in Russ.: Eksperimental'nie issledovanija dlitel'noj prochnosti chromnikelevoj stali v uslovijakh dvustoronnego rastjazhenija). In: Thermal Strength of Materials and Structure Elements (in Russ.: Termoprochnost' materialov i konstrukcionnykh elementov), vol. 3, pp. 77–83 . Naukova Dumka, Kiev (1965a)
121. Lebedev, A.A.: Generalized criterion for the fatigue strength (in Russ.: Obobshennij kriterij dlitel'noj prochnosti). In: Thermal Strength of Materials and Structure Elements (in Russ.: Termoprochnost' materialov i konstrukcionnykh elementov), vol. 3, pp. 69–76. Naukova Dumka, Kiev (1965b)
122. Lebedev, A.A.: On a possible combination of a yield criterion with a criterion for brittle failure (in Russ.: O vozmozhnom sovmeshenii uslovij plastichnosti i khrupkogo razrushenija). Prikladnaja. Mechanika **4**(8), 85–93 (1968)
123. Lebedev, A.A., Panchin, V.V.: Geometrical interpretation of the generalized criterion for the fatigue strength (in Russ.: Geometricheskaja interpretazija obobshennogo kriterija dlitel'noj prochnosti). In: Thermal Strength of Materials and Structure Elements (in Russ.: Termoprochnost' materialov i konstrukcionnykh elementov), vol. 4, pp. 187–192. Naukova Dumka, Kiev (1967)
124. Lebedev, A.A., Koval'chuk, B.I., Giginjak, F.F., Lamashevsky, V.P.: Handbook of Mechanical Properties of Structural Materials at a Complex Stress State. Begell House, New York (2001)
125. Leckie, F.A., Hayhurst, D.R.: Constitutive equations for creep rupture. Acta Metall. **25**, 1059–1070 (1977)
126. Lemaitre, J., Chaboche, J.L.: Mechanics of Solid Materials. Cambridge University Press, Cambridge (1990)
127. Leon, A.: Über die Rolle des Trennbruches im Rahmen der Mohrschen Anstrengungshypothese. Der Bauingenieur **31**(32), 318–321 (1934)
128. Lequeu, P.H., Gilormini. P., Montheillet. F., Bacroix, B., Jonas, J.J.: Yield surfaces for textured polycrystals. Acta Metall. **35**(2), 439–451, 1159–1174 (1987)
129. Lüpfert, H.P.: Beurteilung der statischen Festigkeit und Dauerfestigkeit metallischer Werkstoffe bei mehrachsiger Beanspruchung. Deutscher Verlag für Grundstoffindustrie, Leipzig (1994)
130. Lurie, A.I.: Theory of Elasticity. Springer, Berlin (2005)
131. Maitra, M., Majumdar, K., Das, A.: Unified plastic yield criterion for ductile solids. AIAA Journal **11**(10), 1428–1429 (1973)
132. Mālmeisters, A., Tamužs, V., Teters, G.: Mechanik der Polymerwerkstoffe. Akademie-Verlag, Berlin (1977)
133. Marciniak, Z.: Graphical representation of states of stress and strain. Arch. Mech. **3**, 261–274 (1971)
134. Mariotte, M.: Traité du mouvement des eaux et des autres corps fluides. J. Jambert, Paris (1700)
135. Mendelson, A.: Plasticity: Theory and Application. Krieger, Malabar, Fla (1968)
136. Mendera, Z.: Wytężenie spoiny czołowej w interpretacji powierzchni granicznych. Przegląd Spawalnictwa SIMP **XVIII**(1), 6–13 (1966)

137. Miles, M., Mills, N.: The yield locus of polycarbonate. J. Polym. Sci.: Polym. Lett. Ed. **11**(9), 563–568 (1973)
138. Mirolyubov, I.N.: On the generalization of the strengt theory based on the octaedral stresses in the case of brittle materials (in Russ.: K voprosu ob obobshenii teorii prochnosti oktaedticheskikh kasatelnyh naprjazhenij na khrupkie materialy). Trudy Leningradskogo Technologicheskogo Instituta pp 42–52 (1953)
139. von Mises, R.: Mechanik des festen Körpers im plastischen deformablen Zustand. Nachrichten der Königlichen Gesellschaft der Wissenschaften Göttingen, Mathematisch-physikalische Klasse pp. 589–592 (1913)
140. von Mises, R.: Mechanik der plastischen Formänderung von Kristallen. ZAMM **8**, 161–185 (1928)
141. Mohr, O.: Welche Umstände bedingen die Elastizitätsgrenze und den Bruch eines Materials. Z VDI **45**, 1524–1530 (1900a)
142. Mohr, O.: Welche Umstände bedingen die Elastizitätsgrenze und den Bruch eines Materials. Z VDI **46**, 1572–1577 (1900b)
143. Mohr, O.: Abhandlungen aus dem Gebiete der technischen Mechanik. Wilhelm & Sohn, Berlin (1914)
144. Müller, R.: Theoretische Untersuchung des Einflusses der Spannungskonzentration durch Kerben bei mehrachsiger Belastung. Ph.D., TH Karlsruhe, Karlsruhe (1987)
145. Murzewski, J., Mendera, Z.: Yield surface of steel determined by semi-empirical method. Bulletin de L'Academie Polonaise des Sciences, Serie des sciences, techniques**XI**(7), 35–42 (1963)
146. Navier, M.: De la resistance des corps solides. Dunand, Paris (1864)
147. Nayak, G., Zienkiewicz, O.: Convenient form of stress invariants for plasticity. In: Proceedings of the ASCE Journal of the Structural Division, vol. 98, pp. 949–953 (1972)
148. Novozhilov, V.: On the principles of the statical analysis of the experimental results for isotropic materials (in Russ.: O prinzipakh obrabotki rezultatov staticheskikh ispytanij izotropnykh materialov). Prikladnaja Matematika i Mechanika **XV**(6), 709–722 (1951a)
149. Novozhilov, V.V.: On the connection between stresses and strains in a nonlinear-elastic continuum (in Russ.: O svjazi mezhdu naprjazhenijami i deformazijami v nelinejno-uprugoj srede). Prikladnaja Matematika i Mechanika **XV**(2):183–194 (1951b)
150. Ottosen, N.S., Ristinmaa, M.: The Mechanics of Constitutive Modeling. Elsevier Science, London (2005)
151. Pae, K.D.: The macroscopic yielding behaviour of polymers in multiaxial stress fields. J. Mater. Sci. **12**, 1209–1214 (1977)
152. Papageorgiou, M.: Optimierung: statische, dynamische, stochastische Verfahren für die Anwendung. Oldenbourg, München (1996)
153. Paul, B.: A modification of the Coulomb-Mohr theory of fracture. J. Mater. Sci. Ser E **28**(2), 259–268 (1961)
154. Paul, B.: Macroscopic plastic flow and brittle fracture. In: Liebowitz, H. (ed.) Fracture: An Advanced Treatise, vol. II, pp. 313–496. Academic Press, New York (1968)
155. Pełczyński, T.: Wpływ stanu napięcia na przejście materiału w stan plastyczny. Przeglad Mechaniczny **7**, 204–208 (1951)
156. Pisarenko, G.S., Lebedev. A.A.: Deformation and Fracture of Materials under Combined Stress (in Russ.: Soprotivlenie materialov deformirovaniju i razrusheniju pri slozhnom naprjazhennom sostojanii). Naukowa Dumka, Kiev (1969)
157. Pisarenko, G.S., Lebedev, A.A.: Deformation and Strength of Materials under Complex Stress State (in Russ.: Deformirovanie i prochnost' materialov pri slozhnom naprjazhennom sostojanii). Naukowa Dumka, Kiev (1976)
158. Pęcherski, R.B., Szeptyński, P., Nowak, M.: An extension of Burzyński hypothesis of material effort accounting for the third invariant of stress tensor. Arch. Metall. Mater. **56**(2), 503–508 (2011)
159. Poncelet, J.V.: Mécanique Industrielle. Meline, Bruxelles (1839)

160. Poynting, J.H.: On pressure perpendicular to the shear planes in finite pure shears, and on the lengthening of loaded wires when twisted. Proc. R. Soc. Lond. Ser. A **82**(557), 546–559 (1909)
161. Poynting, J.H.: On the changes in the dimensions of a steel wire when twisted, and on the pressure of distortional waves in steel. Proc. R. Soc. Lond. Ser. A **86**(590), 534–561 (1912)
162. Poynting, J.H., Thomson, J.J.: A Text-Book of Physics, Properties of Matter. Charles Griffin & Company, London (1927)
163. Prager, W., Hodge, P.: Theorie ideal plastischer Körper. Springer, Wien (1954)
164. Raghava, R., Caddell, R., Yeh, G.: The macroscopic yield behaviour of polymers. J. Mater. Sci. **8**(2), 225–232 (1973)
165. Raniecki, B., Mróz, Z.: Yield or martensitic phase transformation conditions and dissipation functions for isotropic, pressure-insensitive alloys exhibiting sd effect. Acta Mech. **195**, 81–102 (2008)
166. Rankine, W.J.M.: Manual of Applied Mechanics. Griffin, London (1876)
167. Reckling, K.: Plastizitätstheorie und ihre Anwendung auf Festigkeitsprobleme. Springer, Berlin (1967)
168. Reiner, M.: Deformation Strain and Flow. An Elementary Introduction to Rheology. H. K. Lewis & Co. Ltd., London (1960)
169. Reiner, M., Abir, D.: Second-Order Effects in Elasticity, Plasticity and Fluid Dynamics. Jerusalem Academic Press, Jerusalem (1964)
170. Résal, J.: Résistance des matériaux. Librairie polytechnique, Baudry & cie., Paris (1898)
171. Reuss, A.: Vereinfachte Beschreibung der plastischen Formänderungsgeschwindigkeiten bei Voraussetzung der Schubspannungsfließbedingung. ZAMM **13**(5), 356–360 (1933)
172. Rivlin, R.S., Saunders, D.W.: Large elastic deformations of isotropic materials. vii. experiments on the deformation of rubber. Philos. Trans. R. Soc. Lond. Ser. A **243**(865), 251–288 (1951)
173. Roscoe, K.H., Burland, J.B.: On the generalized stress-strain behaviour of 'wet' clay. In: Heyman, J., Leckie, F.A. (eds.) Engineering Plasticity, Papers for Conference held in Cambridge, pp. 535–609. University Press, Cambridge March 1968
174. Sähn, S., Göldner, H., Fischer, K.F., Nickel, J.: Bruch- und Beurteilungskriterien in der Festigkeitslehre. Fachbuchverbuchverlag, Leipzig-Köln (1993)
175. de Saint-Venant, B.: Comptes rendus des séances de l'Académie des sciences (1871)
176. Sandel, G.D.: Über die Festigkeitsbedingungen: ein Beitrag zur Lösung der Frage der zulässigen Anstrengung der Konstruktionsmaterialen. Ph.D. thesis, TeH, Stuttgart (1919)
177. Sauter, J.: Neue und alte statische Festigkeitshypothesen. VDI, Reihe 1: Konstruktionstechnik / Maschinenelente Nr. 191, Düsseldorf (1990)
178. Sayir, M.: Zur Fließbedingung der Plastizitätstheorie. Ing. Arch. **39**, 414–432 (1970)
179. Schleicher, F.: Der Spannungszustand an der Fließgrenze (Plastizitätsbedingung). Ztschr f Math und Mech **6**(3), 199–216 (1926)
180. Schleicher, F.: Über die Sicherheit gegen Überschreiten der Fliessgrenze bei statischer Beanspruchung. Der Bauingenieur **9**(15), 253–261 (1928)
181. Schlimmer, M.: Zeitabhängiges mechanisches Werkstoffverhalten: Grundlagen, Experimente. Rechenverfahren für die Praxis, Springer, Berlin (1984)
182. Schmidt, R.: Über den Zusammenhang von Spannungen und Formänderungen im Verfestigungsgebiet. Ing. Arch. **3**(3), 215–235 (1932)
183. Schneider, W.: Mikromechanische Betrachtung von Bruchkriterien unidirektional verstärkten Schichten aus Glasfaser/Kunststoff. Fachbereich Maschinenbau D 17, Technische Hochschule Darmstadt, Darmstadt (1974)
184. Schneider, W.: Versagenskriterien für Kunststoffe unter mehrachsiger Kurzzeitbeanspruchung. In: Belastungsgrenzen von Kunststoff-Bauteilen, pp. 81–105. VDI-Verlag GmbH, Düsseldorf (1975)
185. Schneider, W., Bardenheier, R.: Versagenskriterien für Kunststoffe. Zeitschrift für Werkstofftechnik (J of Materials Technology) **6**(8), 269–280 (1975)
186. Schofield, A., Wroth, P.: Critical State Soil Mechanics. McGraw-Hill, London (1968)

187. Schreyer, H.: Smooth limit surfaces for metals, concrete, and geotechnical materials. J. Eng. Mech. **115**(9), 1960–1975 (1989)
188. Schur, I., Grunsky, H.: Vorlesungen über Invariantentheorie: Die Grundlehren der mathematischen Wissenschaften in Einzelndarstellungen. Springer, Berlin (1968)
189. Schwartz, R., Dugger, J.: Shear strength of plastic materials. Mod. Plast. **21**, 117–121, 164, 166 (1944)
190. Schwarzl, F., Stavermann, A.J.: Bruchspannung und festigkeit von hochpolymeren. In: Stuart, H. (ed.) Die Physik der Hochpolymeren: Theorie und Molekulare Deutung Technologischer Eigenschaften von Hochpolymeren Werkstoffen, vol. 4, pp. 165–176. Springer, Berlin (1964)
191. Sdobyrev, V.P.: Criterion for the long term strength of some heat-resistant alloys at a multiaxial loading (in Russ.: Kriterij dlitelnoj prochnosti dlja nekotorykh zharoprochnykh splavov pri slozhnom naprjazhennom sostojanii). Izvestija Akademii Nauk SSSR, Otdelenie tekhnicheskikh Nauk, Mechanika i Mashinostroenie **6**, 93–99 (1959)
192. Shanley, F.R.: Strength of Materials. McGraw-Hill, New York (1957)
193. Shesterikov, S.A.: On the theory of ideal plastic solid (in Russ.: K postroeniju teorii ideal'no plastichnogo tela). Prikladnaja matematika i mechanika, Rossijskaja Akademija Nauk **24**(3), 412–415 (1960)
194. Skrzypek, J.J.: Plasticity and Creep: Theory. CRC Press, Boca Raton, Examples and Problems (1993)
195. Sokolovsky, V.V.: Theory of Plasticity (in Russ.: Teorija plastichnosti). Gos. izd. tekhn.-teor. literatury, Moscow (1950)
196. Stadler, W.: Multicriteria Optimization in Engineering and the Sciences. Mathematical Concepts and Methods in Science and Engineering, vo. 37. Plenum Press, New York (1988)
197. Stepin, P.A.: Strength of Materials. Gordon & Breach, New York (1963)
198. Sternstein, S., Ongchin, L.: Yield criteria for plastic deformation of glassy high polymers in general stress fields. Div. Polym. Chem. **10**, 1117–1121 (1969)
199. Stockton, F.D., Drucker, D.C.: Fitting mathematical theory of plasticity to experimental results. J. Colloid Sci. **5**(3), 239–250 (1950)
200. Swift, H.W.: Plastic strain in an isotropic strain hardening material. Engineering: for innovators in technology, manufacturing and management **163**, 381–389 (1946)
201. Tarasenko, I.I.: On the criteria of brittle strength of materials (in Russ.: O kriterijach khrupkoj prochnosti materialov). Sbornik nauchnykh trudov, Leningradskij inzhenerno-stroitelnij institut **26**, 161–168 (1957)
202. Theocaris, P.: A general yield criterion for engineering materials, depending on void growth. Meccanica **21**(2), 97–105 (1986)
203. Thorkildsen, R.: Mechanical behaviour. In: Baer, E. (ed.) Engineering Design for Plastics, pp. 227–399. Reinhold, New York (1964)
204. Timoshenko, S.P.: History of Strength of Materials: With a Brief Account of the History of Theory of Elasticity and Theory of Structure. McGraw-Hill, New York (1953)
205. Timoshenko, S.P., Goodier, J.N.: Theory of Elasticity. McGraw-Hill, New York (1987)
206. Timoshenko, S.P., Young, D.H.: Elements of Strength of Materials. D. van Nostrand Company, Princeton (1962)
207. Torre, C.: Einfluss der mittleren Hauptnormalspannung auf die Fließ- und Bruchgrenze. Österreichisches Ingenieur-Archiv **I**(4/5), 316–342 (1947)
208. Torre, C.: Grenzbedingung für spröden Bruch und plastisches Verhalten bildsamer Metalle. Österreichisches, Ingenieur-Archiv **IV**(2):174–189 (1950)
209. Tresca, H.: Mémoire sur l'ecoulement des corps solides. Mémoires Pres par Div Savants **18**, 733–799 (1868)
210. Tschoegl, N.W.: Failure surfaces in principial stress space. J. Polym. Sci., Part C: Polym. Symp. **32**, 239–267 (1971)
211. Tsvelodub, I.Y.: Stability postulate and its applications in the creep theory for metallic materials (in Russ.: Postulat ustojchivosti i ego prilozhenija v teorii polzuchesti metallicheskich materialov). Institut Gidromechaniki, Novosibirsk (1991)

212. Tsvelodub, I.Y.: Multimodulus elasticity theory. J. Appl. Mech. Technical Phys. **49**(1), 129–135 (2008)
213. Vesik, S.: Handbook of Strength of Materials (in Russ.: Spravochnik po soprotivleniju materialov). Budivelnik, Kiev (1970)
214. Volkov, S.D.: Basics of the statistical theory of strength (in Russ.: Osnovy statisticheskoj teorii prochnosti). In: Ioffe, A.F., Kurdjymov, G.B., Zhurkov, S.N. (eds.) Nekotorye problemy prochnosti tverdogo tela, Izdatel'stvo Akademii Nauk SSSR, pp. 325–333. Leningrad, Moscow (1959)
215. Wack, B.: The torsion of a tube (or a rod): General cylindrical kinematics and some axial deformation and ratchet measurements. Acta Mech. **80**(1), 39–59 (1989)
216. Wang, D.A., Pan, J.: A non-quadratic yield function for polymeric foams. Int. J. Plast. **22**(3), 434–458 (2006)
217. Weigler, H., Becker, G.: Über das Bruch- und Verformungsverhalten von Beton bei mehrachsiger Beanspruchung. Der Bauingenieur **36**(10), 390–396 (1961)
218. Westergaard, H.M.: On the resitance of ductile materials to combined stress in two or three directions perpendicular to one another. J. Franklin Inst. **189**, 627–640 (1920)
219. Williams, J.G.: Stress Analysis of Polymers. Longman, London (1973)
220. Yagn, Y.I.: New methods of strength prediction (in Russ.: Novye metody pascheta na prochnost'). Vestnik inzhenerov i tekhnikov **6**, 237–244 (1931)
221. Yagn, Y.I.: Strength of Materials: Theory and Problems (in Russ.: Soprotivlenie materialov: teorja i zadachnik). Kubuch, Leningrad (1933)
222. Yu, M.H.: General behaviour of isotropic yield function (in Chinese). Scientific and Technological Research Paper of Xi'an Jiaotong University, pp 1–11 (1961)
223. Yu, M.H.: Brittle fracture and plastic yield criterion (in Chinese). Scientific and Technological Research Paper of Xi'an Jiaotong University, pp 1–25 (1962)
224. Yu, M.H.: Twin shear stress yield criterion. Int. J. Mech. Sci. **25**(1), 71–74 (1983a)
225. Yu, M.H.: Twin shear stress yield criterion. Int. J. Mech. Sci. **25**(11), 845–846 (1983b)
226. Yu, M.H.: Researches on the twin shear stress strength theory (in Chinese). Xi'an Jiaotong University Press, Xi'an (1988)
227. Yu, M.H.: Engineering Strength Theory (in Chinese). Higher Education Press, Beijing (1999)
228. Yu, M.H.: Advances in strength theories for materials under complex stress state in the 20th century. Appl. Mech. Rev. **55**(5), 169–218 (2002)
229. Yu, M.H.: Unified Strength Theory and its Applications. Springer, Berlin (2004)
230. Yu, M.H., He, L., Song, L.: Twin shear stress theory and its generalization. Scientia Sinica, Series A-Mathematical, Physical, Astronomical and Technical Sciences **28**(11), 1174–1183 (1985)
231. Zawadzki, J.: Ciśnienie zredukowane jako jeden z parametrów wytężenia (Przyrost właściwej energii swobodnej jako miara wytężenia). Rozprawy Inzynierskie **LXXIII**, 358–398 (1957)
232. Ziegler, H.: Zum plastischen Potential der Bodenmechanik. Z f angew Math und Phys **20**, 659–675 (1969)
233. Zienkiewicz, O., Pande, G.: Some useful forms of isotropic yield surfaces for soil and rock mechanics. In: Gudehus, G. (ed.) Finite Elements in Geomechanics, pp. 179–198. John Wiley, London, New York (1977)
234. Zyczkowski, M.: Combined Loadings in the Theory of Plasticity. PWN-Polish Scientific Publ, Warszawa (1981)
235. Zyczkowski, M.: Discontinuous bifurcations in the case of the Burzyński-Torre yield condition. Acta Mech. **132**(1), 19–35 (1999)